GIMA
Geographical Information Management and Applications

Crop Monitoring in Intercropping Systems: Assessing Maize Height patterns using UAV-imagery

Lara Gillham
Student number: 4987608
Email: l.z.gillham@students.uu.nl
Supervisors: Prof. Lammert Kooistra and Jan Peter van der Hoeve
Responsible professor: Prof. Arnold Bregt

Universiteit Utrecht
TU Delft
UNIVERSITY OF TWENTE.
WAGENINGEN UR

Preface

This report, entitled "Crop Monitoring in Intercropping Systems: Assessing Maize Height Patterns Using UAV Imagery," marks one of the big steps of my journey in the Geographical Information Management and Application (GIMA) master's program. Spanning six months, from September 2023 to February 2024, this thesis period has been both challenging and rewarding.

I give my gratitude to Prof. Lammert Kooistra and Jan Peter van der Hoeve for their invaluable supervision. My sincere thanks to Jan Peter van der Hoeve for his guidance throughout the fieldwork, providing me with all the required field data and showing active interest throughout the research. His insights have been pivotal in shaping my understanding and approach. I am equally grateful to Prof. Lammert Kooistra for his great advice and weekly meetings where he encouraged the preparation of presentations, significantly enriching my thought process and sustaining my enthusiasm for the research topic. Also a thanks to Dirk van Apeldoorn for providing the R script essential for this research.

Lara Gillham,

Utrecht, February 22nd**.**

Abstract

In the quest for sustainable agriculture, intercropping is emerging as a promising solution to monoculture. Nevertheless, the existing research on phenotyping in intercropping systems is insufficient. Unmanned Aerial Vehicles (UAVs), especially when equipped with RGB and LiDAR imagery, offer a promising avenue for estimating plant height. The accuracy of these two methods in estimating maize height in a strip intercropping field, focusing on individual and row levels, and observing height patterns throughout the growing season were estimated. A crop height model (CHM) for both types of imagery was created by subtracting a digital surface model (DSM) from a digital terrain model (DTM). Various percentiles and buffer sizes were tested, and the correlation between UAV-estimated plant height and ground truth plant height was evaluated using the coefficient of determination (R^2) and root mean square error (RMSE) to determine the most suitable parameters. The results indicated that LiDAR was more accurate in capturing maize tassel height, with higher results for individual crop observations (R^2= 0.9, RMSE= 13.41cm) than for row observations (R^2 = 0.89, RMSE = 20.89cm). RGB imagery yielded an R^2 of 0.88 and RMSE of 27.88 cm for individual crop height and an R^2 of 0.91 and RMSE of 25.97cm for row observations. Once the optimal parameters are identified, the height patterns in rows and over time could be observed within the field experiment. Height variations were noted within the experimental field, with southern rows typically having lower height values. The influence of neighboring crops was also apparent, as maize plots exhibited lower height values with beans as neighboring crop compared to neighboring maize. To increase accuracy and automation, future studies should consider using tassel detection. Growth curves were observed as highly unique to the different genotypes. This study suggests that LiDAR imagery can offer a reliable assessment of individual maize heights in intercropping fields and that the noticeable height patterns between rows should be taken into account when discerning differences in the behavior of different crops and cultivars in intercropping systems.

Contents

Figures

Tables

List of abbreviations

RS - Remote Sensing

UAV - Unmanned Aerial Vehicle

RGB - Red-green-blue

LiDAR - Light detection and ranging

SfM - Structure from Motion

DTM – Digital Terrain Model

DSM – Digital Surface Model

DEM – Digital Elevation Model

CHM – Canopy Height Model

GCP – Ground control points

ROI - Region of Interest

R^2 - Coefficient of determination

RMSE – Root Square Mean Error

DAP – Days after planting

GP –Growth period

1. Introduction

1.1. Overview of the topic

As the global human population is projected to reach 8.5 billion by the year 2030 (Population Estimates and Projections | DataBank, n.d.), the imperative to sustain livelihoods on a large scale has transformed monoculture into an agricultural standard, driven by the rapid advancements in modern industrial practices (Foley, 2011). Nevertheless, this approach has given rise to a series of pressing concerns, including biodiversity loss, soil degradation and over-reliance on non-renewable resources (Bourke et al., 2021). To confront these challenges, it may be crucial to contemplate a shift towards agricultural methodologies harmonizing with natural cycles, encompassing factors such as crop diversity. Intercropping stands out as a promising practice for mitigating the environmental impacts associated with modern agriculture while maintaining high yields (Bourke et al., 2021). Over time, maize has demonstrated its potential as a crop within intercropping systems (Seran & Brintha, 2010). Nevertheless, the successful implementation of intercropping demands attentive planning, involving intricate agricultural designs and the careful selection of cultivars optimized for such systems (Bourke et al., 2021).

To maximize the benefit of intercropping systems, breeding programs must be tailored to accommodate the complexity of inter-specific interactions. Accurately measuring height data throughout the entire crop cycle assumes significance as it enables the characterization of growth rates, overall crop health, and the detection of any requirements for additional care (Anthony et al., 2014). Consequently, the utilization of phenomics observations becomes imperative to assess the underlying genetic variations (Bourke et al., 2021). The diverse growth stages of crops introduce nuances in height definitions, necessitating adjustments in the measuring methodology through the growth of the crop. Wang et al. (2020) emphasize the critical importance of acknowledging potential variations across different rows in intercropping scenarios.

Traditional manual field phenotyping approaches are labour-intensive, prone to damage, and susceptible to human error. Recent research has shown a growing interest in utilizing Remote Sensing (RS) systems, such as Unmanned Aerial Vehicles (UAVs), for monitoring crop traits, aiming to detect phenotypic variations within the crops. The use of UAVs allows a higher temporal and spatial resolution scale with low cost and operational flexibility (Berni et al., 2009). Red-green-blue (RGB) cameras, multi/hyperspectral cameras, Light detection and ranging (LiDAR) sensors, and thermal and fluorescence imaging sensors can all be mounted on UAVs to gather RS data for crop phenotyping (Araus et al., 2018; Xie & Yang, 2020). Araus et al. (2018) specifically identify RGB and LiDAR images as the most effective tools for measuring crop height. Although the use of LiDAR has been perceived as more accurate than SfM RGB, its higher cost and complexity make it less appealing to farmers to implement (Malachy et al., 2022). The use of LiDAR, commonly used in forestry studies, is still little researched for crop management purposes (Gao et al., 2022).

1.2. Problem definition

Intercropping is rising as a good alternative to monoculture offering a solution to its negative environmental impacts. Currently, intercropping is primarily employed on small-scale farms,

but as its implementation expands, there arises a need to explore efficient methods in phenotyping for acquiring knowledge. The utilization of UAVs in crop monitoring within intercropping systems has shown promising potential in allowing more efficient measuring, yet the current body of research in this domain remains relatively recent and requires further development. A crop's phenotype in intercropping systems intricately depends on a variety of factors, including spatial arrangement, crop species interactions, resource availability, environmental influences, and temporal dynamics (Bourke et al., 2021). This interplay of elements weaves a complex system of research considerations, underscoring the need for more comprehensive exploration and augmentation of existing knowledge in the research field. Despite the Netherlands significant agricultural presence, studies specifically focusing on maize phenotyping remain scarce.

Maize is one of the world's leading cereals, with 11 per cent of it being produced in Europe (Erenstein et al., 2022). While studies have focused on investigating crop height for maize at a field scale and in monoculture, there's a notable gap when it comes to understanding how individual maize behaves in intercropping systems. Acknowledging the distinctiveness of the selected study area, characterized by its diverse array of genotypes, our objective is to bridge a notable research gap within complex intercropping systems. This is why we use maize as the focal point for our study, aiming to shed light on its behavior in intercropping scenarios. Height has also been noted to correlate with other traits, including yield, serving as a dependable predictor for various essential crop characteristics (Qiu et al., 2022; Jamil et al., 2022). By observing the possible different height patterns in cultivars, the study hopes to obtain further knowledge on maize phenotyping.

1.3. Research objectives

The general research objective of this thesis is to assess the feasibility of two UAV-based methods, more specifically using RGB and LiDAR imagery, for monitoring maize height in intercropping systems. The most accurate method will then be applied to observe height patterns between and within the plots of an experimental field. Here are the research questions that will be answered throughout this study:

- What key factors should be considered when assessing the effectiveness of UAVs in measuring maize height within intercropping systems?

- What is the accuracy of the two proposed UAV imagery-based methods (RGB and LiDAR) for observing maize height in the context of intercropping?

- Are there differences in height dynamics between the inner and outer maize rows in maize intercropping strips and do we see variation in these differences between the different maize cultivars?

- Is there variation in the growth dynamics between different maize cultivars in intercropping systems when analyzing their height at multiple time points using UAV data?

1.4. Scope and limitations

This study comes with certain limitations that need to be acknowledged. Firstly, it should be noted that the research focuses on maize crops, with a particular emphasis on different

cultivars. Unlike most field experiments that encompass one or two cultivars, this study delves into the examination of 32 cultivars which makes it unique. However, it's essential to recognize that height monitoring methods are highly crop-specific, as indicated by Jamil (2022). As a result, this investigation will focus exclusively on identifying a method suitable for maize crops.

The primary focus of this study revolves around assessing the capabilities of RS for intercropping. While the results will be employed to observe intercropping patterns, it's important to highlight that the underlying reasons for these patterns will not be explored in this thesis. This would require observations of additional environmental factors which we do not possess for this study, as well as some genotypic analysis. Nevertheless, it is our aspiration that this research will establish a solid foundation for future agricultural investigations.

In this study, our focus is not primarily on determining the superior method for maize height measurement in intercropping systems, as this assessment would entail consideration of various factors, including a cost-benefit analysis. Instead, our objective is to present results obtained from two distinct methodologies and to draw comparisons with findings from other studies. By doing so, we aim to contribute to the broader understanding of potential methodologies without imposing a definitive ranking. Moving forward, the UAV method demonstrating the highest accuracy will be selected to analyse growth patterns. This strategic choice ensures optimal accuracy in subsequent results.

2. Literature review

2.1. Crop height monitoring in intercropping systems

2.1.1. Intercropping: A sustainable agricultural practice

Monocultures took a big rise in the 19th century with the appearance of mechanization, such as steam tractors, which gave farmers the possibility for financial and organizational benefits (Struik & Kuyper, 2017). Opting for monoculture relieved farmers from the complex production requirements of diverse crops, allowing them to maintain high-yield production with minimal compromises. However, as our understanding of environmental issues has advanced in recent decades (Power & Follett, 1987), monoculture's dominant role in modern agriculture comes with strong concern about its disruption of natural cycles, including water pollution, soil erosion, biodiversity loss and over-reliance on non-renewable resources (Steffen et al., 2015; Chen et al., 2016). In their early study, Power & Follett (1987) mention how soil erosion acceleration and pest damage are being caused by repetitively growing a single cop on a field. Giam et al. (2015) shed light on the severe loss of freshwater biodiversity through oil palm monocultures in Southeast Asia. Given the studied environmental degradation, the sustainability of monoculture as an agricultural practice is beyond dispute.

Intercropping, as defined by Vandermeer (1992), is an agricultural practice in which two or more different crops are strategically grown together in the same field. This approach initiates a complex web of interactions among the crops, as they jointly access and compete for essential resources, including nutrients, water, light, oxygen, and carbon dioxide (Power & Follett, 1987). When the elements of an intercropping system exhibit divergent resource utilization patterns, effectively complementing each other's environmental use, the result becomes more resource-efficient compared to monoculture practices (Jensen, 1996). Notably, the intercropping of maize with leguminous plants has exhibited substantial advantages in nutrient uptake compared to monoculture maize cultivation (Seran & Brintha, 2010). Simultaneously cultivating multiple crops, which may even include various genotypes of a single crop species, has thereby demonstrated remarkable outcomes in increased yields, improved yield consistency, and enhanced food security (Raseduzzaman and Jensen, 2017; Li et al., 2021). Intercropping benefits extend beyond resource optimization, offering a spectrum of environmental benefits, including reductions in pest damage (Tooker & Frank, 2012), enhanced soil fertility (Li et al., 2021), and the amelioration of water erosion (Power & Follett, 1987). Because of the advantages it offers, intercropping appears as a hopeful approach for establishing sustainability in agriculture (Figure 1).

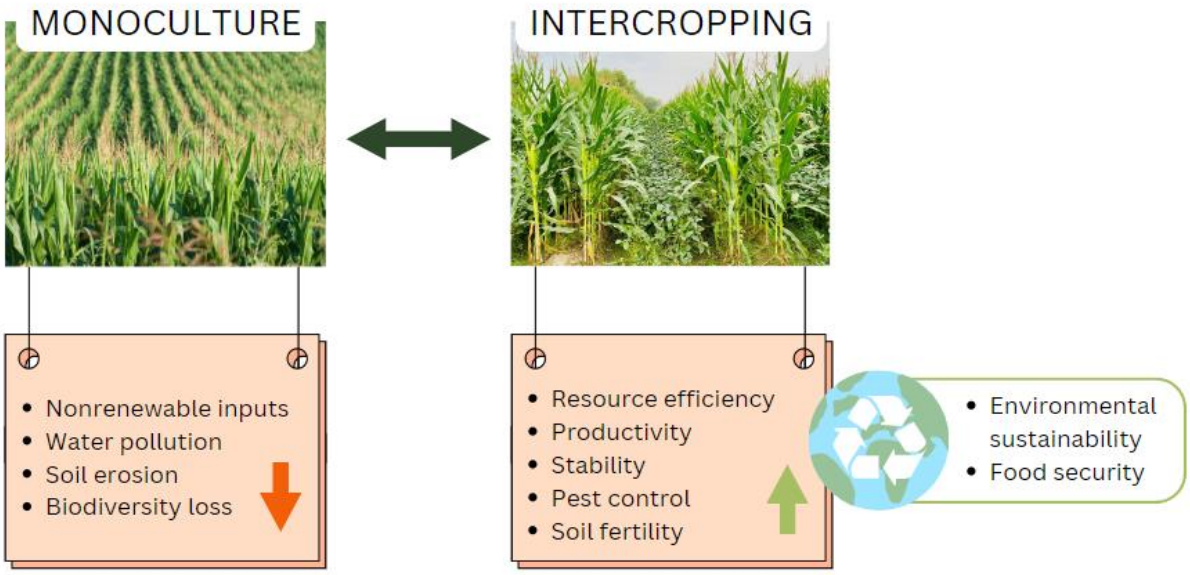

Figure 1: *Intercropping as a sustainable agricultural system.*

Intercropping embodies both a traditional and innovative agricultural practice, dependent on one's perspective (Bourke et al., 2021). Its historical roots can already be traced back to ancient civilizations (Yang et al., 2021). In his book, Vandermeer (1992) underscores the numerous intercropping combinations across the globe in the 20th century, with maize-bean intercropping being particularly abundant. In contemporary agriculture, intercropping endures as a prevalent practice among small-scale farmers in diverse regions, including China, Latin America, and Africa (Brooker et al., 2015). In Latin America, up to 90% of bean cultivation is estimated to involve intercropping with maize, potatoes, and other crops (Yang et al., 2021). However, this traditional agricultural method has largely remained confined to small-scale operations and, as Bourke et al. (2021) emphasize, expanding such a system necessitates a reconfiguration of the technology currently employed in modern agricultural systems. In his book, Vandermeer (1992) challenges the notion that intercropping is exclusively for small-scale farmers, arguing that as research technology and machinery for intercrops advance, and specific varieties are developed, intercropping will no longer be limited to smaller producers.

2.1.2. Height phenotyping in intercropping systems

As presented above, the upscaling of intercropping systems necessitates a redesign of the technology currently specialized for modern agricultural systems. Among these advancements, enhanced cultivars have played a substantial role in elevating crop productivity (Bourke et al., 2021). It is however important to recognize that the cultivars optimized for monoculture may not be the most suitable choice for intercropping (Bourke et al., 2021). Current breeding strategies primarily target the selection of the best-performing individual plant genotypes when grown in monoculture, meaning they are cultivated without other plant species. These strategies often disregard the potential benefits that may arise from positive interactions between different crop species or even different genotypes of the same species when cultivated together (Bourke et al., 2021). However, it's becoming increasingly evident that limitations in phenotyping efficiency, particularly in high-throughput field phenotyping, present a significant hurdle to genetic advancements in intercropping programs (Araus et al., 2018). Recognizing

this disparity highlights the importance of tailored field phenotyping approaches in intercropping contexts. According to studies, pertinent traits for phenomics assessment include yield, biomass, height, leaf area index, chlorophyll and nitrogen (Xie & Yang, 2020; van der Meij et al., 2017). Progress in phenotyping is therefore essential for the development of effective breeding programs in intercropping.

One crucial phenotypic trait in intercropping is height, which plays a pivotal role in understanding the dynamics of these complex agricultural systems. Plant height is defined by Perez-Harguindeguy et al., (2013) as the shortest distance between the highest point of the main photosynthetic tissues of a plant and the ground level. Accurate measurement of crop heights is indispensable to evaluate how different species interact and compete for resources within intercropping contexts. Plant height is one of the most accurately quantifiable traits, making it highly valuable for estimating other characteristics within intercropping systems (Van der Meij et al.,2017). This morphological trait is essential in providing information on the overall plant growth across the growing season and serves as a key parameter for determining advanced traits such as biomass and yield (Qiu et al., 2022; Jamil et al., 2022). As a practical example, Zhou et al. (2020) underscores the significance of measuring plant height in the context of lodging. It's important to note that the methods for measuring plant height can vary depending on the crop type and growth stage, as highlighted by Jamil et al. (2022).

Phenotyping plant height in intercropping systems presents a unique set of challenges that distinguish it from phenotyping in traditional monoculture systems. Through the study of pea-barley and faba bean-wheat combinations, Ajal et al. (2022) have demonstrated that the traits of various crop species are affected by the diversity of species. As a result, plants may exhibit more nuanced patterns, making the evaluation of individual crop heights, as opposed to field-scale assessments, a crucial focal point in comprehending their interactions (Jamil et al., 2022). Furthermore, the presence of various crops nearby can obstruct clear measurements and necessitate specialized techniques that consider height variations among different species within the same field. Consequently, height phenotyping in intercropping systems demands advanced technologies, enabling researchers to obtain accurate, high-resolution data (Jamil et al., 2022).

2.2. UAV imagery for precise crop height monitoring

While crop height can, for instance, be measured using a sufficiently tall ruler, obtaining quantitative height data through manual means is labor-intensive, time-consuming, and potentially detrimental to the plants (Araus et al., 2018). However, recent advances in technology have offered a more efficient and non-destructive alternative for crop height monitoring. UAVs, equipped with RS technologies, have gained prominence in precision agriculture (Araus et al., 2018). Utilizing UAVs enables achieving a greater temporal and spatial assessment at a low cost, allowing for the accurate assessment of crop height at multiple growth stages, without causing harm to the plants (Berni et al., 2009). Anderson et al. (2020) observed a significant impact of genetic factors on maize height measurements. Through a comparison of various height measurement approaches, they identified 32 genetic regions associated with plant height. This number surpassed the findings of traditional measurements alone, highlighting the value of advanced methods. Araus et al. (2018) underscore RGB imagery and LiDAR as the most suitable tools for measuring plant/canopy height.

To gain insights into the current state of crop height monitoring through UAVs across various

crops, a targeted search was conducted on Web of Science using the query: ALL=(UAV height crop (RGB OR Lidar)). The resulting 222 publications were subsequently organized chronologically (Figure 2). The histograms illustrate that the exploration of LiDAR and RGB technologies in crop height estimation represents a recent and evolving area of research.

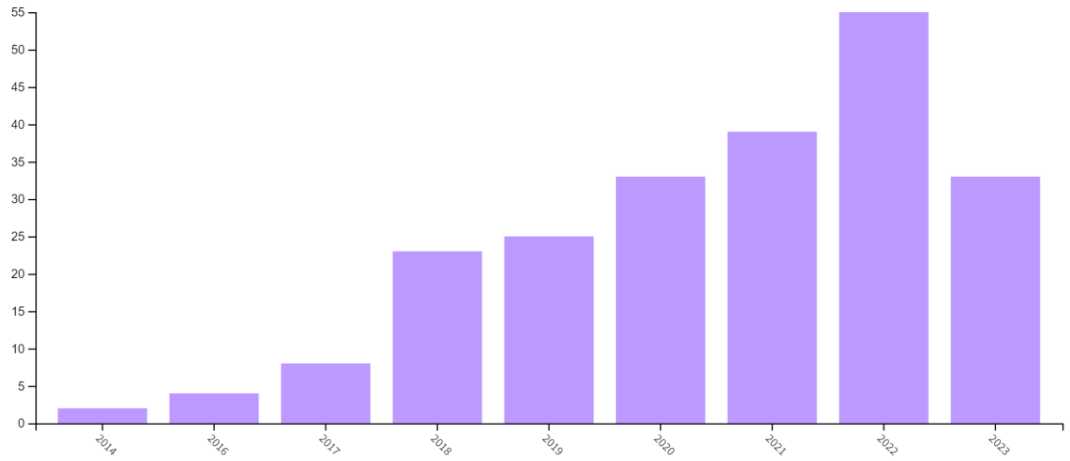

Figure 2: *Distribution of publications on UAV crop height monitoring by publication years. Under the following query: ALL=(UAV height crop (RGB OR Lidar))*.

2.2.1. RGB technology

RGB (Red, Green, Blue) technology, uses the visible spectrum to unveil intricate details in various applications, notably in agriculture. In the context of crop monitoring, RGB imagery has been observed as efficient in discerning subtle variations in plant health, growth, and overall conditions (Araus et al., 2018). RGB imagery is widely seen as advantageous due to its cost-effectiveness, making it easier to persuade breeders to adopt crop phenotyping practices (Araus et al., 2018). Various studies have delved into the realm of crop height measurement, employing the versatile RGB technology and a Structure from Motion (SfM) algorithm as a key instrument in unravelling the intricacies of plant growth (see 2.2.2). In the study by Han et al. (2018), focus was given to plant height assessment, specifically on maize crops. They explored the use of RGB imagery to examine the correlation between UAV-estimated and ground truth plant height of maize plants. The outcome of this study revealed an underestimation of maize height when relying on RGB images. The underestimation is attributed to a lack of point clouds for the full reconstruction of the tassel. Grenzdörffer (2014) also observes an underestimation of maize height when using RGB. According to this study, when the canopy structure is either thin or characterized by the presence of peaks representing the highest points of individual plants, using UAV for crop height determination will result in lower height measurements compared to manual reference measurements. Chang et al. (2017) investigated the height of Sorghum using RGB imagery Their study, involving seven data acquisitions over the growing season, highlighted the potential of UAVs for accurate crop height assessment, suggesting applicability to other crops for precision agriculture management. Jamil et al. (2022) extended the scope to intercropping, concentrating on cabbage, pumpkin, barley, and wheat. While their study demonstrated the potential of RGB imagery for accurate height assessment in cabbage and pumpkin, alternative methods were proposed for barley and wheat due to varying accuracy levels. This collective body of research underscores the versatility of RGB technology in crop height assessment while shedding light

on challenges and potential applications across diverse crop types.

2.2.2. Structure for Motion

Structure for Motion (SfM) is employed in the computation of three-dimensional (3D) models from a sequence of two-dimensional (2D) images captured from diverse perspectives (Westoby et al., 2012). This methodology involves determining the position and orientation of each camera relative to the photographed objects by identifying recurring features, such as corners or edges, within the images. Subsequently, utilizing this information, the object's surface is represented as a set of spatial points, forming a 3D point cloud generated through triangulation. A 3D surface model or mesh of the object is constructed using the obtained point cloud (Khalil, 2020). The resulting model is manipulable by computer and can be applied to diverse tasks, including mapping, surveying, and monitoring changes over time. SfM photogrammetry allows monitoring of vegetation with little cost and technical knowledge (Iglhaut et al., 2019)

2.2.3. LiDAR technology

LiDAR, or Light Detection and Ranging, has emerged as a valuable technology for precise and efficient crop height monitoring. By emitting laser pulses and measuring the time it takes for the light to return after interacting with the crop canopy, LiDAR sensors can create detailed three-dimensional representations of the vegetation (Lefsky et al., 2002). The application of LiDAR, a technology often employed in forestry research, remains relatively unexplored in the context of crop management (Gao et al., 2022). However, this high-resolution data allows for accurate measurements of crop height, offering insights into the vertical structure of crops. LiDAR's ability to penetrate the canopy and provide detailed elevation information makes it particularly advantageous in environments with dense vegetation (Anthony et al., 2014). The study from Harkel et al. (2019), focused on height measurements for potato, sugar beet, and wheat crops using LiDAR technology. Encouraging results were observed for sugar beet and wheat, indicating the efficacy of LiDAR in these contexts. However, the same level of success was not achieved in the case of potato observation. In a separate study by Gao et al. (2022), LiDAR imagery was proposed as an effective tool for monitoring individual crop height within the framework of precision agriculture.

Collectively, these recent studies underscore the specificity associated with the utilization of both RGB and LiDAR technologies for crop height monitoring. The effectiveness of these technologies is contingent upon factors such as crop type, targeted traits, and specific agricultural practices, highlighting the need for tailored approaches in adopting these technologies for crop monitoring purposes.

2.3. Spatiotemporal patterns in maize intercropping

The accuracy obtained through a height extraction process is highly specific to the type of crop, as evidenced by Jamil et al. (2022). This specificity extends to the observation of different cultivars within the same crop as demonstrated by Qiu et al. (2022) in their height assessment of two maize cultivars using LiDAR. For meaningful comparisons, it becomes imperative to conduct a literature review analysis limited to the maize crop.

2.3.1. Growth stage of maize in intercropping

In intercropping systems, the assessment of crop growth stages is pivotal for the success of mixed cultivation systems. The growth stage refers to specific developmental phases in the life cycle of plants, encompassing key events such as germination, vegetative growth, flowering, and grain development (Dambreville et al., 2015). The growth stages of crops are typically divided into the vegetative stage (V) and the reproduction stage (R) (Kling & Edmeades, 1997). Different crops, or even cultivars within a crop, will have varying resource requirements at different stages of their growth. By obtaining phenotype information during different growth stages of maize, farmers can strategically plan the intercropping arrangement to ensure that companion crops with complementary needs are planted together. The growth stage of maize significantly impacts canopy development, especially given its tall and dense nature, influencing sunlight penetration and nutrient availability for companion crops. Figure 3 illustrates the distinct vegetative and reproductive phases of maize.

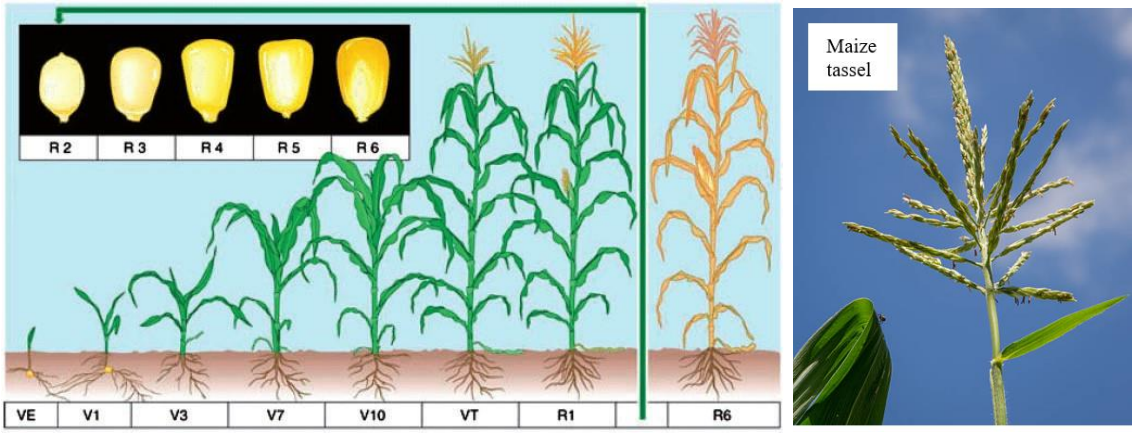

Figure 3: *Vegetative and reproductive stages of a maize plant. Adapted from Zhao et al (2012).*

The initial vegetative stage milestone is the emergence stage (VE), where the seed absorbs water and sprouts from the soil (Nleya et al., 2016). Throughout the remaining vegetative phase, the plant experiences most of its growth, generating an increasing number of leaves. These phases of vegetative growth are identified using numerical divisions, namely V1, V2, V3, and so forth up to Vn. Here, 'n' signifies the count of leaves with visible collars. As the vegetative stage concludes, the tasseling phase (R1) signifies the plant's maximum growth, marked by the full visibility of the tassel and the appearance of pollen. The reproductive stage of a maize plant is critical for the production of grains, making it a key focus for farmers aiming to optimize yield and quality. During the filling sage (R3-R4) nutrients are transported to the cob. Physiological maturity (R6) is the final stage when the kernels reach full size, dry down, and the plant approaches senescence (Nleya et al., 2016).

Considering these stages, critical height measurement points become essential. Guo et al. (2022) focus on the heading (Vn) and tasseling (VT) events as critical height observations, while Yu et al. (2013) consider the emergence (VE) and three-leaf (V3) stages. Moreover, it is important to take into account, especially when working with cultivars, that stages will not necessarily appear at the same time points for every cultivar. Guo et al. (2022) determine the heading and tasseling dates as the day when these phenological events occurred in at least 50 % of maize for each plot. Oehme et al. (2022) observed that the precision in assessing maize plant height through UAV measurements is influenced by both the growth stage of the plant

and the specific manual measurement method used as a comparison. The study noted reduced accuracy during the early growth stage due to the smaller crop size and during the maturity stage due to difficulty in tassel measurement. Additionally, findings indicated that, during the Vn and R1 stages, the manual measurement of the highest straightened leaf correlated more closely with UAV measurements than the measurement of the highest leaf. During the maturity stage (R6), the tassel alone emerged as a suitable metric for crop height, indicating a distinct shift in the preferred height determination measure. In Han et al. (2018) it is however observed that the tasseling period is where the model accuracy is the lowest. During the jointing stage, Qiu et al. (2022) measure the highest point of the central leave.

2.3.2. Row patterns in maize intercropping systems.

Ofori and Stern (1987) mark the three main categories of intercropping as mixed intercropping, row intercropping, and strip intercropping. Strip intercropping involves cultivating two or more crops simultaneously in distinct strips. These strips are sufficiently wide to allow separate cultivation practices but narrow enough to facilitate agronomic interaction between the crops (Li et al., 2013). In their research, Wang et al. (2020) conducted a comprehensive analysis of maize yield in the context of intercropping systems. By observing variances in yield depending on crop proximity, their investigation underscores the significance of assessing crops at the row scale within strip intercropping fields. One of the primary resources observed in species facilitation within intercropping systems is sunlight (Gebru, 2015). The quantity and quality of sunlight reaching the plants can be influenced by factors such as the structure and density of the crop canopy (Munz et al., 2014), as well as the orientation, width of the strips and spacing of the crops (Wang et al., 2017). Border rows of taller plants, such as maize, will benefit from less shading while border rows from shorter plants experience more shading (Munz et al., 2014). The study conducted by Wang et al. (2017) highlights the significant impact of row orientation on sunlight absorption when analysing maize height observations across different row configurations (Figure 4). Notably, they observe a discernible variance between the border and inner rows within intercropping strips comprising four rows, with the inner rows demonstrating superior height values. Maize strips with two rows, which can be considered as border rows, exhibit heights similar to the border row values of the four-row strip configuration. Maize grown in a monoculture setting portrays the highest height values throughout the flowering phase and was the closest to the values of intercropping inner rows.

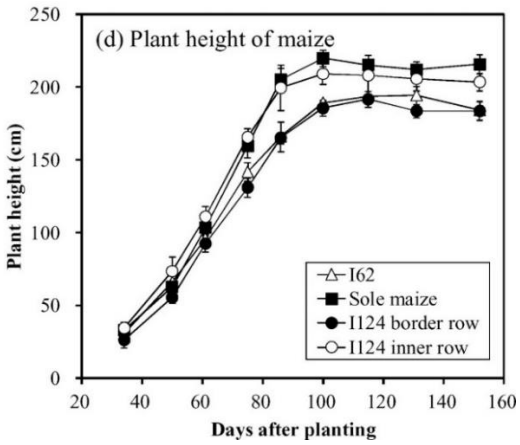

Figure 4: *Maize height in intercropping configurations (162= 2 rows, 1124= 4 rows) and monoculture (sole maize) during the growing period in 2013. Wang et al. (2017), adapted from Figure 4.*

The study notes that maize plants exhibit phenotypic plasticity, allowing them to grow in ways that enhance light capture, a key factor in their successful adaptation to intercropping systems.

2.4. Maize height estimation methods

As stated, above, height observation is extremely dependent on the crop morphology. To gain insight into the research made on maize height estimation through UAV methods, understand the possible methodologies, and thereby pinpoint specific knowledge gaps, a more precise query search was conducted on Web of Science. The goal was to select publications that specifically address the observation of maize height monitoring using RGB and/or LiDAR imagery. Through trial, the following query was regarded as the most appropriate: *TI=(height OR growth) AND (AB = ((maize OR corn)(RGB OR LiDAR))) NOT AB=(machine learning))*. A total of 29 results were identified and analyzed. The 29 obtained results, which all regard maize crop, were then categorized by the imagery and methods used, giving a good overview of the research on the topic (Table 1). The two different ground altitude methods are explained in the following section.

Table 1: *TI=(height) AND (AB = ((maize OR corn)(RGB OR Lidar))) NOT AB=(machine learning). Out of the 29 studies, 8 were estimated as out of scope. The total observed studies is n = 21.*

Imagery	Ground altitude method	Plant extraction scale	Studies	Statistical parameters
RGB n = 14	Classification within DSM n= 8	Individual n = 1	Qiu et al., 2022	Jointing stage (Vn) Measurmeent of the highest point of central leave n = 38 Jiongnongke 728: R^2 = 0.96, RMSE = 0.013 m Nongda 84: R^2 = 0.98, RMSE = 0.011 m
		Plot n = 7	Oehme et al., 2022	Matirity stage (R6) Measurement of the tassel n = 400 400 different genotypes: R^2 = 0.38, RMSE = 0.33 m
			Raj et al., 2023	No manual measurement – height data used to estimate health index
			Malambolo et al., 2018	Reproductive stage (R) Measurement of the tassel n = 144 99th percentile: R^2 = 0.77, RMSE = 0.11
			Lu et al., 2021	Grain filling stage (R3-R4) Measurement of the tassel n = 36 99.5th percentile: R^2 = 0.68 99.9th percentile: R^2 = 0.69 Maximum: R^2 = 0.64
			Anderson et al., 2020	No manual measurement - height used to test Weibull sigmoidal function accuracy for modeled plant growth
			Li et al., 2022	Combination of 4 different growth stages 90th percentile:

				R^2 = 0.80, RMSE = 0.15 m
			Tirado et al., 2020	Reproductive stage: R^2 = 0.72
	DTM from off-season DSM n = 6	Individual n = 0	-	-
		Plot n = 6	Han et al., 2018	487 plots Throughout four stages Measurements of the tassel R^2 = 0.896, RMSE=0.21m
			Gilliot et al., 2021	Reproductive stage Measurements of the tassel n = 38 R^2 = 0.90, RMSE= 0.16m
			Guo et al., 2022	Heading and tasseling stages n = 100 points 90th percentile R^2= 0.938, RMSE= 0.302 m
			Fathipoor et al., 2019	Vegetative stage (V12) No tassel measurement n = 66 R^2 = 0.85, RMSE = 0.067 m
			Li et al., 2016	Growth stage not provided R^2 = 0.74, RMSE = 0.21 m
			Xiao et al., 2023	Vegetative stage (V12) No tassel measurement n = 20 R^2 = 0.84, RMSE = 0.16 m
LiDAR n = 7	Classification within DSM n= 5	Individual n = 0	-	-
		Plot n = 5	Luo et al., 2021	Growth stage not specified n = 41 R^2 = 0.649, RMSE = 0.237 m
			Zhou et al., 2020	Lodging n = 50 R^2 = 0.964, RMSE = 0.127 m
			Luo et al., 2016	-n = 42 Growth stage not specified: R^2 = 0.833, RMSE= 0.230 m
			Luo et al., 2019	- n = 42 Growth stage not specified: R^2 = 0.812, RMSE = 0.238 m
			Li et al., 2015	Grain filling stage (R3-R4) n = 16 R^2 = 0.63, RMSE= 0.17 m
	DTM from off-season DSM n = 2	Individual n = 1	Gao et al., 2022	Tasseling stage Measurement of the tassel n = 289 100th percentile RMSE = 3.04 cm Whole growth stage R^2 = 0.96
		Plot n = 1	Crommelinck & Höfle., 2016	Reproductive stage n = 119 RMSE = 0.16 m

The current state of research on maize height monitoring using UAVs reveals several noteworthy trends and gaps. Overall, there is a noticeable deficiency in comprehensive studies on this subject. There are discernibly more studies discussing RGB technology results over LiDAR. At the individual plot scale, the shortage of research is even more pronounced. Only one of the studies has explored individual maize height using RGB, employing the classification method. This investigation focused on the jointing stage (Vn), meaning that it did

not involve tassel measurement. Similarly, with LiDAR, there is a singular study at the individual scale, this time utilizing the off-season Digital Terrain Model (DTM) method, specifically during the tasseling stage. The evident knowledge gap in individual-level maize studies is apparent. Regarding the ground altitude method, there are more studies employing the classification method for both LiDAR and RGB. However, the employment of off-season Digital Surface model (DSM) appears to yield superior results compared to the classification method for both RGB and LiDAR. The results from the existing literature will be further considered in the discussion section.

2.4.1. Ground altitude extraction

When measuring height, the selected Ground Altitude (GA) plays a crucial role in achieving precise results. Fujiwara et al. (2022) address this significance by introducing three distinct methods: (1) Ground and Canopy Classification Method, (2) DTM derived from an off-season DSM, and (3) DTM generated through surface information from outside the Region of Interest (ROI). The last was however not presented in any of the studies related to maize height crops and will thereby not be studied any further.

In the classification method, variables are allocated to distinguish between ground and canopy cover within a singular DSM. Oehme et al. (2022) applied this method to observe maize at various growth stages on a plot scale. While promising results were achieved during mid-stages, challenges arose when measuring height from the tassel. Similarly, Raj et al. (2023) employed the classification method proposed in Raj et al. (2021) which notices an increased root mean square error (RMSE) toward the end of the growth period, meaning a lower suitability of the method during the reproductive period. Qui et al. (2022) confirms these findings by observing the classification method is was the least suitable when observing the reproductive stage of the maize. Luo et al. (2021) observed that the classification method might not be most appropriate for densely planted crops because of the insufficient availability of ground point cloud information.

The off-season DSM method uses an early on DSM, with absent crops, as DTM. The DSM is then subtracted from the DTM to create the Canopy Height Model (CHM) (Figure 5). Han et al. (2018) created a CHM by subtracting the DSM from the Digital Elevation Model (DEM) at various growth stages. While overall results were positive, an underestimation in the tassel stage was observed. Wang et al. (2019) confirmed these findings using a similar methodology, noting satisfactory results. They conducted individual stage analyses, revealing an increasing correlation between UAV and ground truth from seedling to the reproductive stage, possibly due to increased plant density forming a continuous canopy. Gilliot et al. (2021) adopted a similar method, focusing solely on the reproductive period, and reported commendable results in aligning UAV imagery with manual methods. Guo et al. (2022) extended the exploration by comparing the DSM method with an indirect approach using multi-indicators, including RGB-based vegetation indices, demonstrating satisfactory results for both techniques. The findings in Luo et al. (2021) indicate that models for estimation of height, utilizing LiDAR variables, demonstrated greater accuracy in estimation compared to models relying on CHMs derived from LiDAR data.

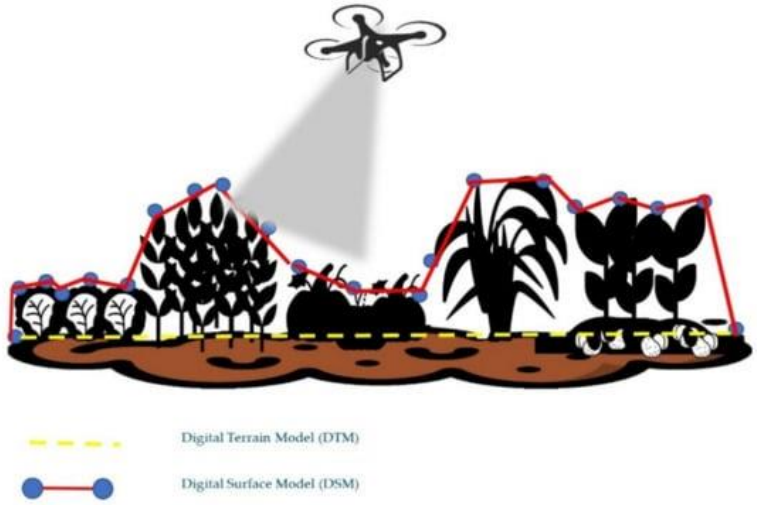

Figure 5: *Canopy height model (CHM) extracted from difference between DSM and DTM. Taken from: Jamil et al. (2022).*

2.4.2. Metrics for crop height extraction

In the realm of crop height estimation, metrics play a pivotal role in quantifying the vertical dimension of plant growth. Metrics, in this context, refer to numerical parameters or measures that are applied to datasets derived from RS technologies, such as RGB imagery, to determine the height of crops. Various studies have delved into identifying the most effective metrics for accurate crop height estimation. Several studies have investigated the optimal metrics for crop height estimation. Malambolo et al. (2018) explored percentiles such as 90^{th}, 95^{th}, 99^{th}, and the maximum for Maize and Sorghum. Notably, the study found that the 90^{th} percentile was most effective for sorghum estimation, while the 99th percentile was better suited for Maize. This observation aligns with the crop-specific nature of the most suitable metric, as confirmed by Malachy et al. (2022) and Jamil et al. (2021). Lu et al. (2021) delved into the use of maximum, 99.9^{th}, and 99.5^{th} percentiles. Their findings suggested that, during the grain-filling period, the 99.9th percentile of the point cloud provided the most accurate estimation of plant height. Guo et al. (2022) explored the average, 75^{th} percentile, and 90^{th} percentile over multiple years, ultimately obtaining better results with the 90^{th} percentile. Qui et al. (2022) chose to observe the 98^{th} percentile of the CHM. Whilst these studies all seem to favor higher percentile metrics, the study by Li et al. (2022) determined that the 90^{th} percentile outperformed the 95^{th} percentile in measuring maize cultivar heights across various stages of growth. Luo et al. (2016) argue that single LiDAR metric consistently serves as the optimal variable for estimating biophysical parameters of vegetation across various vegetation types, LiDAR data, environments, and study areas.

3. Methodology

This section presents an outline of the materials and methods employed in this research. To address the above-mentioned research questions, this thesis will be structured into two parts. In the first part, RGB and LiDAR imageries will be investigated in assessing maize height in intercropping systems. This evaluation will involve a comparative analysis between the UAV-derived imagery and ground truth data. Section 3.1 gives a description of the experimental site. Section 3.2 provides an account of the UAV image acquisition process while field measurements are described in Section 3.3. The procedures for estimating plant height from UAV imagery are outlined in Section 3.4. The second part on observing different height patterns according to data retrieved from parameters defined in the first part. 3.5 highlights the assessment of growth patterns within the intercropping field.

3.1. Experimental site

In the 2023 growing season, a substantial intercropping field experiment was conducted at Wageningen's experimental sites (at approximately 51.988352° N latitude and 5.656963° E longitude). The field was created by combining 32 different cultivars of maize (Table 2) with 32 different cultivars of faba bean.

Table 2: *List of 32 different maize cultivars used in the intercropping field experiment.*

Nr	Cultivar	Nr	Cultivar	Nr	Cultivar	Nr	Cultivar
1	Remus	9	LG31207	17	Damaun	25	Benco
2	LG31238	10	Ashley	18	NM09	26	Skandik
3	LG32257	11	Crosbey	19	NM01	27	Liberty
4	Golden Bamtam	12	MEZDI KS	20	Flynt	28	Prospect
5	LG31276	13	Black popcorn maize	21	Ambient	29	Vitamin
6	Calo	14	Stowell's evergreem	22	Joy	30	Micheleen
7	Jakleen	15	Mergoscia	23	SA0060COSMOS	31	Nomad
8	LG31206	16	Black tortilla maize	24	Silverbull	32	LG31218

Subsequently, due to some damage, a portion of the faba bean crops was replaced with four cultivars of pumpkin. The uniqueness of this field experiment lies in the diverse array of cultivars, presenting an exceptional opportunity for uncovering novel intercropping discoveries (Figure 6). The primary aim of the field was to assess the interaction effects among the various cultivars within each crop with their neighboring crop. Each cultivar plot was configured as a rectangular area comprising rows. Each rows possessed a width of 1.5 meters and a length of 5 meters. A set of ten ground control points (GCP) were established around the experimental site for georeferencing purposes.

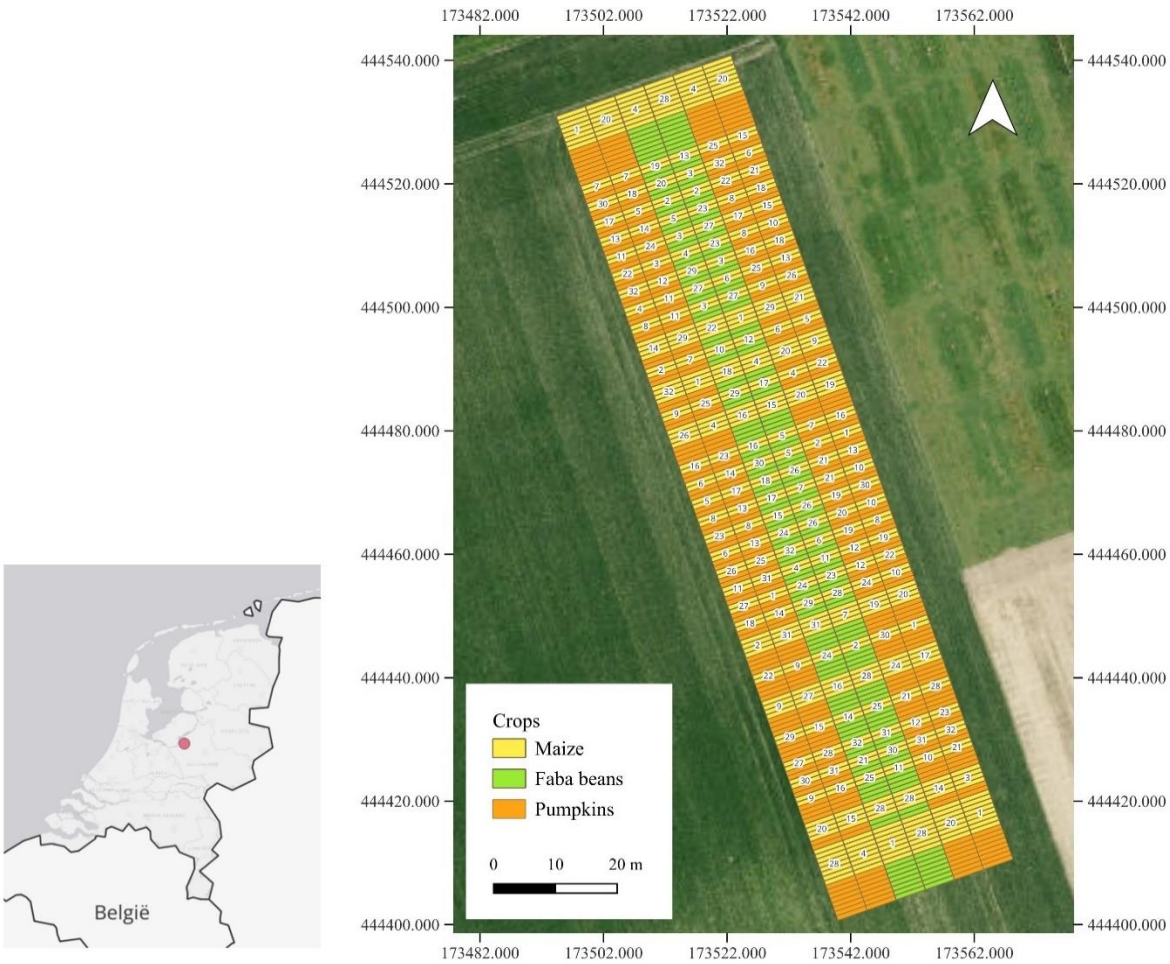

Figure 6: *Overview of strip-cropping experiment: spatial distribution of maize (yellow), faba beans (green), and pumpkins (orange) across plots, including randomized maize genotypes.*

3.2. UAV imagery acquisition

RGB and LiDAR imagery were acquired through UAV flight at various time intervals of the 2023 crop season, spaced 14 days apart, spanning from the initial germination phase (20th April) to the harvesting stage (11th September). It is important to note that the data was collected independently and provided to the author for use in this study. Further details relating to the survey data can be found in Figure 7.

Number of images:	1,371	Camera stations:	1,371
Flying altitude:	14.7 m	Tie points:	6,507,498
Ground resolution:	1.83 mm/pix	Projections:	22,816,821
Coverage area:	0.0154 km²	Reprojection error:	0.275 pix

Camera Model	Resolution	Focal Length	Pixel Size	Precalibrated
ZenmuseP1 (35mm)	8192 x 5460	35 mm	4.39 x 4.39 µm	No

a) Table 1. Cameras.

Number of images:	1,030	Camera stations:	1,030
Flying altitude:	13.9 m	Tie points:	3,790,904
Ground resolution:	1.81 mm/pix	Projections:	8,975,269
Coverage area:	0.0126 km²	Reprojection error:	0.694 pix

Camera Model	Resolution	Focal Length	Pixel Size	Precalibrated
ZenmuseP1 (35mm)	8192 x 5460	35 mm	4.39 x 4.39 µm	No

b) Table 1. Cameras.

Figure 7: *Survey data for RGB at (a) germination and (b) harvesting stage.*

3.3. Field data collection

Ground truth data was collected to evaluate the UAV data accuracy. The field data was measured during the harvest stage on the 11th of September 2023, on the same day as the last drone flight to ensure proper comparison. Maize height was measured from the base of the soil to the top of the tassel as presented in previous studies (Anthony et al., 2014; Gao et al., 2022) To do so, a measuring tool composed of a sliding measuring allowed reading of the value at an easier viewpoint instead of having to look at the top of the plant (Figure 8).

Figure 8: *Method and location for maize height measurement: from base to tassel top.*

The height measurements were made on multiple maize rows at different areas of the field to ensure a representative sample. Two crops were measured per row by estimating a distance of 1m50 from the edge of each row. The observed crops were checked visually and confirmed to be representative. This means that the crops didn't have a broken tassel or a noticeably different height compared to their neighbors. In addition, two individual plants per plot were measured on the outside of the rows. In total, 208 maize plants were measured in 42 different plots. The fieldwork was done by one person in a time frame of approximately 6 hours.

3.4. Crop height esimation from UAV imagery

In this section, we detail the methodology for generating CHMs through DSMs, outline the

plant extraction approach employed, and provide insight into the statistical analysis conducted. An overview of the analysis workflow that was used to conduct these steps is presented below using a flowchart (Figure 9).

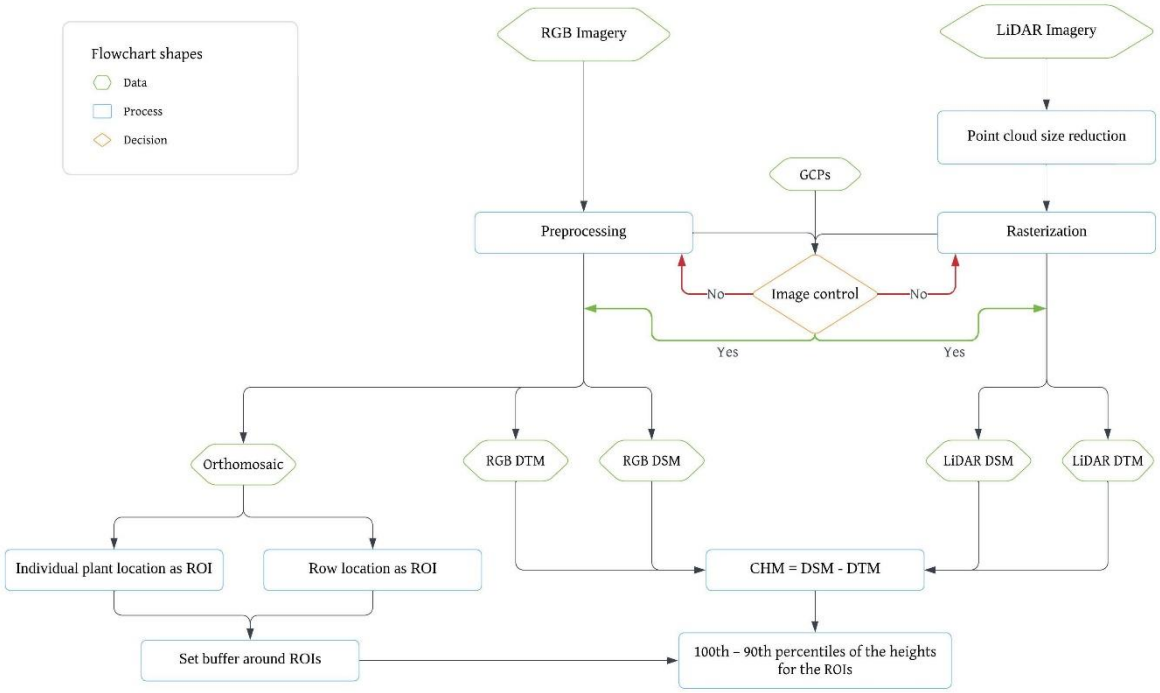

Figure 9: *Flowchart depicting the general overview of the methodology for calculating the canopy height model (CHM) and the height of the regions of interest (ROIs) at two different scale: individual plant and row.*

The analyses conducted in this study leverage a selection of advanced software tools, specifically QGIS, ArcGIS Pro, and R. Section 3.4.1 provides a detailed account of the steps involved in generating DSMs. Following this, Section 3.4.2 outlines the process for creating CHMs, and Section 3.4.3 explains how these models are utilized to extract plant heights for both individual crops and rows. Finally, Section 3.4.4 delves into the statistical analysis employed to derive quantitative results.

3.4.1. Digital Surface Models (DSM)

The RGB imagery DSMs were pre-generated using the SfM technique, aligning with the photogrammetric procedures detailed in the investigation by Jamil et al. (2022). This involved the creation of high-resolution rasters with a cell size of 0.0036x0.0036m. The SfM approach allowed for the reconstruction of 3D surface models from the RGB imagery, ensuring comprehensive coverage and precise spatial representation. Following the established methodology, these DSMs formed the foundation for subsequent analyses and height extraction procedures in our study. The DSM layers were clipped using the study area polygon as a mask through the *Clip Raster by Mask Layer* function. This step is deemed necessary due to the substantial file sizes, facilitating more efficient processing.

The LiDAR images (.las), with their significant size containing up to 600 million points per layer, were imported into QGIS for processing. To manage the layers more effectively, the *LAS clip* tool from the *LAS tools* package in QGIS was employed to crop the layers based on the study area polygon. The conversion process was conducted utilizing the *LAS Dataset to Raster* tool within ArcGIS Pro. The preference for this tool over the *LAS2DEM* tool in QGIS was driven by its capacity to analyze a larger volume of points with increased speed and efficiency. The application of the maximum interpolation method during this conversion facilitated the accurate capture of the uppermost points of the vegetation, providing a suitable representation of the vertical extent of the plant cover. The resolution was set to match that of the RGB data, at 0.0036x0.0036 meters.

Before commencing any analysis, a thorough examination of the DSMs is imperative to identify and rectify possible errors or discrepancies. This entails confirming the uniformity of coordinate systems in the images (EPSG:28992 - Amersfoort / RD New in our case), ensuring alignment with GCPs, and visually inspecting for any curvature or unexpected value patterns. Given the fine nature of maize tassels under investigation, precise observation is crucial for accurate analysis and interpretation. An error in the values of the various RGB DSM layers was identified and attributed to a variance in the coordinate system calibration of the drones, specifically concerning GCPs. To rectify this discrepancy, the DSM layers underwent recalibration, resulting in the alignment of values. Additionally, another anomaly was detected in the LiDAR data, characterized by distorted lines indicating a lack of image alignment in specific areas. This issue was successfully addressed through a new round of pre-processing, ultimately resolving the observed irregularities.

3.4.2. Canopy Height Model (CHM) generation

According to Luo et al. (2021), classification within a DSM is deemed suboptimal for densely vegetated crops, a characteristic reflective of our study context. Moreover, research employing the off-season DSM methodology appears to achieve heightened accuracy in results (Table 1). Additionally, our possession of high-resolution DSMs depicting the field absence of crops further solidifies our decision to generate a CHM from an off-season DTM, as opposed to utilizing a classification method reliant on a singular DSM. The methodology employed in this study aligns with the framework proposed by Jamil et al. (2022), which defines the CHM as the disparity between the DSM and the DTM. To implement this methodology, the DTM and DSM datasets are imported into QGIS. The *Raster Calculator* in QGIS is then employed to calculate the CHM by subtracting the DTM from the DSM.

In the final stage of the CHM generation, the distinction between vegetation and ground elevation was introduced. Due to the ground being obscured by grass and weeds, utilizing vegetation indices for the distinction of vegetation and non-vegetation was not feasible. Instead, a threshold value was selected to delineate the boundary between ground and crops based on height. After trial the threshold value of 25cm was chosen as most suitable. This methodological step holds significance for various reasons. Firstly, considering the magnitude of the dataset, characterized by extensive spatial coverage and high-resolution measurements, computational operations are highly resource-intensive. Focusing the analysis solely on the vegetation component, with ground elevation falling outside the scope of our research, has resulted in a substantial acceleration of processing times. Moreover, the presence of varying ground elevations across the study area could distort percentile observation when exploring

different percentiles and buffers to optimize crop height observations. By excluding ground data from our analysis, we ensure a focused and accurate exploration of individual maize crop heights, free from the confounding influences of ground-related variations. This strategic refinement ensures that the ensuing analysis is tailored to the nuanced objectives of our RS investigation.

3.4.3. Plant height extraction

Han et al. (2018) recommend individual measurements as the optimal approach to mitigate the influence of potential leaves from neighbouring plants. In cases where precise plant locations are unavailable, a ROI is employed (Malachy et al., 2022). In the context of this study, the field data encompasses both exact measurements of individual plant locations and semi-randomized row measurements. Consequently, two distinct methods of height extraction are implemented.

Individual crop height extraction

In assessing individual crops, the initial step involves the manual placement of points on the RGB Ortho mosaic image corresponding to the harvesting period for each measured plant (shown in Figure 8). While the potential for automation exists (Zan et al., 2020), such a process falls beyond the scope of our study. Luo et al. (2016) emphasize that there is no universal set of LiDAR metrics that always works optimally for estimating vegetation parameters across different study areas. Therefore, different metrics are tested in this study. Given the spatial arrangement of individual plants and their distance from neighbouring ones, higher values within these buffers are anticipated to effectively represent individual plant height. According to the literature, seven distinct metrics (90^{th}, 95^{th}, 98^{th}, 99^{th}, 99.5^{th} 99.9^{th}, and 100^{th}) are chosen and investigated for their suitability in this context. Following this, buffer zones (Figure 10) are established around these points utilizing the Buffer tool. Subsequently, the *Zonal Statistics as Table* tool in ArcGIS Pro is employed to extract statistical values from the CHM within these buffers. This tool is recommended over the *v.rast.stats* tool in QGIS, as the one in QGIS only allows the observation of rounded up percentile. The acquired datasets and field measurement values are then imported into R for subsequent in-depth analysis.

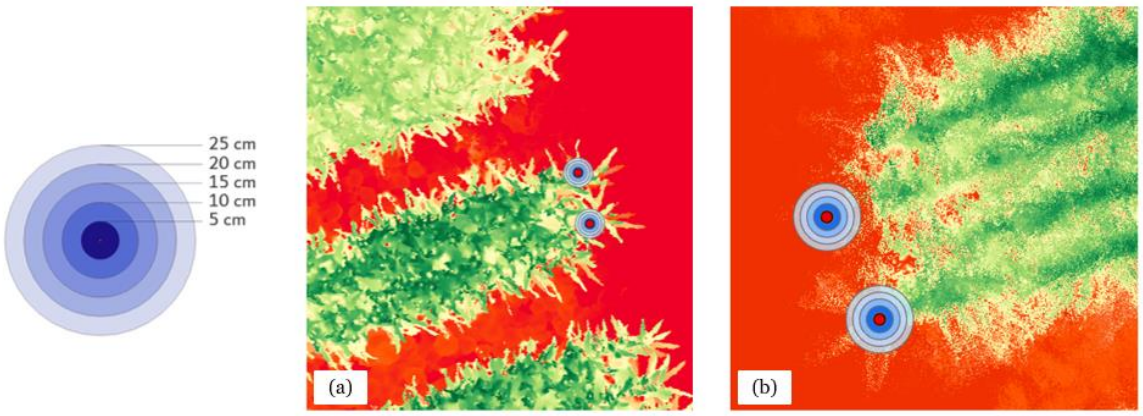

Figure 10: *Buffers around individual crop measurement points visualized with (a) RGB imagery and (b) LiDAR data.*

Row height extraction

When evaluating height at the row scale, the initial step involves the generation of an individual row shapefile. To do so, an R script originally created by Dirk van Apeldoorn was modified to generate a shapefile containing polygons (0.3m x 2.5m) representing each maize row. Drawing insights from Malachy et al. (2022), who emphasized the potential impact of leaves at the row edges on height extraction, we implemented a 10cm gap between neighbouring rows to spare our data from any neighbouring effects. An additional 4cm gap was added between the two inner rows, accounting for spacing introduced during crop planting. The adjusted shapefile is imported into QGIS, and a distinct layer is established to isolate rows subjected to manual measurements. Two additional buffer sizes are then considered: one with an additional 4 cm buffer, and the other one with a 4cm negative buffer representing a loss of gaps between the rows (Figure 11).

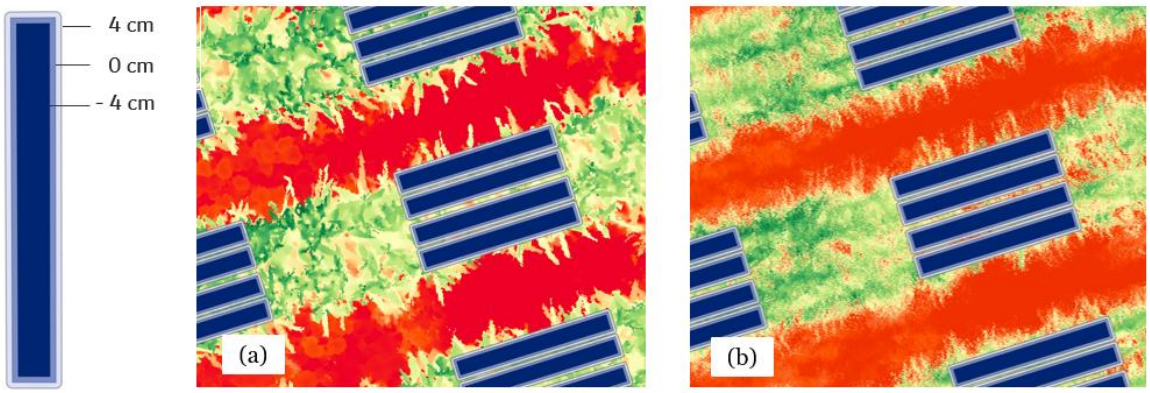

Figure 11: *Buffers around row ROI visualized with (a) RGB imagery and (b) LiDAR data.*

3.4.4. Statistical Analysis – UAV and ground measurements

Upon obtaining height values from both RGB and LiDAR imagery at both individual crop and row scale, the acquired data for ground truth measurements and RS are imported into R for subsequent analysis. A comparative examination between ground truth measurements and UAV-derived imagery is conducted to assess the accuracy of the estimation of plant height using UAV imagery. Two different metrics are used, the coefficient of determination (R^2) and the RMSE as indicated by previous research (Jamil et al., 2022), with the following equations:

$$R^2 = \frac{\sum_{i=1}^{n} (y_i - \hat{y}_i)^2}{\sum_{i=1}^{n} (y_i - \bar{y}_i)^2} \quad (1)$$

$$\mathrm{RMSE} = \sqrt{\sum_{i=1}^{n} \frac{(\hat{y}_i - y_i)^2}{n}} \quad (2)$$

In these equations, *n* signifies the count of individual plant samples. The variable yi represents the ground-truth-measured height of plant *i*, while $\hat{yi}$ signifies the estimated height of the same plant derived from UAV data and $\bar{y}i$ represents the average(mean).

The selection of suitable parameters for height observation involves balancing the achieved R^2 and RMSE values. This judgment should align with the specific characteristics of the observed case. The R^2 value captures the goodness of fit, representing the overall relationship between variables. This metric is pertinent for discerning patterns among height values of different rows and genotypes. Observing RMSE is crucial for obtaining values that accurately reflect reality. This parameter becomes particularly relevant in this study when observing the temporal changes in height differences among rows. In this case, it is crucial not to singularly focus on one of these variables, but rather to consider both in tandem. Scatter plots illustrating the regression model between UAV-estimated values and ground truth values are generated for both individual crop and row scales.

The constraints of limited ground truth data collection prohibit a direct validation of the most suitable model. To address this challenge, a CHM was generated for the 14th of August, a time period that is part of the tasselling stage when the height undergoes minimal change (as elaborated in section 2.3.1). The height values were then extracted with the judged optimal parameters – including imagery type, buffer and percentile -. Subsequently, a regression model was developed to compare the heights obtained on the 11th of September with those on the 14th of August. This comparative analysis serves as a form of validation, allowing us to assess whether similar data are obtained between these two periods.

3.5. Height patterns data analysis

Upon evaluating the accuracy of utilizing UAV imagery for maize height observation within an intercropping system, the dataset obtained through the estimated optimized parameters - encompassing imagery type, buffer, and percentile - can be applied to observe pattern within the experimental field. The datasets includes information on maize height, rows, genotype of maize and genotype of neighbouring crop. This analysis focuses on the discovery of patterns within the data. This exploratory approach allows us to highlight the complexities and nuances in the data, laying the groundwork for future research that can delve into these patterns with a more detailed statistical analysis through additional data on environmental and genotypic factors.

3.5.1. Height patterns between rows

To examine potential height variations between rows, we generated two separate maps. One map displayed the average height of each individual maize row, while the other visualized the average height differences between rows. To create the second map, additional data was generated using the *Raster Calculator* tool. This involved subtracting the values of each pair of neighbouring rows within a plot and then averaging these differences. By adopting this approach, we are looking at the difference in variations within plots of different size (4 rows, 8 rows, and monocultures), and thereby ascertain whether rows located closer to other crops exhibit more significant height changes (in which case plots with 4 rows would have a higher value). Accompanying diagrams facilitate a clearer interpretation of genotype-specific values, overcoming the challenges posed by the spatial dispersion of values on the map.

3.5.2. Growth dynamics between cultivars

In the subsequent section, our analysis extends to encompass two additional timeframes, necessitating the creation of CHMs for new time periods using the same methodology elucidated earlier. The two newly observed time periods are June 7th and July 18th, selected based on the LiDAR image quality and the maize growth cycle (as detailed in section 2.3.1). Once the CHMs are created, height values are collected for each row of the two new dates, and a map for each date, displaying the height per row, is generated. Additional, two extra maps are created to reflect the height different between the different periods, thereby evaluating the height difference over time of the different genotypes. Diagrams are once again created to visualise the data by genotype.

4. Results

4.1. Development of CHM

Figure 12 portrays the derived CHMs obtained from both RGB and LiDAR imagery. The CHMs exclusively display vegetation features, achieved through a suppression of values below 25cm. The CHM derived from RGB imagery indicates height values up to 288cm, whereas the CHM derived from LiDAR imagery exhibits height values extending up to 314cm.

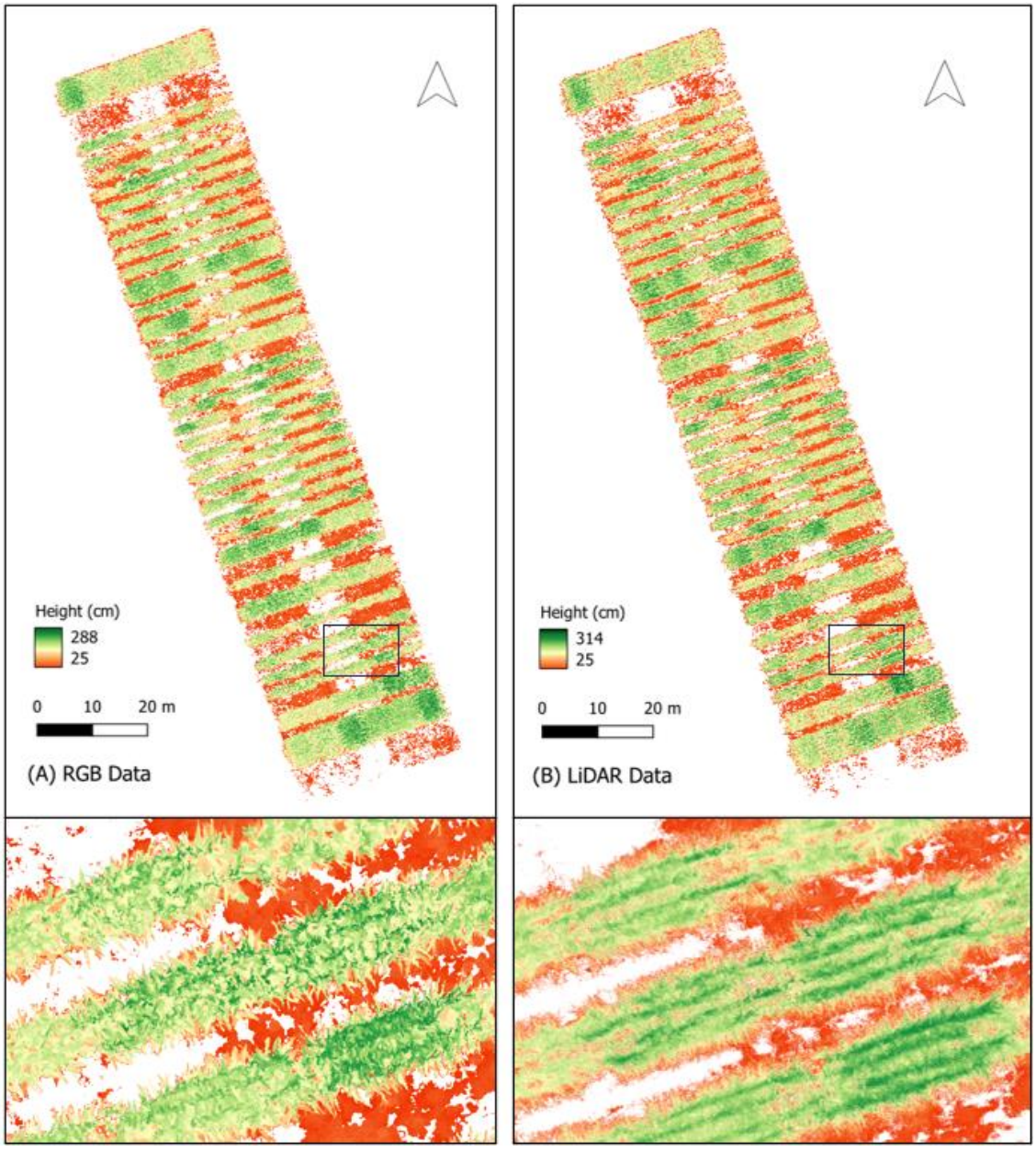

Figure 12: *Canopy Height Models (CHMs) derived from (a) RGB and (b) LiDAR imagery. The CHMs were generated using DTMs from imagery captured on 20th April (germination period) and the DSMs from imagery captured on the 11th September (harvesting period). Values below 25 cm, indicative of ground surfaces, were removed from the analysis.*

The CHMs depicted in Figure 12 were standardized with the same colour scale to facilitate direct visual comparison of height values. Upon initial inspection, both models yield comparable data, however with distinct visual characteristics. The CHM derived from RGB imagery offers a vibrant and detailed depiction of the study area, emphasizing the diversity of vegetation. In contrast, the CHM derived from LiDAR imagery presents vegetation with less clarity. However, it offers a more nuanced depiction of vertical structures, featuring both lower values and higher values visible within the rows. This distinction can be observed in the zoomed view provided at the lower part of the figure 12 and is further highlighted by the higher values in the LiDAR imagery legend.

4.2. Optimal settings for maize height estimation through UAV

To derive plant height from the CHMs, the optimal parameters for the buffer area surrounding the measurement point and the distribution threshold (cut-off percentile) for the selected pixels within the buffer have to be established. These parameters play a crucial role in ensuring the accuracy of the height estimation process.

4.2.1. Individual crop height extraction

Figure 13 and Figure 14 provide a detailed analysis of the accuracy metrics involved in estimating individual crop height observations using UAV imagery in comparison with ground-truth measurements. The evaluation encompasses two key metrics: the R^2 on the left and the RMSE on the right. This analysis was conducted across a range of distribution thresholds, spanning from the 100th to the 90th percentile, and buffer sizes varying from 5cm to 25cm around the crop. These figures present a comprehensive visual representation of the performance of the height estimation process under different distribution thresholds and buffer sizes. By systematically assessing the impact of these parameters on the accuracy of height estimation, the figures facilitate informed decision-making in selecting optimal settings for subsequent analyses.

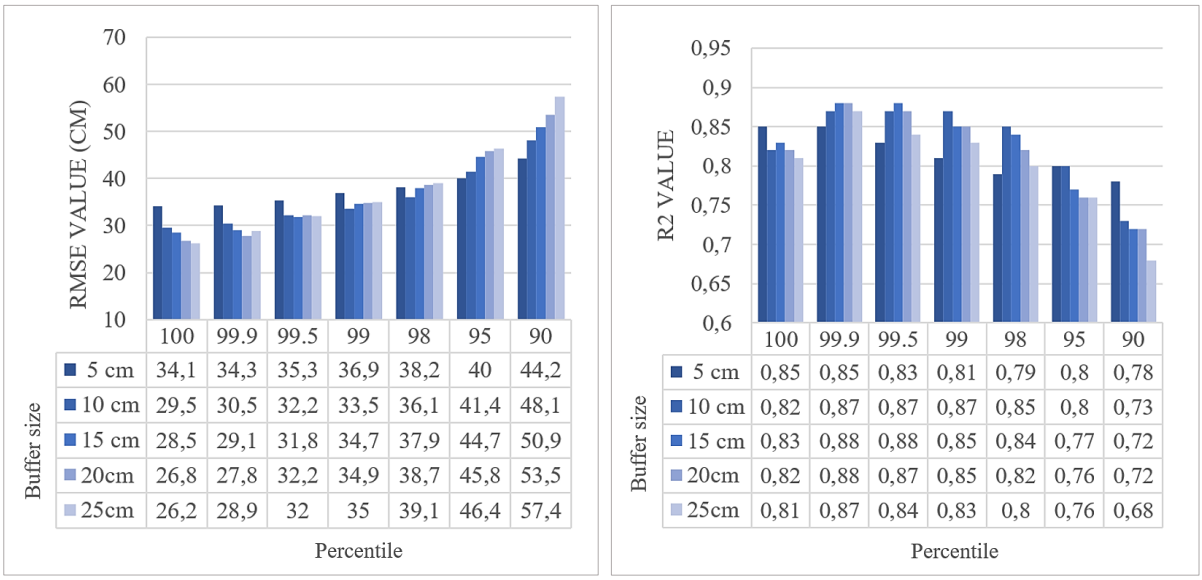

Buffer size	100	99.9	99.5	99	98	95	90
5 cm	34,1	34,3	35,3	36,9	38,2	40	44,2
10 cm	29,5	30,5	32,2	33,5	36,1	41,4	48,1
15 cm	28,5	29,1	31,8	34,7	37,9	44,7	50,9
20cm	26,8	27,8	32,2	34,9	38,7	45,8	53,5
25cm	26,2	28,9	32	35	39,1	46,4	57,4

Buffer size	100	99.9	99.5	99	98	95	90
5 cm	0,85	0,85	0,83	0,81	0,79	0,8	0,78
10 cm	0,82	0,87	0,87	0,87	0,85	0,8	0,73
15 cm	0,83	0,88	0,88	0,85	0,84	0,77	0,72
20cm	0,82	0,88	0,87	0,85	0,82	0,76	0,72
25cm	0,81	0,87	0,84	0,83	0,8	0,76	0,68

Figure 13: *RMSE (on the left) and R^2 (on the right) values at different buffer sizes and percentiles from individual crop measurements using RGB imagery.*

In the analysis of RGB imagery for individual crop height observation (Figure 14), an upward trend in percentile correlates with a general decrease in the RMSE value. Notably, an escalation in percentile from the 90th to the 99.9th percentile corresponds to an increase in the R^2 value. However, an anomaly surfaces as the R^2 value experiences a decline at the 100th percentile. At lower percentiles, a reduction in buffer size is associated with a decrease in RMSE values. This trend undergoes a reversal post the 99.5th percentile, wherein a smaller buffer size now contributes to an augmented RMSE value. No discernible pattern emerges between buffer size and R^2 values at different percentiles. The lowest RMSE value (26.2cm) is obtained with a 25cm buffer at the 100th percentile and the highest value (57.4cm) with a 25cm buffer at the 90th percentile. A maximal R^2 value (0.88) is obtained with a 20cm buffer at the 99,9th percentile and the lowest value (0.68) with a 25cm buffer at the 90th percentile.

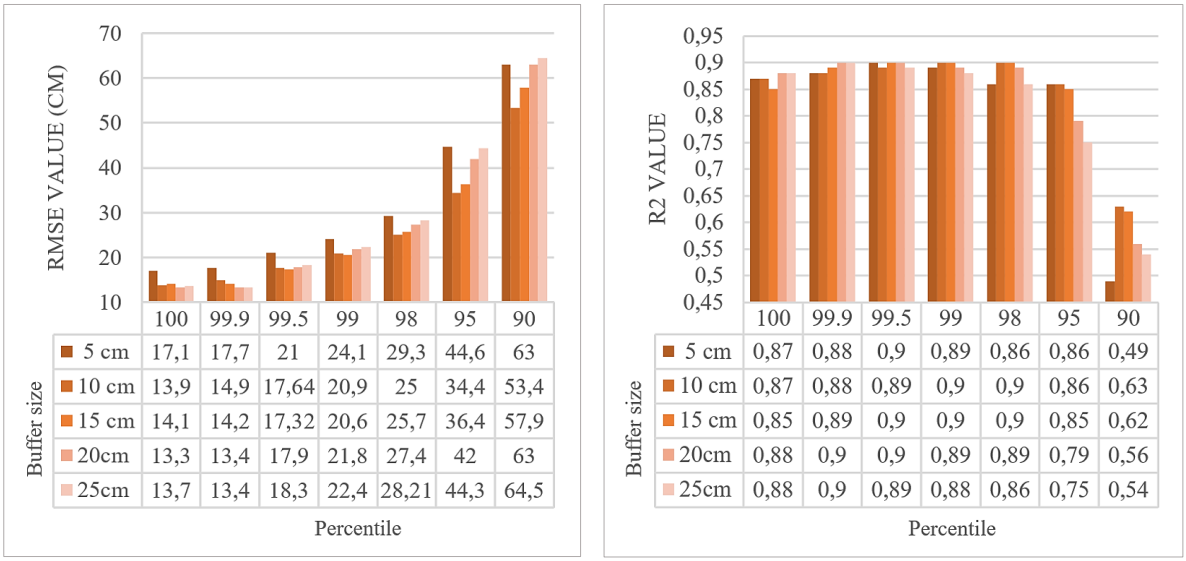

Figure 14: *R^2 and RMSE values at different buffer sizes and percentiles from individual crop measurements using LiDAR data.*

In the examination of LiDAR imagery (Figure 15), an increase in percentiles also corresponds to an exponential decrease in RMSE values. Notably, smaller buffer sizes typically yield lower RMSE values, although an exception arises with the lowest buffer size (5cm), which exhibits a notably higher RMSE. Throughout the analysis, the R^2 value consistently hovers around 0.9 across various buffer sizes, with the exception of the 90th percentile, where the R^2 value dips. No apparent pattern emerges between buffer size and R^2 values at different percentiles. The lowest RMSE (13,3cm) is achieved with a 20cm buffer at the 100th percentile, while the highest (64,5cm) is observed with a 25cm buffer at the 90th percentile. Similarly, a maximum R^2 value (0.9) is obtained with a 20cm buffer at the 99.9th percentile, contrasting with the lowest R^2 value (54) observed with a 5cm buffer at the 90th percentile.

The selection of optimal parameters for individual crop height measurements through UAV imagery involved a balance between RMSE and R^2 values. The optimal settings for both imagery types were determined to be an observation of the 99,9th percentile with a buffer of 20cm around the crop. Despite the accompanying decrease in R^2 value, the lower RMSE indicates that the model yields more precise estimations, particularly at the extremes of the height distribution. Figure 15 is showcasing scatter plots (n=40) depicting the alignment between field measurements and values derived from RGB and LiDAR imagery, underscoring

the trade-offs between precision and goodness of fit in height estimation.

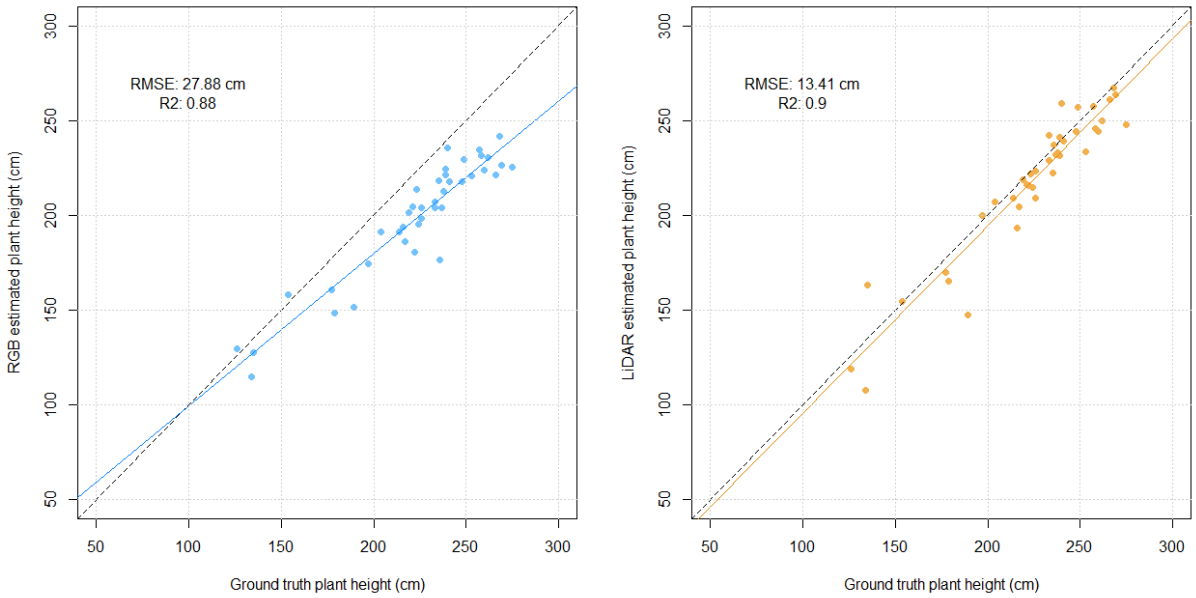

Figure 15: *Scatter plots indicating the (a) RGB imagery and (b) LiDAR data values in comparison to ground truth measurements, at the individual crop scale. (99.9th percentile and a 20cm buffer).*

The scatter plot associated with RGB imagery exhibits a R^2 of 0.88 and a RMSE of 27.88cm. In comparison, the scatter plot corresponding to LiDAR imagery demonstrates a higher R^2 value of 0.90, accompanied by a substantially lower RMSE of 13.41cm. These statistics reflect the stronger correlation and higher precision from LiDAR imagery compared to those derived from RGB imagery.

4.2.2. Row height extraction

Figure 16 and Figure 17 depict a detailed analysis of R^2 and RMSE values, this time for estimating row height observations. This analysis was conducted across a spectrum of distribution thresholds, ranging from the 100th to the 90th percentile, and buffer sizes varying from 4cm to -4cm around the row polygon around the crop.

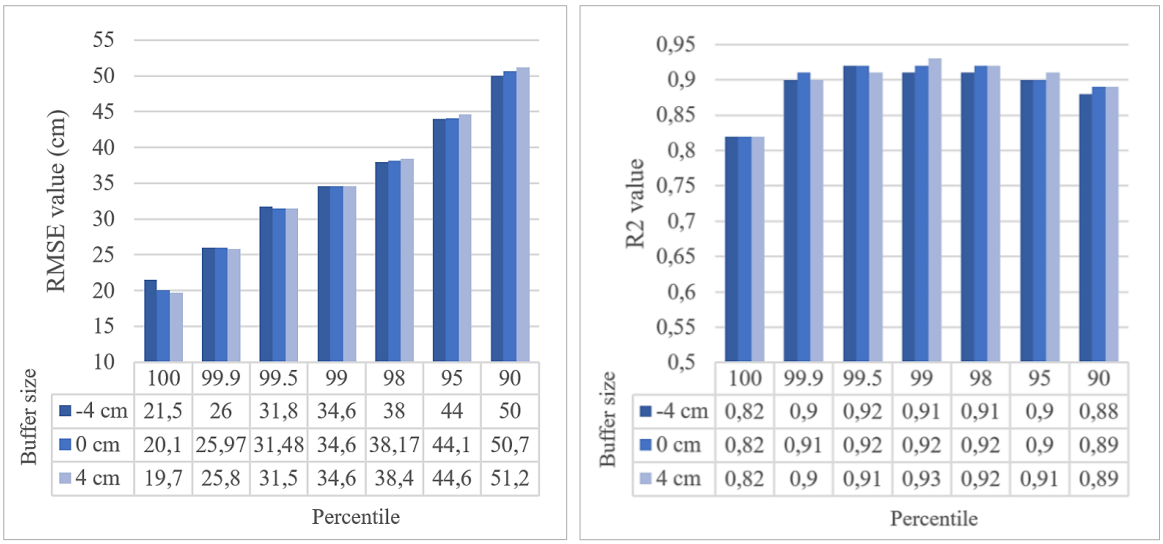

***Figure 16**: RMSE (on the left) and R^2 (on the right) values at different buffer sizes and percentiles from row measurements using RGB imagery.*

In the analysis of RGB imagery for row height measurement (Figure 16), a notable pattern emerges where increasing percentiles are associated with a consistent decrease in the RMSE value, indicative of improved precision in height estimation. From the 90th to the 98th percentile, a slight rise in the R^2 value is observed, followed by a stabilization until the 99.9th percentile. However, a significant drop in the R^2 value is evident at the 100th percentile. Furthermore, at lower percentiles, a reduction in buffer size correlates with a decrease in RMSE values. At lower percentiles, a reduction in buffer size is associated with a decrease in RMSE values. This trend undergoes a reversal post the 99th percentile, wherein a smaller buffer size now contributes to an augmented RMSE value. No discernible pattern is observed between buffer size and R^2 values across different percentiles. The lowest RMSE value (19,7cm) is obtained with a 4cm buffer at the 100th percentile and the highest (51,2cm) with a 4cm buffer at the 90th percentile. A maximal R^2 value (0.93) is obtained with a 4cm buffer at the 99th percentile and the lowest (0,82) at the 100th percentile.

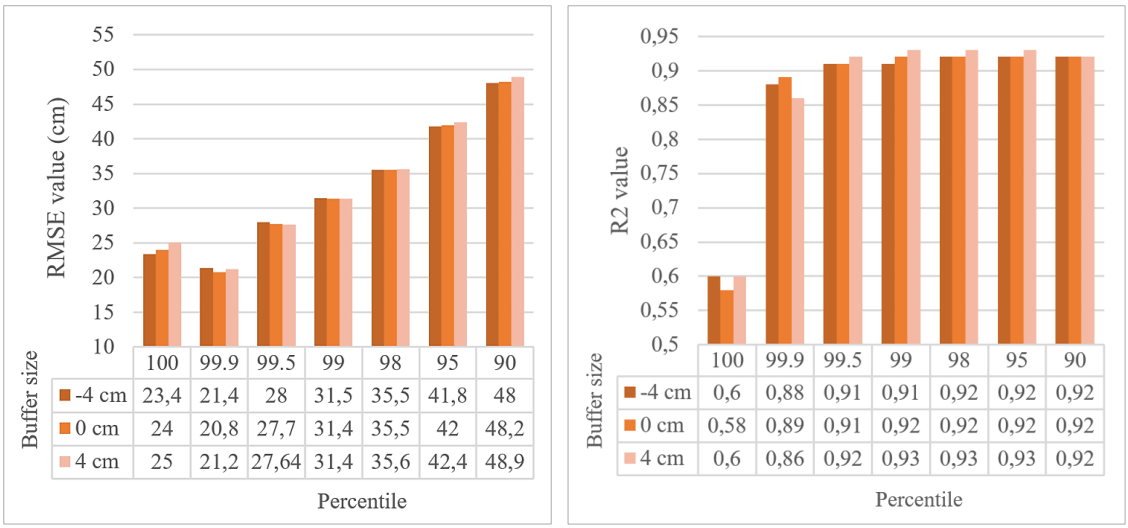

***Figure 17:** R^2 and RMSE values at different buffer sizes and percentiles from row measurements using LiDAR data.*

In the evaluation of LiDAR imagery for row height measurements (Figure 14), there is an observed trend where increasing percentiles lead to a substantial decrease in RMSE values, with the exception of the 100th percentile, where the RMSE value increases once again. Interestingly, there is minimal variation in RMSE values across different buffer sizes. Throughout the analysis, the R^2 value remains consistently high, hovering around 0.9 across various buffer sizes, except for a dip observed at the 100^{th} percentile. Notably, no discernible pattern emerges between buffer size and R^2 values at different percentiles. The lowest RMSE (20,8cm) is achieved with a 0cm buffer at the 99.9^{th} percentile, while the highest (48,9cm) is observed with a 4cm buffer at the 90^{th} percentile. A maximum R^2 value (0.9) is attained with a 4cm buffer at the 99^{th} percentile, contrasting with the lowest R^2 value (0,58) observed with a 0cm buffer at the 100^{th} percentile.

Just as for the individual crop height observation, the process of selecting optimal parameters for measuring row height using UAV imagery required careful consideration of both metrics. The most effective settings for both types of imagery were identified as observing the 99.9^{th} percentile with a 0cm buffer around the row polygon. In the case of RGB imagery, although the 100th percentile yielded a slightly smaller RMSE, it resulted in a significant reduction in model suitability (R^2). Similarly, for LiDAR imagery, while the 99.5^{th} percentile exhibited a higher R^2 value, it was accompanied by a notably larger RMSE value. The corresponding scatter plots (n=84) are featured in Figure 18.

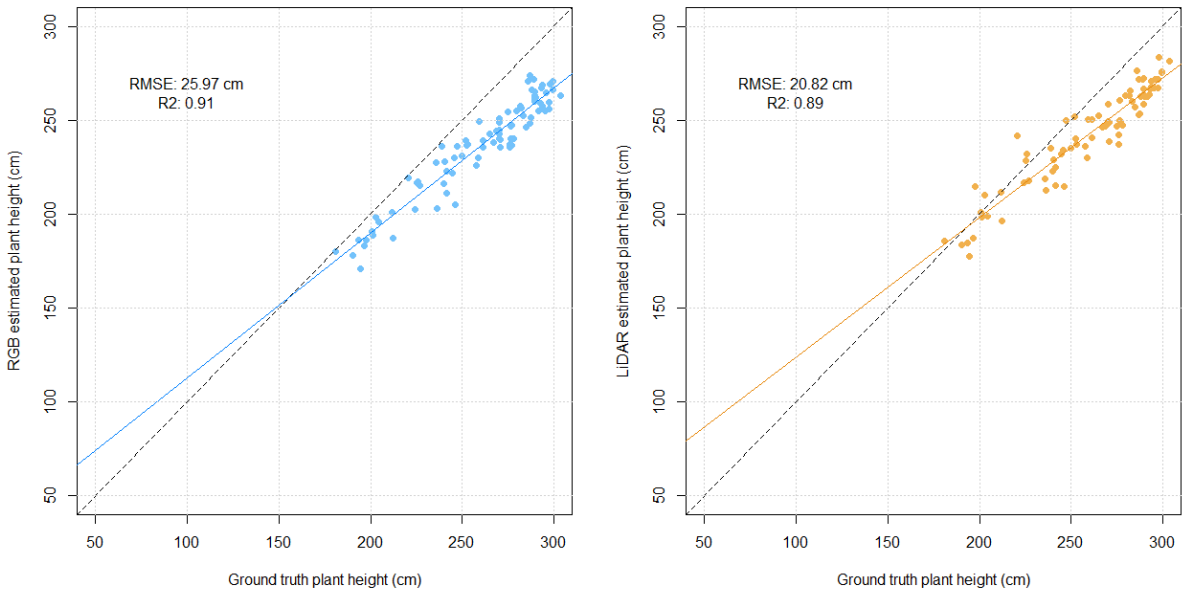

Figure 18: *Scatter plots indicating (a) RGB and (b) LiDAR data values in comparison to ground truth measurements, at the row scale (99.9th percentile and a 0cm buffer)*

The scatter plots depicted in Figure 19 present the relationship between field measurements and values derived from RGB and LiDAR imagery for row observations. The scatter plot associated with RGB imagery exhibits a R^2 of 0.91 and a RMSE of 25,97cm. In comparison, the scatter plot corresponding to LiDAR imagery demonstrates a lower R^2 value of 0.89, however accompanied by a lower RMSE of 13.41cm. In this case, both RGB and LiDAR have high R^2 values, suggesting a strong correlation between the imagery and the tassel height. The slight difference may not be substantial enough to be the sole factor in choosing one over the other. LiDAR, with its lower RMSE, appears to provide more accurate estimations of maize

tassel height compared to RGB. It is thereby concluded that the LiDAR imagery with the proposed polygons and the 99.9th percentile presents the optimal parameters for the further investigation of patterns within the experimental site.

The constraints of limited ground truth data collection prohibit a direct validation of the most suitable model. To address this challenge, a CHM was generated for the 14th of August, a time period that is part of the tasselling stage when the height undergoes minimal change (as elaborated in section 2.3.1). Figure 19 shows the regression model between the heights per row measured on the 14th of August and the 11th of September. Each colour corresponds to a genotype allowing for comparison in growth.

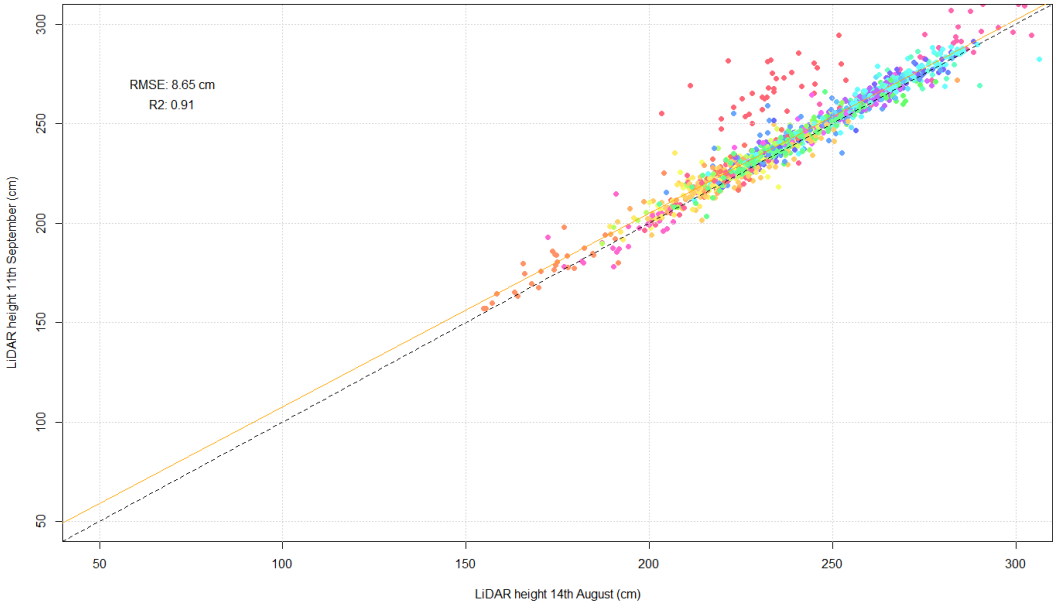

Figure 19: *Scatter plot displaying LiDAR data values on the September 11th and August 14th at row scale (99.9th percentile and 0cm buffer). Each genotype is represented by a unique colour.*

With an R^2 of 0.90, the scatter plot exhibits a robust correlation between the height estimates obtained from LiDAR at these two time points. Additionally, a closer examination of the data reveals that the outliers, contributing to an RMSE of 8.64 cm, are predominantly linked to genotype. This observation suggests that the discrepancies in height measurements are not random but rather can be attributed to the ongoing growth variations within this particular genotype, further attesting to the precision and reliability of LiDAR measurements in capturing dynamic growth patterns in maize.

4.3. Growth patterns within experimental site

Additionally to testing out the reliability of UAV-derived height measurements in an intercropping context, this thesis wishes to apply the proposed methodology (see 4.2.) to collect insight on the height distribution patterns of the experimental site.

4.3.1. Height patterns observations

Figure 20 presents the distribution of maize crop heights across different rows within the experimental field on September 11th, where measured heights spanned from 157 cm to 329 cm. This visualization reveals significant height variations not only among distinct plots but also within the rows of a single plot. These initial results display the presence of different height dynamics within the field and can be used for the identification of underlying patterns that contribute to the variations in crop height observed within the study area, thereby enhancing our understanding of the spatial dynamics affecting maize growth.

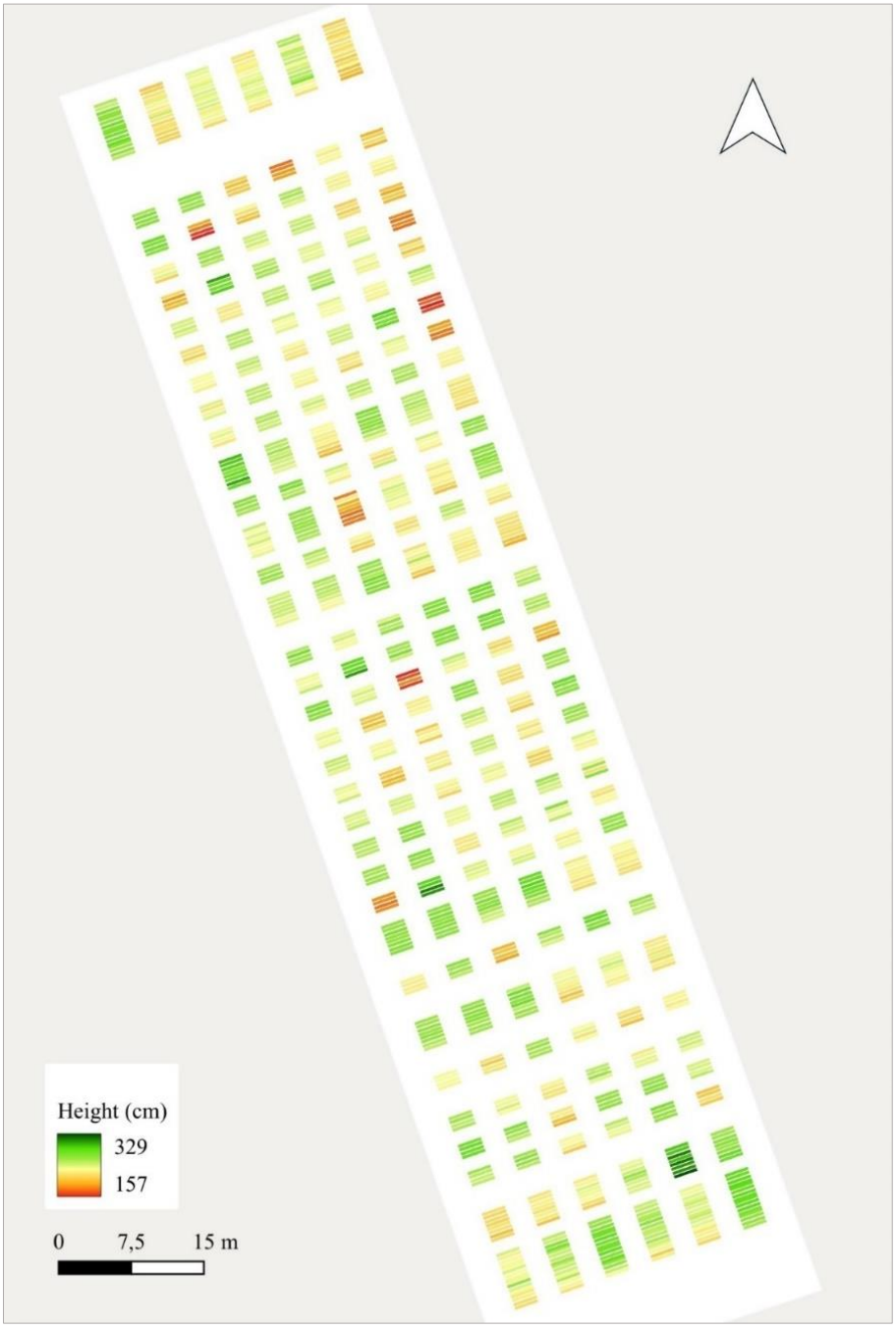

Figure 20: *Spatial distribution of the average tassel height for each row on September 11th, utilizing the 99.9th percentile value of the LiDAR imagery.*

Figure 21 provides an overview of row height distributions across the 32 different genotypes, initially introduced in Figure 5.

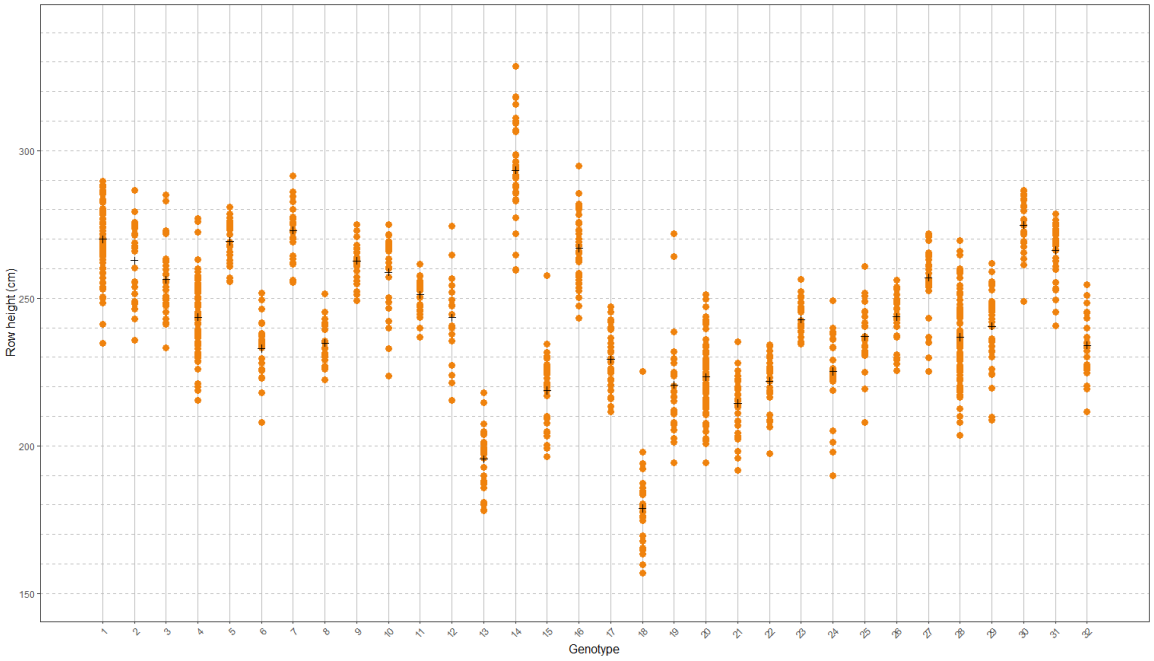

Figure 21: *Phenotypic diversity in maize cultivars based on height distributions from September 11th.*

The analysis of maize genotypes' height distributions reveals a spectrum of phenotypic diversity. The genotypes display distinct phenotypes, with some characterized by generally shorter plants and others by consistently taller plants. For instance, genotype 18 exhibits a relatively short height, with an average height of 178 cm, while genotype 14 stands out for its consistently tall plants, with an average of 294 cm. Furthermore, the distribution of height values within each genotype varies significantly. Some genotypes demonstrate a relatively uniform distribution of plant heights, suggesting homogeneity, such as genotype 23 with a standard deviation of 24 cm. Conversely, other genotypes display extensive variations in height, indicating pronounced heterogeneity, as seen in genotype 28 with a standard deviation of 68 cm. This variation not only highlights the phenotypic diversity among different genotypes but also within the populations of each genotype.

Figure 22 puts light on the height distribution according to rows in the two different intercropping configurations of the field: four rows and eight rows. The complexity of phenotypic expression, as depicted through the distribution of row height values in the top plots, underscores an inherent variability within genotypes. Thereby, we observe that genotypes do not only display difference in height between plots but also between rows. The corresponding lower plots depict the average plant height distribution per row for the two intercropping configurations. Intriguingly, both configurations exhibit a noticeable downward slope towards the southern side, featuring a decline of around 10 cm, with the lowest values observed in the southernmost row. Additionally, the configuration with 8 rows exhibits another similar slope among the three most northern rows with a decline of about 5 cm. The presence of observable row patterns, particularly evident in the southernmost rows, suggests interaction with environmental factors. To further understand these interactions, the height distributions for each genotype were analysed separately through comparable graphs (Appendix A).

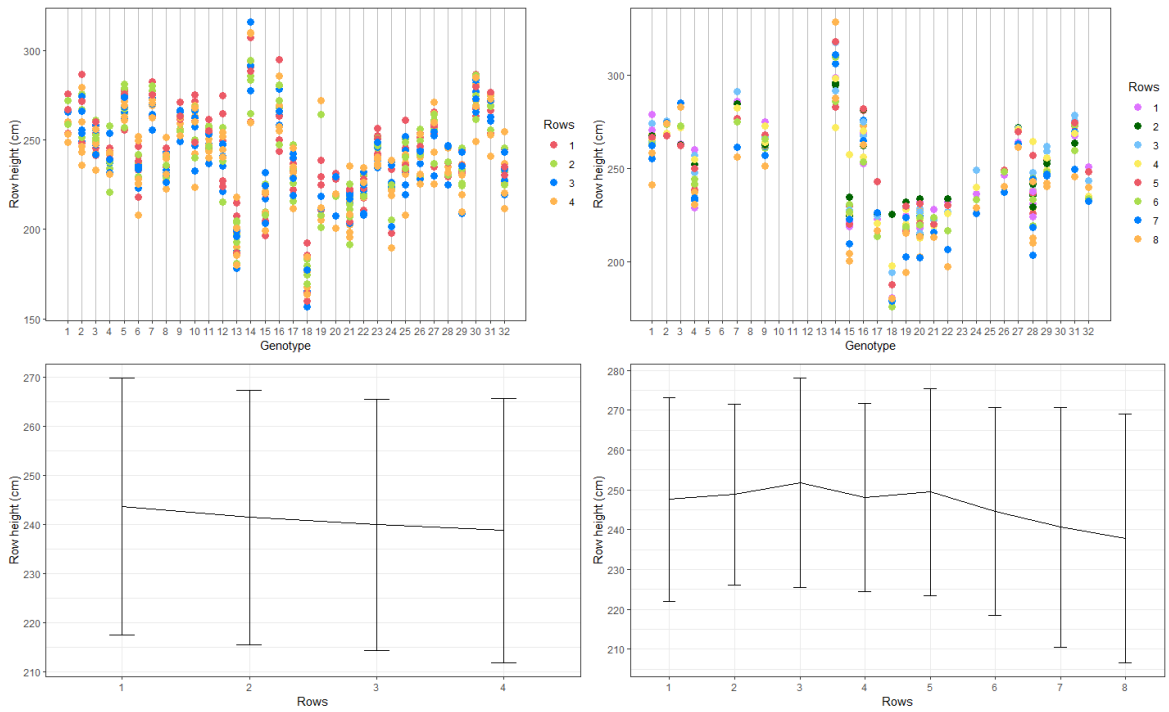

Figure 22: *Height distribution across rows by genotypes (top) in two intercropping configurations (left = 4 rows, right = 8 rows) on September 11th.*

Figure 23 presents an overview of the observed height patterns in rows for the different genotypes for the two intercropping configurations: 4 rows and 8 rows. It not only quantifies these patterns but also includes illustrative examples for each, offering a comprehensive overview of the dataset.

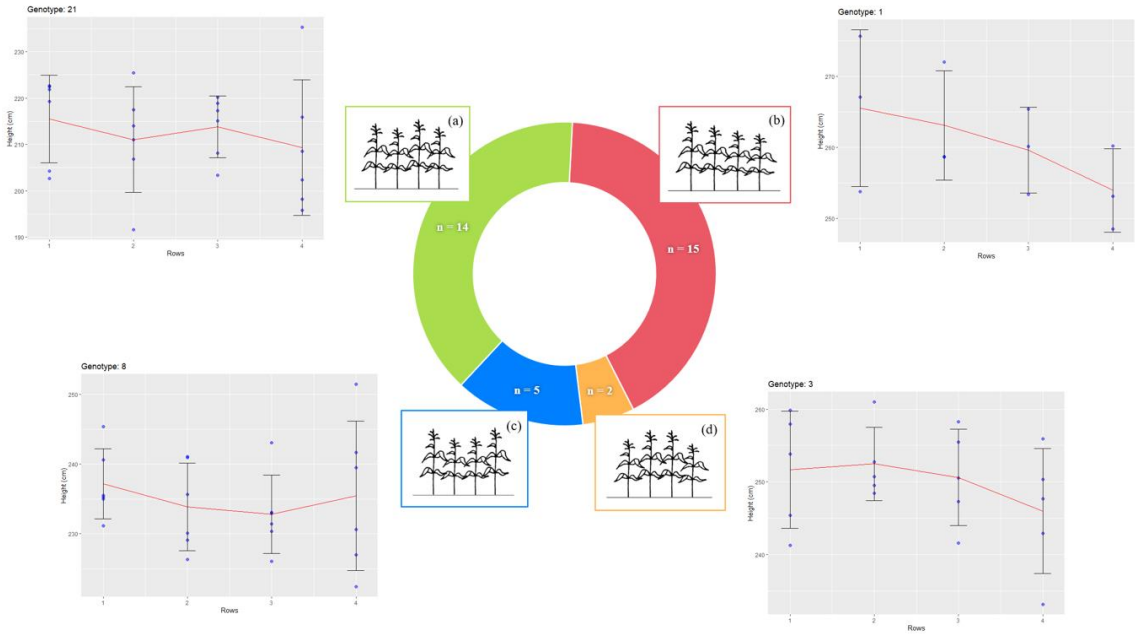

Figure 23: *Overview of the observed height variations across rows by genotypes on September 11th. Four types of height patterns are observed: (a) alternating, (b) slope with southern decline, (c) convex, and (d) concave.*

This analysis reveals that different genotypes reflect distinct patterns between rows, contributing to the overall variability in plant height. Most of the genotypes reflected either a southern sloped tendency (n=15) or an alternating distribution (n=14). Although present in a few cases, the observation of convex (n=5) or concave (n=2) patterns were less frequent. These findings underscore the complex relationship between genotypes and environmental factors, as well as the grouping of different patterns from genotypes.

In Figure 24, the analysis focused on evaluating the average height of different cultivars of maize grown in proximity to varying neighbouring crops. The graphs illustrate the type of crop in the right neighbouring strip, categorized as maize (yellow), beans (green), or pumpkin (orange). Results show that, on average, crops adjacent to beans exhibited a lower mean height compared to those neighbouring maize and pumpkin. This trend varied across genotypes but consistently pointed towards a positive influence of beans on crop height.

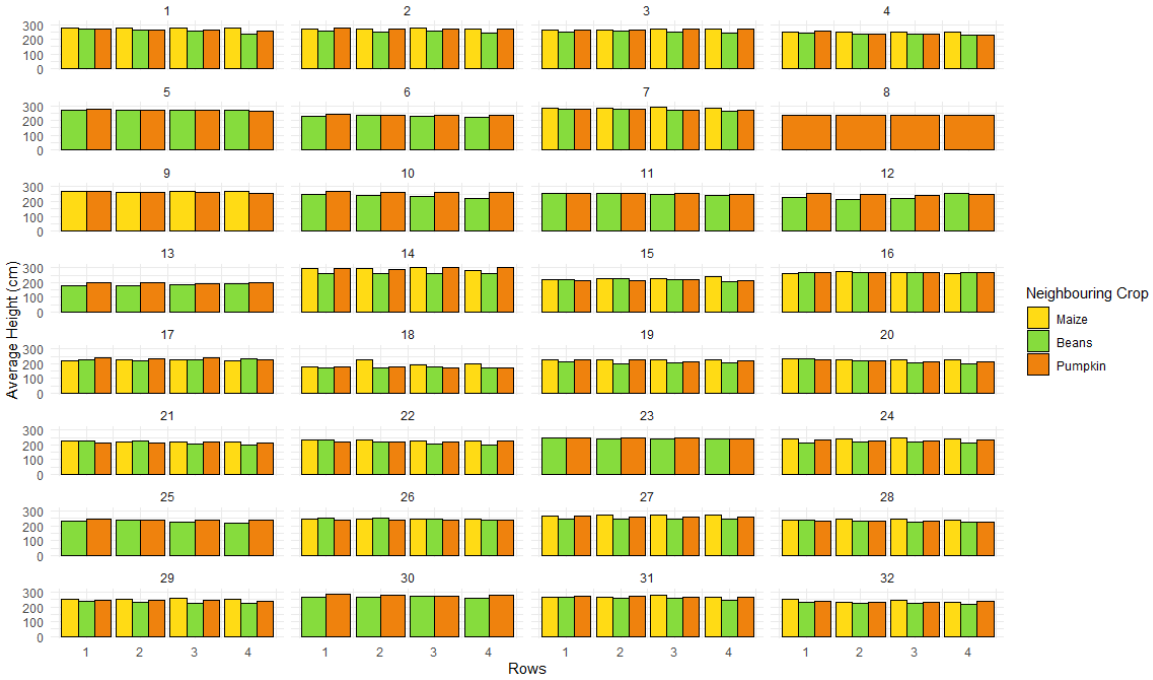

Figure 24: Height (cm) per row for each genotype on September 11th using LiDAR data.

Results from Figure 25 shed light on the average height differences between neighbouring rows within each plot. This analysis offers insights into how plot configurations, such as those with 4 rows, 8 rows, or monoculture plots, may influence the variability in height within a plot. Specifically, the map seeks to determine whether rows situated closer to different types of crops (i.e., border rows) exhibit greater height variation compared to rows located farther from neighbouring crops (i.e., inner-rows). If this is the case, it would be expected that plots with 4 rows would display higher values, as they contain fewer inner rows, which would lower the average variation. The map was generated using a Natural Break (Jenks) classification, allowing the observation of different groups within a continuous dataset based on natural breaks in the data. Upon visual inspection, it is observed that while variations between row configurations cannot be detected, variations are observable within genotypes.

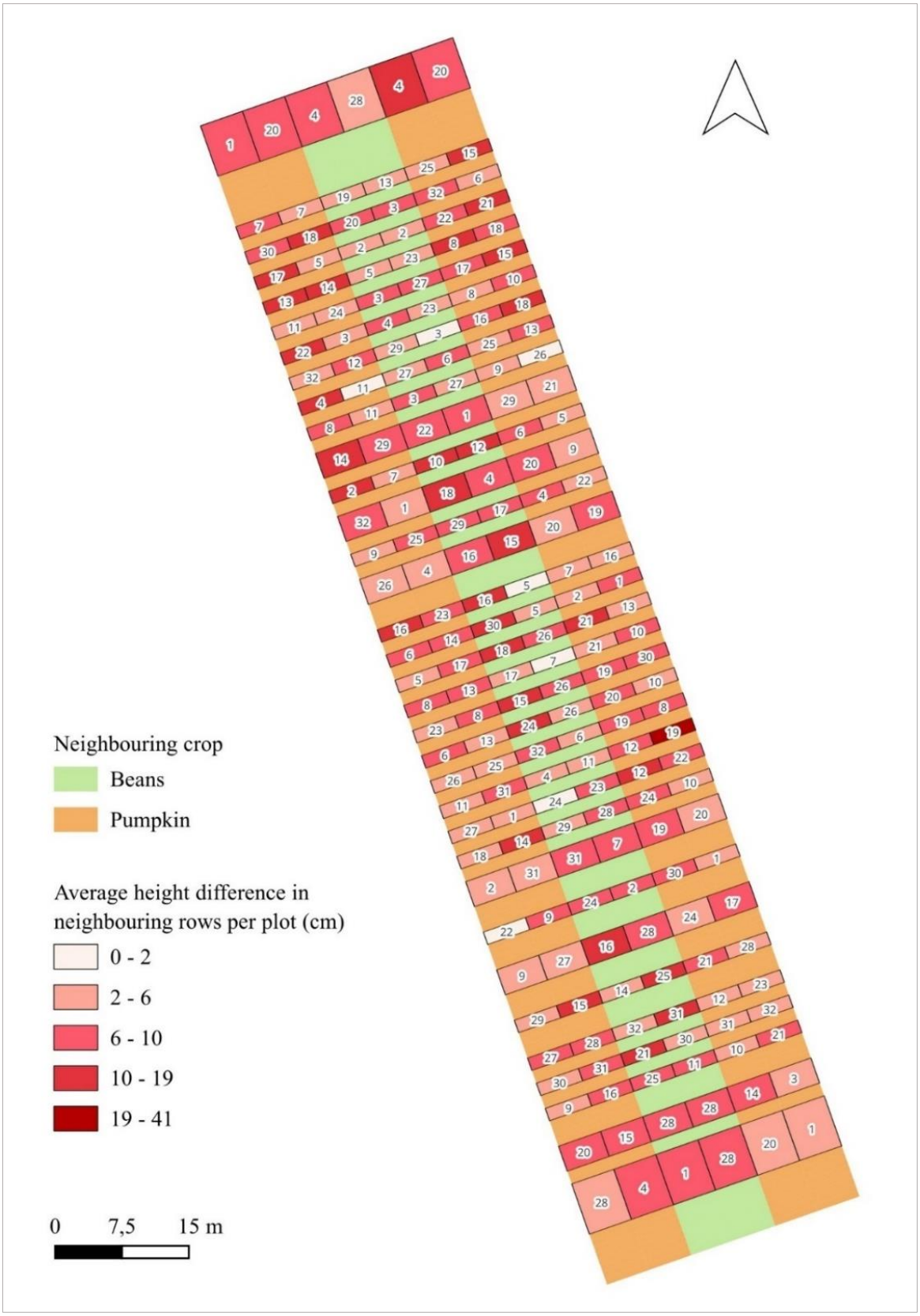

Figure 25: *Average height differences between rows per plot. Observed on September 11th with LiDAR data.*

4.3.2. Temporal patterns

Additionally to observing spatial patterns, height growth observation could also be obtained through the observation of two more dates: the 7th of June and the 18th of July. Maps displaying the height of the maize during these two time periods can be found in Appendix B.

The two growth periods (GPs) are presented in Figure 24. To make the difference in height through time easier to observe, a new dataset with the differences between the June 7th and July 18th (GP1), and the difference between the July 18th and September 11th was created. An equal interval classification was chosen in order to make the two time period maps easily comparable.

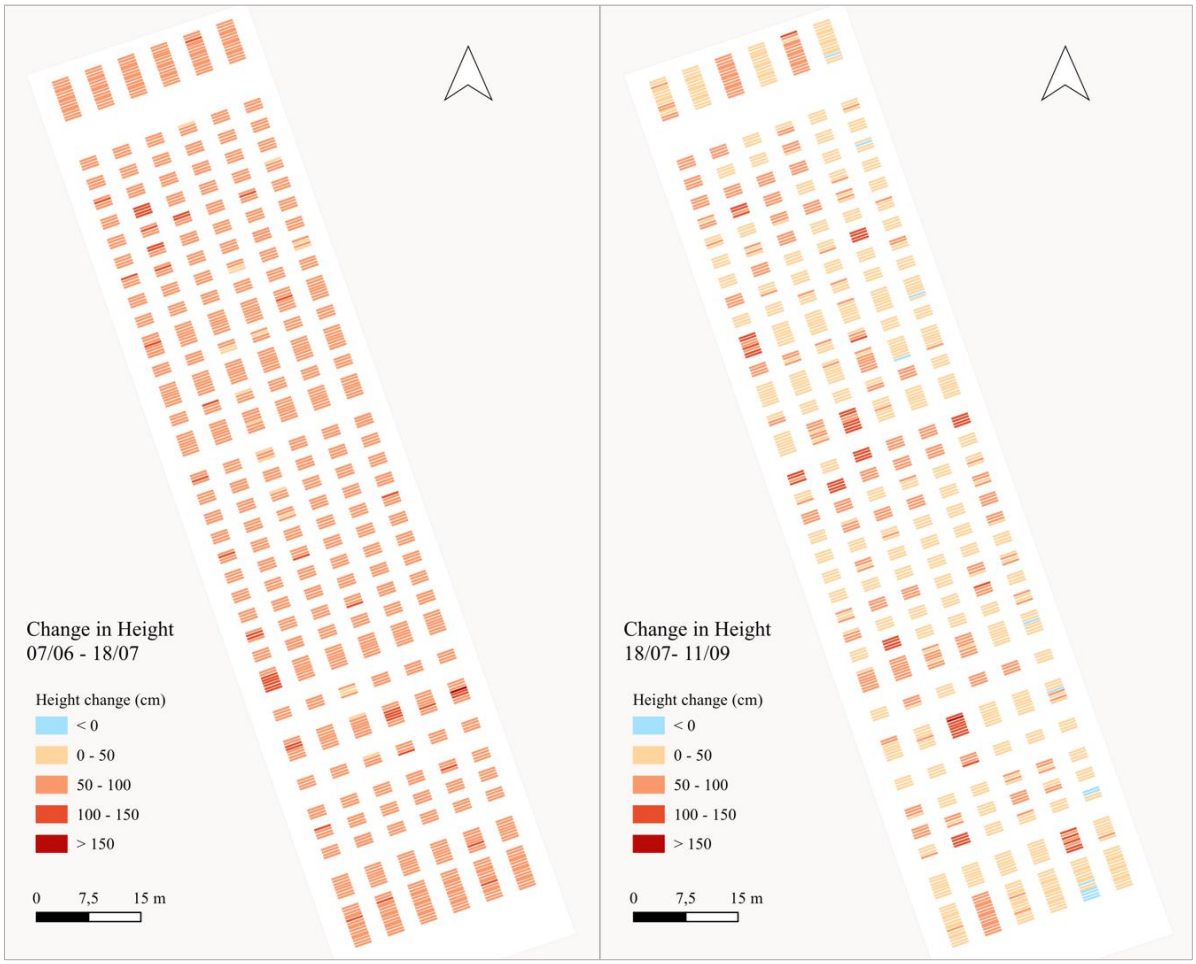

Figure 26: *Average height differences between rows per plot using LiDAR data. Observed for the tie periods of (a) June 7th to July 18th and (b) July 18th to September 11th.*

The GP1 witnesses a notable and relatively homogeneous increase in height across the experimental plots. However, within a few patches, distinctive differences are observed, often accompanied by even more pronounced increases in height. To receive more clarity on these observations, these patches were examined using corresponding ortho and LiDAR images for both dates. Upon close examination of imagery from June 7th, anomalies were identified as lodging areas, shedding light on the observed patterns (see Figure 25).

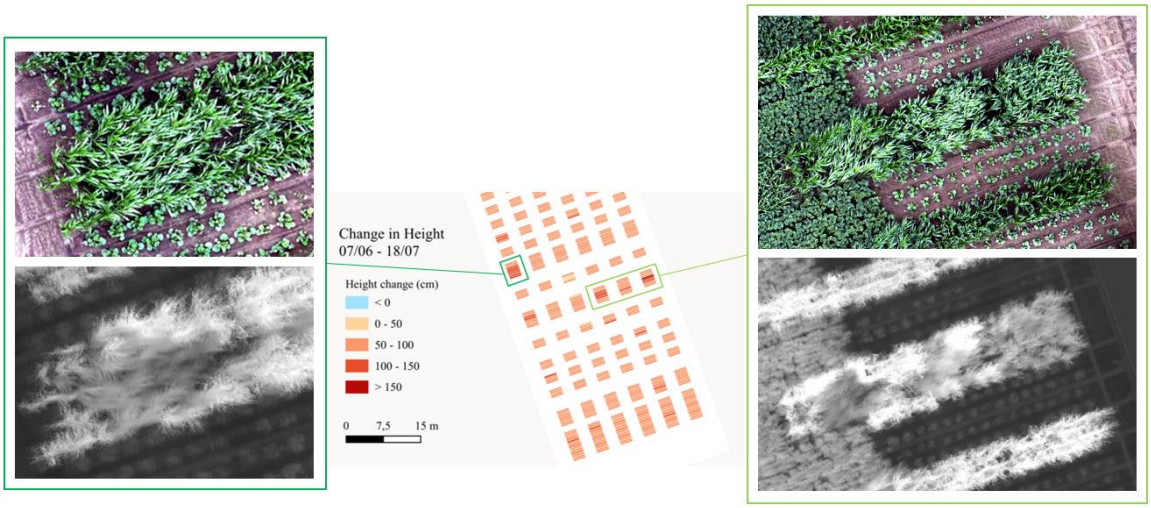

Figure 27: *Detection of lodging areas in the experimental site on June 7th using LiDAR data*

The GP2 is characterised by an overall lower increase in height change compared to the previous period. However, the value are much more heterogeneous with a much greater variation in height. Some rows even show a decrease in height with values under 0cm.

Figure 28 illustrates the growth dynamics of various genotypes across four key stages of the growing season, marked by days after planting (DAP): June 7th (DAP 54), July 18th (DAP 95), August 14th (DAP 122), and September 11th (DAP 150). This figure plots the average height per row of each genotype at these intervals to showcase their growth trajectories. While the initial phase saw a rapid increase in height for most genotypes, a select few demonstrated a notable growth spurt in the subsequent period. Towards the latter part of the season, most of the genotypes reached a plateau in growth, with the exception of one cultivar, which continues to exhibit robust growth. Detailed observations for each genotype are provided in Appendix C and a table with the average heights are presented in Appendix D.

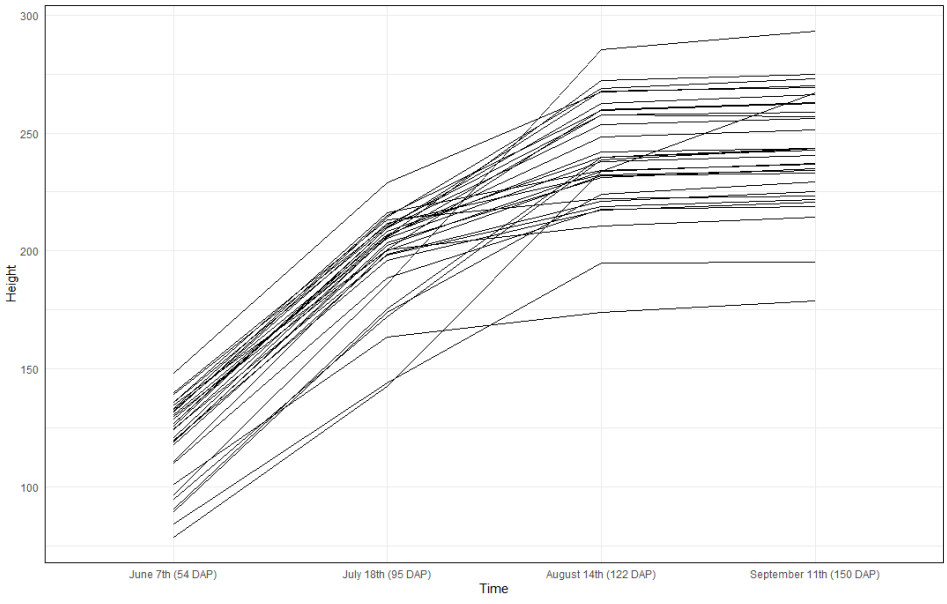

Figure 28: *Comparative growth dynamics of plant genotypes over the growing season.*

5. Discussion

5.1. UAV-based height estimation for maize height in intercropping

The primary aim of this study was to evaluate the effectiveness of UAV-based imagery in detecting maize height within intercropping systems. By having comparable conditions and settings for both imagery types, our analysis was able to directly compare the performances of LiDAR and RGB imagery in correlating with measured ground truth data.

At first, an observation of maize at the individual scale was conducted. Following the identification of the optimal settings, notably an observation of the 99.9th percentile with a 20cm buffer, our findings revealed that LiDAR imagery outperformed RGB imagery in correlating with individual crop ground truth data. Specifically, LiDAR imagery exhibited stronger model suitability (R^2=0.9) and lower root mean square error (RMSE=13.41cm) compared to RGB imagery (R^2=0.88, RMSE=27.88cm). These results, demonstrate the superior performance of LiDAR technology in detecting maize tassels thereby capturing higher values, as evident in through scatter plots (Figure 15) and the maximal heights in the CHMs (Figure 12). The study conducted by Qiu et al. (2022) used RGB imagery to assess individual maize height and reported strong accuracy results for two different genotypes, with R^2 values of 0.96 and 0.98, and RMSE values of 1.3 cm and 1.1 cm, respectively. However, the study observed maize at the height of the leaves in the jointing which has been associated to higher acracy result than looking at the tassel height (Qiu et al., 2022). Our study is innovative in the observation of tassel height at the individual scale through RGB imagery. In the investigation conducted by Gao et al. (2022), LiDAR imagery was employed to evaluate individual maize height, yielding superior results (R^2=0.96, RMSE=3.04 cm) compared to our own study. This difference in results may be attributed to several factors. Notably, the former study possessed a larger sample size, potentially reducing the likelihood of errors associated with manual measurements. Additionally, the study by Gao et al. (2022) utilized individual crop detection, which likely contributed to the accuracy of their measurements. In contrast, our study relied on manual detection of tassel location, which could introduce additional human-induced errors. Furthermore, it is pertinent to reiterate that this research was conducted across a field hosting 32 distinct maize cultivars. As demonstrated in Qiu et al. (2022), height accuracy observations vary between cultivar due to difference in phenotype, making here common accurate observation more challenging. This genotypic diversity underscores the robustness of our methodology, as the accuracy of our results reflects the capability to discern and characterize a multitude of phenotypic expressions within a single analytical framework.

We furthered our study by observing maize height through UAV imagery at row scale. The optimal observations were once again observed at the 99.9th percentile with no buffer surrounding the initially created polygon. In comparison to the individual scale, we observed similar R^2 values with 0.91 for RGB and 0.89 for LiDAR but much higher RMSE value for both LiDAR and RGB imageries with values of 20.82cm and 25.97cm for RGB respectively (Figure 18). LiDAR imagery was once again associated to better accuracy results. A strong explanation for the similar R^2 values between the row scale and the individual scale measurements is the increased number of manual measurements at the row scale, which mitigates the impact of human error and reduces the number of induced outliers. The results obtained from row observation in this study align with previous research, showcasing consistent results across various methodologies. For instance, Han et al. (2018) and Gilliot et

al. (2021) both obtained a R^2 value of 0.9 and RMSE values of 21 cm and 16 cm through RGB imagery. Similarly, the study by Crommelinck & Hofle (2016), which focused on LiDAR for plot maize height estimation, yielded a comparable RMSE value of 16 cm.

In both individual and row scale observations, the optimal percentile to measure the maize's height (99.9^{th}) did not correspond to the highest percentile. This finding aligns with the study by Lu et al. (2021) in which the highest results for tassel height detection were also observed at the 99.9^{th} percentile. Shorter crops such as wheat and barley may require the consideration of lower percentiles due to the presence of weeds which may become higher that the crops (Jamil et al., 2022). However, in our study, we focused on maize, a tall crop, and selected dates where the crop height had already surpassed that of the weeds (Figure 12), effectively neutralizing this issue. Another and more probable reasoning for this observation is the presence of leaves from neighboring crops, which may results in a higher LiDAR-measured value than the tassel of the observed individual maize plant.

This study successfully demonstrates LiDAR technology's potential to accurately measure maize height during the reproductive stage. Through comparison with an earlier reproductive stage date where minimal height changes were anticipated (Figure 19), a high correlation (R^2=0.91) was established. Moreover, it was identified that the outliers originated from the same cultivar, showcasing higher values on the later date and indicating ongoing growth in this genotype. This observation highlights the accuracy and reliability of LiDAR technology in capturing maize height, suggesting promising applications in agriculture.

5.2. Uncertainties and limitations in UAV derived height accuracy

Our study encountered several limitations that may have impacted the reliability and accuracy of our maize height estimations. Firstly, we were constrained by the limited number of individual crop field measurements that were collected. Manual measurements are prone to human errors, as maize stalks are thin and therefore prone to crop movement from wind making the reading of the high crops height value tricky (Gao et al., 2022). With more measurements, and more field workers, we would have been able to give less focus to the human-errors. To achieve a more comprehensive comparison between cultivars, a greater number of measurements would have been necessary, as suggested by Perez-Harguindeguy et al. (2013). For the row observation, we also only got to measure two crops per row, which could have hindered our ability to capture the full spectrum of maize height variation within the rows.

Moreover, locating the tassels was a big challenge in this study. We did not have the exact location of the individual crop that we measured and we therefore relied on the ortho picture to pinpoint the crops. Because we were on the outside of the rows where it was not dense we could afford to use a higher buffer, therefore ensuring that the highest tassel value was included in our measures. However, this would not have been possible in the center of the rows where there is much denser vegetation. While we attempted to account for the location of rows based on the movement of crop growth, the generalization of polygons created per row across all plots may have led to a slight deviation from the true row placement, potentially impacting our results. Incorporating machine learning techniques for individual crop detection could enhance the accuracy of our methodology by detecting the exact location of crops and thereby also generate unique row placements. This would also have promoted the automation of the process and not have to manually select the individual crops. Various approaches are proposed by different studies, such as tassel detection (Zan et al., 2020) and seedling detection (Gao et al., 2022).

5.3. Height dynamics between rows of maize cultivars in intercropping

The investigation of maize height patterns in intercropping systems through different cultivars marks a pioneering research in agricultural research. Given the nascent stage of this field, our study primarily engaged in an exploration of height patterns between genotypes, rows and neighboring crops, laying the groundwork for future analyses. Our initial observations on September 11th delineate two primary patterns of height variability: differences between plots and significant variations within rows (Figure 20).

Analysis of height distributions across genotypes revealed significant variability in the phenotypic profiles of different cultivars (Figure 21). This pronounced variability underscores the pivotal role of genotypic variation as a primary driver of height disparities among maize plots. Further examination into the effects of adjacent crops on maize height revealed another noteworthy pattern in plots: plots adjacent to bean crops generally exhibited lower height values, whereas those neighboring other maize crops displayed higher values (Figure 24). This observation is particularly intriguing given the phenotype difference between beans, which are relatively low-growing plants, and maize, which reach greater heights. This pattern aligns with and lends support to the findings of Muntz et al (2014), suggesting that the impact of neighboring crops on plant height is significant. The lower stature of bean plants adjacent to maize may exert a competitive or complementary influence on the growth dynamics of maize, resulting in varied height outcomes. These observations not only highlight the critical influence of genotype on maize plant height but also underscore the importance of interspecific interactions within crop systems. The discernible effect of neighboring crops on plant height emphasizes the need for further research into the strategic placement of crops to optimize growth outcomes and agricultural productivity.

In addition to the observed height differences between plots, a detailed investigation into the height variations within rows was conducted. Analysis of maize height distribution across four-row configurations unveiled a notable slope trend, with the southernmost rows consistently exhibiting the lowest height values (Figure 22). To mitigate the influence of genotype variability on this pattern, an individual analysis for each genotype was performed (Appendix B). This slope pattern, still evident in the majority of genotypes (Figure 23), points to sunlight exposure as a pivotal factor affecting row height. This observation aligns with the conclusions drawn by Wang et al. (2017), who linked variations in maize crop heights to differences in sunlight absorption. However, our diverges from the symmetrical border row effect described by Wang et al. Instead of a uniform effect across rows, we observe a pronounced impact in the southernmost row. This discrepancy may be explained by our specific row orientation, which differs from the conditions examined by Wang et al. (2017) by being more southern faced, thereby influencing the observed growth patterns (Figure 29).

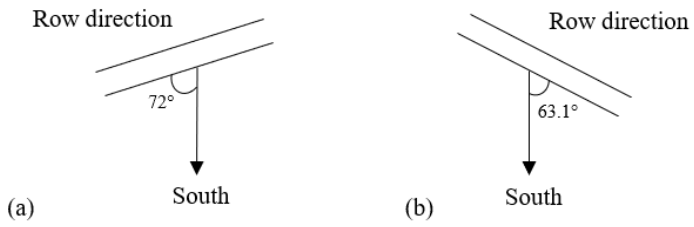

Figure 29: *Row orientation illustrations comparing (a) this study with (b) the Wang et al. (2017) study.*

In addition to the observed slope pattern, certain genotypes exhibited alternating, convex and concave patterns. This morphological variability was accompanied by a high degree of variance within the rows, indicating that the growth patterns are not solely determined by genotype and orientation but are also influenced by additional environmental factors. Such complexity suggests that multiple interacting elements contribute to the observed growth dynamics, underscoring the intricate interplay between genetic and environmental influences on crop development. Subsequent communication revealed that some discrepancies in the observed patterns could be attributed to planting errors, with variations in genotypes between rows 1 and 3 and between rows 2 and 4. These inconsistencies partially account for the alternating growth patterns observed in some plots. Another explanation differences in phenotypic plasticity between cultivars. Fully understanding the maize's different height profile would suggest observing environmental factors sch as sunlight quantity, water absorption and crop properties.

5.4. Growth dynamics of maize cultivars in intercropping

For this section, height were observed on June 7th (DAP 54), July 18th (DAP 95) and September 11th (DAP 150). Through our analysis, we observed very different growth patterns between the two periods (Figure 26). The GP from June 7th to July 18th was marked by a higher maize height change with a general height difference between 50cm and 100cm. Changes outside of these values were primarily attributed to lodging areas (Figure 27). Lodging, a disruption caused by environmental stressors such as wind or rain, can physically bend or break maize stalks, affecting their apparent height (Zhou et al., 2020). In the GP from July 18th to September 11th, lower growth values were noticed with changes that are generally more around 0 to 50cm. Some cultivars even showed regression in height, which can be linked to tassel breakage and maize plants drying down. This observed pattern of growth is characteristic of maize's developmental stages, where the early vegetative phase is marked by rapid stem elongation, transitioning into a reproductive phase where energy is redirected towards flowering and seed production, thus slowing stem growth (Nleya et al., 2016). These results resonate with the observations of Wang et al. (2017) where high growth was observed till about DAP 100 and then stabilization of the growth (Figure 4). However, when looking at the variation between plots (Figure 26) and the growth curves by genotypes (Figure 28), we observe that some genotypes actually show more height during the second period than during the first one. Furthermore, while most cultivars exhibit minimal height variation between August 18th and September 11th, cultivar 16, distinguished as the sole black maize in the experimental field, continues to demonstrate significant growth. This unique growth pattern is also evident in the height comparison between these dates (Figure 19). These observations clearly indicate that whilst the expected pattern is generally observed, cultivars have their own growth curve thereby having a different resource interaction from each other.

5.5. Key factors in assessing UAV based observation of maize height in intercropping

Exploring the effectiveness of UAV maize height within intercropping systems is a pivotal yet recent area of research. A meticulous examination of pertinent literature underscores key factors that must be considered when delving into a pertinent assessment of the subject.

Firstly, the selection of imagery requires careful consideration. According to Araus et al. (2018), the adoption of RGB and LiDAR imagery is most suitable for achieving accurate crop height measurements. Additionally, the scale of observation assumes paramount significance within intercropping contexts. Precision is vital to capture nuanced inter-specific patterns among neighboring genotypes. Our study addresses this necessity by conducting height

measurements at both row and individual crop scales. The diverse range of genotypes within intercropping systems necessitates tailored methodological approaches. Different maize cultivars will have different accuracy values to a proposed height extraction (Gao et al., 2022; Qiu et al., 2022). In our study, this emphasized the need for a methodology capable of accurately assessing the different maize genotypes with their unique morphologies. Furthermore, the method employed for height extraction carries considerable weight. Particularly in dense vegetation scenarios like maize fields, the utilization of off-season DTMs has shown superior accuracy (Table 1). The crop growth stage emerges as a pivotal consideration due to its profound impact on crop morphology. Maize undergoes notable morphological changes during its growth stages, such as the emergence of the tassel during the reproductive phase (Oehme et al., 2022). With the tassel being a thin and thereby not easily detectable object, more precise imagery is expected to be required than when looking at the crop leaves. Height extraction parameters, such as observed percentiles and buffer sizes, represent nuanced yet critical determinants. Tailoring these parameters to specific study contexts is imperative, as their efficacy is highly dependent on the nature of the observation. Finally, striking a judicious balance between accuracy and cost is indispensable. While heightened accuracy is desirable, it often comes with elevated costs. Thus, pragmatic considerations regarding cost must be carefully weighed against the imperative for precision. By meticulously addressing these key factors, our study was established with a robust methodology for measuring maize height within intercropping systems. This holistic approach sets the stage for further investigation.

5.6. Future work

In this study, we have provided additional knowledge for further exploration into the use of UAV imagery in assessing phenotypic traits in intercropping systems. Moving forward, there are several avenues for continued research and refinement.

The diverse set of maize cultivars used in this study offers a unique opportunity to delve deeper into the genetic factors that influence plant height in intercropping systems. Future plant investigations can focus on correlating height observations with yield, root systems, and overall plant health, shedding light on the specific genetic determinants of maize height variation. The complexity of the experimental field, including neighboring crops like faba beans and pumpkins, provides a platform for studying the interplay between different crop types. Shifting the focus of height pattern analysis to these neighboring crops using the same field experiment can offer insights into how maize height interacts with other plant species in intercropping systems. In this study, a hypothesis regarding the lack of accuracy due to imprecise tassel identification warrants further investigation was made. A comparative analysis between manual observations and tassel detection methods using UAV imagery can shed light on the power of automatization in using RS for phenotyping in intercropping systems. The use of pre-disposed pre-processing settings in this study provides a basis for exploring the impact of different parameters on UAV performance in intercropping systems. Fine-tuning these parameters can enhance the accuracy of height measurements not only for maize but also for other crops in intercropping scenarios. Finally, while this study has focused on maize, there is scope for comparative studies on optimal methodologies across different crops in intercropping systems. Assessing the accuracy of UAV imagery in measuring height across various crops can provide valuable insights into the unique challenges and opportunities presented by different plant species.

By addressing these areas in future research, we can further refine the application of UAV technology in assessing crop height and morphology, contributing to more precise and efficient agricultural practices in intercropping systems.

6. Conclusion

This study has provided valuable insights into the utility of UAV-based imagery for measuring maize height in intercropping systems, emphasising the need for several considerations. Firstly, the selection of precise imagery is essential for accurately capturing smaller features like tassels, with RGB and LiDAR emerging as the most effective technologies for assessing crop height. Furthermore, the scale of observation plays a crucial role, especially since intercropping effects are pronounced at the row level. Precision at an individual plant scale has the advantage of mitigating the impact of foliage. Moreover, accurately choosing the most appropriate method for plant height extraction and its parameters has been identified as highly dependent to the observed experimental field. For densely vegetated fields and when early data are available, integrating a DTM with a DSM proves to be the most efficient approach. Finally, the variability introduced by the presence of multiple cultivars and differing growth stages necessitates a flexible methodology that can accommodate these complexities, which may differ from the methodology observed for a specific cultivar or growth stage.

Comparing the performance of LiDAR and RGB imagery with ground truth data, the study demonstrated the superior accuracy of LiDAR in capturing maize tassel height. Specifically, higher accuracy was observed for individual crop observations (R2= 0.9 , RMSE= 13.41cm) compared to row observations (R2 = 0.89, RMSE = 20.89cm). RGB imagery yielded results of R^2 = 0.88, RMSE = 27.88 cm for individual crop height and R^2 = 0.91, RMSE = 25.97cm for row observations. However, using LiDAR data has shown extra complications, such as the need for high storage capacities and elevated processing time. Using LiDAR may also be more costly than RGB Imagery, although technology advancements are gradually reducing this cost disparity.

The research revealed significant height variation influenced by genotypic differences, row configurations, and environmental factors, with notable impacts from neighbouring crops on maize height. The variability observed within rows for different cultivars suggests a high impact of sunlight exposure. However, with a complex interactions at play, the need for an in-depth exploration of the relationship between maize genotypes and their specific growing conditions is required.

Our research also established patterns in maize growth dynamics, exhibiting a pronounced increase in height during the initial vegetative phase followed by a more gradual growth as the plants transition into the reproductive stage. However, growth pattern were noticed as highly unique to cultivars. In particular, the black maize, showed a much later growth phase than the other cultivars. Through observation of growth patterns we were also able to display the potential of RS in detecting lodging areas.

Challenges such as limited sample sizes and the need for manual tassel detection suggest areas for methodological refinement. Future studies should explore the method's robustness across different crops and intercropping systems, automate data processing, and further investigate the genetic basis of height variability among cultivars.

References

Ajal, J., Kiær, L. P., Pakeman, R. J., Scherber, C., & Weih, M. (2022). Intercropping drives plant phenotypic plasticity and changes in functional trait space. *Basic and Applied Ecology, 61*, 41-52.
https://doi.org/10.1016/j.baae.2022.03.009

Anderson, S. L., Murray, S. C., Chen, Y., Malambo, L., Chang, A., Popescu, S., ... & Jung, J. (2020). Unoccupied aerial system enabled functional modeling of maize height reveals dynamic expression of loci. *Plant Direct*, 4(5), e00223.
https://doi.org/10.1002/pld3.223

Anthony, D., Elbaum, S., Lorenz, A., & Detweiler, C. (2014, September). On crop height estimation with UAVs. In *2014 IEEE/RSJ International Conference on Intelligent Robots and Systems* (pp. 4805-4812). IEEE.
https://doi.org/10.1109/IROS.2014.6943245

Araus, J. L., Kefauver, S. C., Zaman-Allah, M., Olsen, M. S., & Cairns, J. E. (2018). Translating high-throughput phenotyping into genetic gain. *Trends in plant science*, *23*(5), 451-466.
https://doi.org/10.1016/j.tplants.2018.02.001

Berni, J. A., Zarco-Tejada, P. J., Suárez, L., & Fereres, E. (2009). Thermal and narrowband multispectral remote sensing for vegetation monitoring from an unmanned aerial vehicle. *IEEE Transactions on geoscience and Remote Sensing*, *47*(3), 722-738.
https://doi.org/10.1109/TGRS.2008.2010457

Bourke, P. M., Evers, J. B., Bijma, P., van Apeldoorn, D. F., Smulders, M. J., Kuyper, T. W., ... & Bonnema, G. (2021). Breeding beyond monoculture: putting the "intercrop" into crops. *Frontiers in Plant Science*, *12*, 734167.
https://doi.org/10.3389/fpls.2021.734167

Brooker, R. W., Bennett, A. E., Cong, W. F., Daniell, T. J., George, T. S., Hallett, P. D., ... & White, P. J. (2015). Improving intercropping: a synthesis of research in agronomy, plant physiology and ecology. *New Phytologist*, 206(1), 107-117.
https://doi.org/10.1111/nph.13132

Chang, A., Jung, J., Maeda, M. M., & Landivar, J. (2017). Crop height monitoring with digital imagery from Unmanned Aerial System (UAS). *Computers and Electronics in Agriculture*, 141, 232-237.
https://doi.org/10.1016/j.compag.2017.07.008

Chen, H., Yi, Z. F., Schmidt-Vogt, D., Ahrends, A., Beckschäfer, P., Kleinn, C., ... & Xu, J. (2016). Pushing the limits: The pattern and dynamics of rubber monoculture expansion in Xishuangbanna, SW China. *PloS one*, 11(2), e0150062.
https://doi.org/10.1371/journal.pone.0150062

Crommelinck, S., & Höfle, B. (2016). Simulating an autonomously operating low-cost static

terrestrial LiDAR for multitemporal maize crop height measurements. *Remote sensing*, 8(3), 205.
https://doi.org/10.3390/rs8030205

Dambreville, A., Lauri, P. E., Normand, F., & Guédon, Y. (2015). Analysing growth and development of plants jointly using developmental growth stages. *Annals of Botany*, 115(1), 93-105.
https://doi.org/10.1093/aob/mcu227

Erenstein, O., Jaleta, M., Sonder, K., Mottaleb, K., & Prasanna, B. M. (2022). Global maize production, consumption and trade: Trends and R&D implications. *Food Security*, 14(5), 1295-1319.

Fathipoor, H., Arefi, H., Shah-Hosseini, R., & Moghadam, H. (2019). Corn forage yield prediction using unmanned aerial vehicle images at mid-season growth stage. *Journal of Applied Remote Sensing*, 13(3), 034503-034503.
https://doi.org/10.1117/1.JRS.13.034503

Foley, J.A., 2011. Can we feed the world & sustain the planet? Sci. Am. 305, 60–65. https://www.jstor.org/stable/26002878

Gao, M., Yang, F., Wei, H., & Liu, X. (2022). Individual maize location and height estimation in field from uav-borne lidar and rgb images. *Remote Sensing*, *14*(10), 2292. https://doi.org/10.3390/rs14102292

Gebru, H. (2015). A review on the comparative advantages of intercropping to mono-cropping system. Journal of Biology, *Agriculture and Healthcare*, 5(9), 1-13.

Giam, X., Hadiaty, R. K., Tan, H. H., Parenti, L. R., Wowor, D., Sauri, S., ... & Wilcove, D. S. (2015). Mitigating the impact of oil-palm monoculture on freshwater fishes in Southeast Asia. *Conservation Biology*, 29(5), 1357-1367.
https://doi.org/10.1111/cobi.12483

Gilliot, J. M., Michelin, J., Hadjard, D., & Houot, S. (2021). An accurate method for predicting spatial variability of maize yield from UAV-based plant height estimation: A tool for monitoring agronomic field experiments. *Precision Agriculture*, 22(3), 897-921.

Grenzdörffer, G. J. (2014). Crop height determination with UAS point clouds. The International Archives of the Photogrammetry, *Remote Sensing and Spatial Information Sciences*, 40, 135-140.
https://doi.org/10.5194/isprsarchives-XL-1-135-2014

Guo, Y., Xiao, Y., Li, M., Hao, F., Zhang, X., Sun, H., ... & He, Y. (2022). Identifying crop phenology using maize height constructed from multi-sources images. *International Journal of Applied Earth Observation and Geoinformation*, 115, 103121.
https://doi.org/10.1016/j.jag.2022.103121

Han, L., Yang, G., Yang, H., Xu, B., Li, Z., & Yang, X. (2018). Clustering field-based maize phenotyping of plant-height growth and canopy spectral dynamics using a UAV remote-

sensing approach. *Frontiers in plant science*, 9, 1638.
https://doi.org/10.3389/fpls.2018.01638

Iglhaut, J., Cabo, C., Puliti, S., Piermattei, L., O'Connor, J., & Rosette, J. (2019). Structure from motion photogrammetry in forestry: A review. *Current Forestry Reports*, 5, 155-168.

Jamil, N., Kootstra, G., & Kooistra, L. (2022). Evaluation of Individual Plant Growth Estimation in an Intercropping Field with UAV Imagery. *Agriculture*, *12*(1), 102. MDPI AG. https://doi.org/10.3390/agriculture12010102

Jensen, E. S. (1996). Barley uptake of N deposited in the rhizosphere of associated field pea. *Soil Biology and Biochemistry*, 28(2), 159-168.
https://doi.org/10.1016/0038-0717(95)00134-4

Khalil, O. A. (2020). Structure from motion (SfM) photogrammetry as an alternative to laser scanning for 3D modeling of historical monuments. *Open Science Journal*, 5(2). https://doi.org/10.23954/osj.v5i2.2327

Kling, J., & Edmeades, G. O. (1997). Morphology and growth of maize: *IITA research guide*, No. 9.
https://hdl.handle.net/20.500.12478/3968

Lefsky, M. A., Cohen, W. B., Parker, G. G., & Harding, D. J. (2002). Lidar remote sensing for ecosystem studies: Lidar, an emerging remote sensing technology that directly measures the three-dimensional distribution of plant canopies, can accurately estimate vegetation structural attributes and should be of particular interest to forest, landscape, and global ecologists. *BioScience*, 52(1), 19-30.
https://doi.org/10.1641/0006-3568(2002)052[0019:LRSFES]2.0.CO;2

Li, L.; Zhang, L.Z.; Zhang, F.Z. Crop mixtures and the mechanisms of over yielding. In Encyclopedia of Biodiversity, 2nd ed.; Levin, S.A., Ed.; Academic Press: Waltham, MA, USA, 2013; Volume 2, pp. 382–395.
http://dx.doi.org/10.1016/B978-0-12-384719-5.00363-4

Li, W., Niu, Z., Wang, C., Huang, W., Chen, H., Gao, S., ... & Muhammad, S. (2015). Combined use of airborne LiDAR and satellite GF-1 data to estimate leaf area index, height, and aboveground biomass of maize during peak growing season. *IEEE Journal of Selected Topics in Applied Earth Observations and Remote Sensing*, 8(9), 4489-4501.

Li, W., Niu, Z., Chen, H., Li, D., Wu, M., & Zhao, W. (2016). Remote estimation of canopy height and aboveground biomass of maize using high-resolution stereo images from a low-cost unmanned aerial vehicle system. *Ecological indicators*, 67, 637-648.
https://doi.org/10.1016/j.ecolind.2016.03.036

Li, X. F., Wang, Z. G., Bao, X. G., Sun, J. H., Yang, S. C., Wang, P., ... & Li, L. (2021). Long-term increased grain yield and soil fertility from intercropping. *Nature Sustainability*, 4(11), 943-950.
https://doi.org/10.1038/s41893-021-00767-7

Li, M., Shamshiri, R. R., Schirrmann, M., Weltzien, C., Shafian, S., & Laursen, M. S. (2022). UAV oblique imagery with an adaptive micro-terrain model for estimation of leaf area index and height of maize canopy from 3D point clouds. *Remote Sensing*, 14(3), 585. https://doi.org/10.3390/rs14030585

Lu, J., Cheng, D., Geng, C., Zhang, Z., Xiang, Y., & Hu, T. (2021). Combining plant height, canopy coverage and vegetation index from UAV-based RGB images to estimate leaf nitrogen concentration of summer maize. *Biosystems Engineering*, 202, 42-54. https://doi.org/10.1016/j.biosystemseng.2020.11.010

Luo, S., Chen, J. M., Wang, C., Xi, X., Zeng, H., Peng, D., & Li, D. (2016). Effects of LiDAR point density, sampling size and height threshold on estimation accuracy of crop biophysical parameters. *Optics express*, 24(11), 11578-11593. https://doi.org/10.1364/OE.24.011578

Luo, S., Wang, C., Xi, X., Nie, S., Fan, X., Chen, H., ... & Zhou, G. (2019). Combining hyperspectral imagery and LiDAR pseudo-waveform for predicting crop LAI, canopy height and above-ground biomass. *Ecological Indicators*, 102, 801-812. https://doi.org/10.1016/j.ecolind.2019.03.011

Luo, S., Liu, W., Zhang, Y., Wang, C., Xi, X., Nie, S., ... & Zhou, G. (2021). Maize and soybean heights estimation from unmanned aerial vehicle (UAV) LiDAR data. *Computers and Electronics in Agriculture*, 182, 106005. https://doi.org/10.1016/j.compag.2021.106005

Malachy, N., Zadak, I., & Rozenstein, O. (2022). Comparing methods to extract crop height and estimate crop coefficient from UAV imagery using structure from motion. *Remote Sensing*, 14(4), 810. https://doi.org/10.3390/rs14040810

Malambo, L., Popescu, S. C., Murray, S. C., Putman, E., Pugh, N. A., Horne, D. W., ... & Bishop, M. (2018). Multitemporal field-based plant height estimation using 3D point clouds generated from small unmanned aerial systems high-resolution imagery. *International Journal of Applied Earth Observation and Geoinformation*, 64, 31-42. https://doi.org/10.1016/j.jag.2017.08.014

Munz, S., Graeff-Hönninger, S., Lizaso, J. I., Chen, Q., & Claupein, W. (2014). Modeling light availability for a subordinate crop within a strip–intercropping system. *Field Crops Research*, 155, 77-89. https://doi.org/10.1016/j.fcr.2013.09.020

Nleya, T., Chungu, C., & Kleinjan, J. (2016). Corn growth and development. Grow Corn Best Manag. *Pract.*

Oehme, L. H., Reineke, A.-J., Weiß, T. M., Würschum, T., He, X., & Müller, J. (2022). Remote Sensing of Maize Plant Height at Different Growth Stages Using UAV-Based Digital Surface Models (DSM). *Agronomy*, 12(4), 958. https://doi.org/10.3390/agronomy12040958

Ofori, F., & Stern, W. R. (1987). Cereal–legume intercropping systems. *Advances in agronomy*, 41, 41-90.
https://doi.org/10.1016/S0065-2113(08)60802-0

Perez-Harguindeguy, N., Diaz, S., Garnier, E., Lavorel, S., Poorter, H., Jaureguiberry, P., ... & Cornelissen, J. H. C. (2013). New handbook for standardised measurement of plant functional traits worldwide. Aust. Bot. 61, 167–234.

Population estimates and projections | DataBank. (n.d.).
https://databank.worldbank.org/source/population-estimates-and-projections

Power, J. F., & Follett, R. F. (1987). Monoculture. *Scientific American*, 256(3), 78-87.
https://www.jstor.org/stable/24979342

Qiu, R., Zhang, M., & He, Y. (2022). Field estimation of maize plant height at jointing stage using an RGB-D camera. *The Crop Journal*, 10(5), 1274-1283.
https://doi.org/10.1016/j.cj.2022.07.010

Raj, R., Walker, J. P., Pingale, R., Nandan, R., Naik, B., & Jagarlapudi, A. (2021). Leaf area index estimation using top-of-canopy airborne RGB images. *International Journal of Applied Earth Observation and Geoinformation*, 96, 102282.
https://doi.org/10.1016/j.jag.2020.102282

Raj, R., Walker, J. P., & Jagarlapudi, A. (2023). Maize On-Farm Stressed Area Identification Using Airborne RGB Images Derived Leaf Area Index and Canopy Height. *Agriculture*, 13(7), 1292.
https://doi.org/10.3390/agriculture13071292

Raseduzzaman, M. D., & Jensen, E. S. (2017). Does intercropping enhance yield stability in arable crop production? A meta-analysis. *European Journal of Agronomy*, 91, 25-33.
Seran, T. H., & Brintha, I. (2010). Review on maize based intercropping. Journal of agronomy, 9(3), 135-145.
https://doi.org/10.1016/j.eja.2017.09.009

Steffen, W., Richardson, K., Rockström, J., Cornell, S. E., Fetzer, I., Bennett, E. M., ... & Sörlin, S. (2015). Planetary boundaries: Guiding human development on a changing planet. *Science*, 347(6223), 1259855.
https://doi.org/10.1126/science.1259855

Struik, P. C., & Kuyper, T. W. (2017). Sustainable intensification in agriculture: the richer shade of green. A review. *Agronomy for sustainable development*, 37, 1-15.

ten Harkel, J., Bartholomeus, H., & Kooistra, L. (2019). Biomass and Crop Height Estimation of Different Crops Using UAV-Based Lidar. *Remote Sensing*, *12*(1), 17. MDPI AG. Retrieved from
http://dx.doi.org/10.3390/rs12010017

Tirado, S. B., Hirsch, C. N., & Springer, N. M. (2020). UAV-based imaging platform for monitoring maize growth throughout development. *Plant Direct*, 4(6), e00230.

https://doi.org/10.1002/pld3.230

Tooker, J. F., & Frank, S. D. (2012). Genotypically diverse cultivar mixtures for insect pest management and increased crop yields. *Journal of Applied Ecology*, 49(5), 974-985. https://doi.org/10.1111/j.1365-2664.2012.02173.x

Vandermeer, J. H. (1992). The ecology of intercropping. Cambridge university press, p.13.
van der Meij, B., Kooistra, L., Suomalainen, J., Barel, J. M., and De Deyn, G. B.: Remote sensing of plant trait responses to field-based plant–soil feedback using UAV-based optical sensors, *Biogeosciences*, 14, 733–749, 2017.

Wang, Z., Zhao, X., Wu, P., Gao, Y., Yang, Q., & Shen, Y. (2017). Border row effects on light interception in wheat/maize strip intercropping systems. *Field Crops Research*, 214, 1-13. https://doi.org/10.1016/j.fcr.2017.08.017

Wang, R., Sun, Z., Zhang, L., Yang, N., Feng, L., Bai, W., ... & van der Werf, W. (2020). Border-row proportion determines strength of interspecific interactions and crop yields in maize/peanut strip intercropping. *Field Crops Research*, *253*, 107819. https://doi.org/10.1016/j.fcr.2020.107819

Westoby, M. J., Brasington, J., Glasser, N. F., Hambrey, M. J., & Reynolds, J. V. (2012), 'Structure-from-Motion' photogrammetry: A low-cost, effective tool for geoscience applications. Geomorphology, 179, 300–314. https://doi.org/10.1016/j.geomorph.2012.08.021

Xiao, J., Suab, S. A., Chen, X., Singh, C. K., Singh, D., Aggarwal, A. K., ... & Avtar, R. (2023). Enhancing assessment of corn growth performance using unmanned aerial vehicles (UAVs) and deep learning. *Measurement*, 214, 112764. https://doi.org/10.1016/j.measurement.2023.112764

Xie, C., & Yang, C. (2020). A review on plant high-throughput phenotyping traits using UAV-based sensors. *Computers and Electronics in Agriculture*, *178*, 105731. https://doi.org/10.1016/j.compag.2020.105731

Yang, H., Zhang, W., & Li, L. (2021). Intercropping: Feed more people and build more sustainable agroecosystems. *Frontiers of Agricultural Science and Engineering*, 8(3), 373-386. https://doi.org/10.15302/J-FASE-2021398

Yu, Z., Cao, Z., Wu, X., Bai, X., Qin, Y., Zhuo, W., ... & Xue, H. (2013). Automatic image-based detection technology for two critical growth stages of maize: Emergence and three-leaf stage. *Agricultural and forest meteorology*, 174, 65-84. https://doi.org/10.1016/j.agrformet.2013.02.011

Zhao, X., Tong, C., Pang, X., Wang, Z., Guo, Y., Du, F., & Wu, R. (2012). Functional mapping of ontogeny in flowering plants. *Briefings in bioinformatics*, 13(3), 317-328. https://doi.org/10.1093/bib/bbr054

Zhou, L., Gu, X., Cheng, S., Yang, G., Shu, M., & Sun, Q. (2020). Analysis of plant height

changes of lodged maize using UAV-LiDAR data. *Agriculture*, 10(5), 146. https://doi.org/10.3390/agriculture10050146

Appendix A: Variability in maize height across rows by genotype on September 11th.

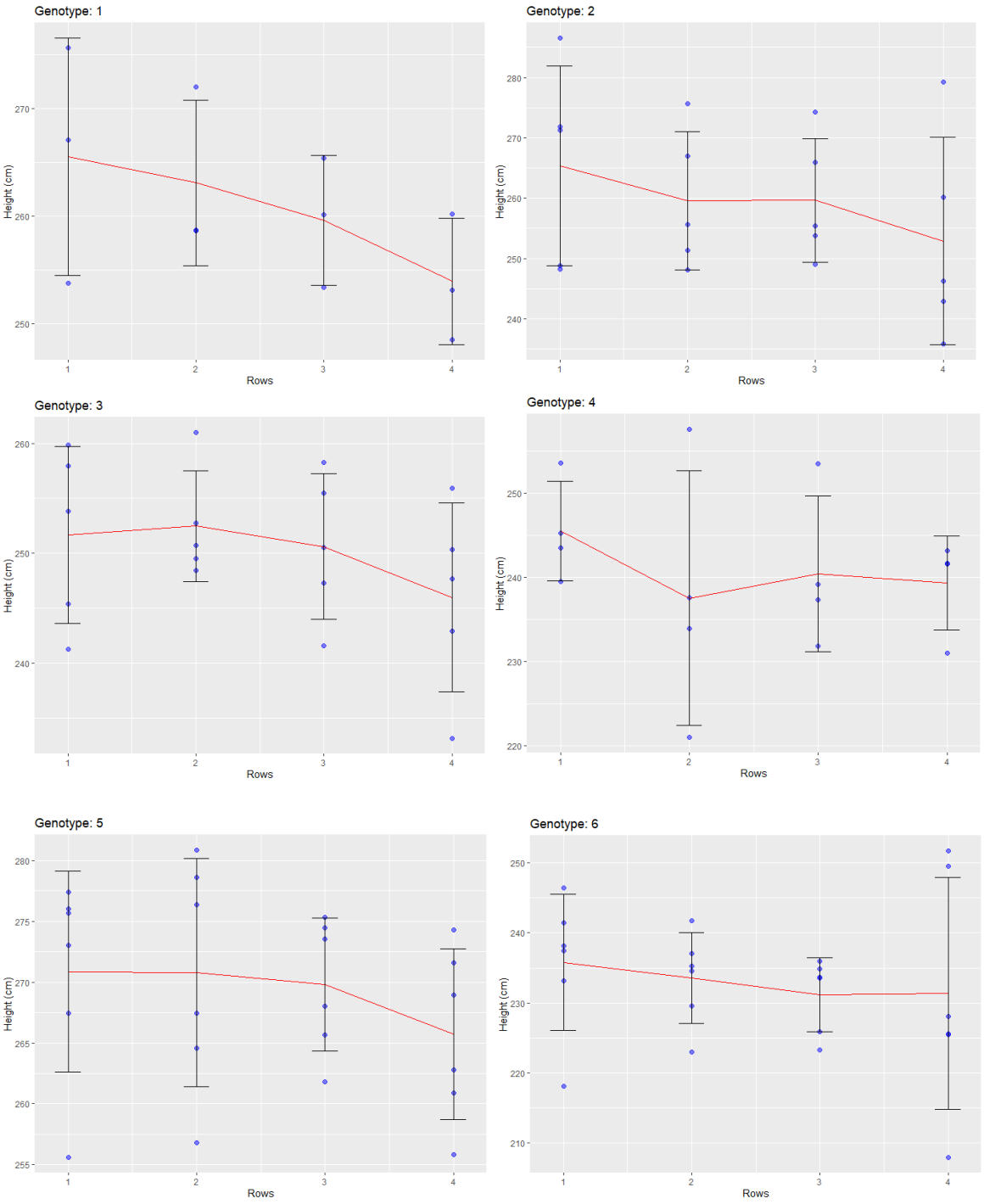

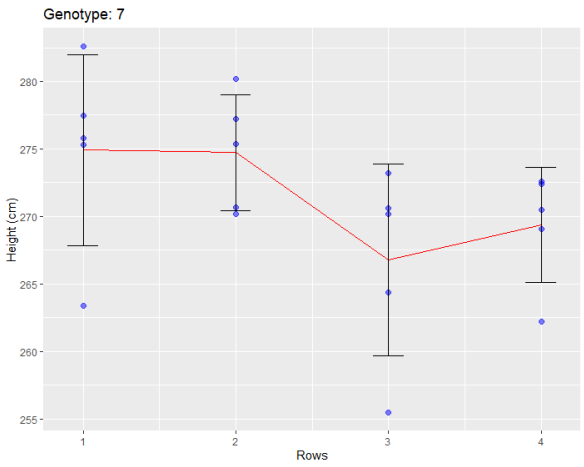
Genotype: 7
Height (cm)
280
275
270
265
260
255
1
2
3
4
Rows

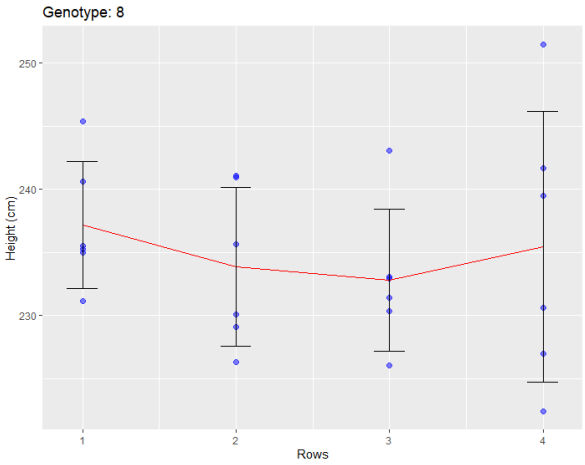
Genotype: 8
Height (cm)
250
240
230
1
2
3
4
Rows

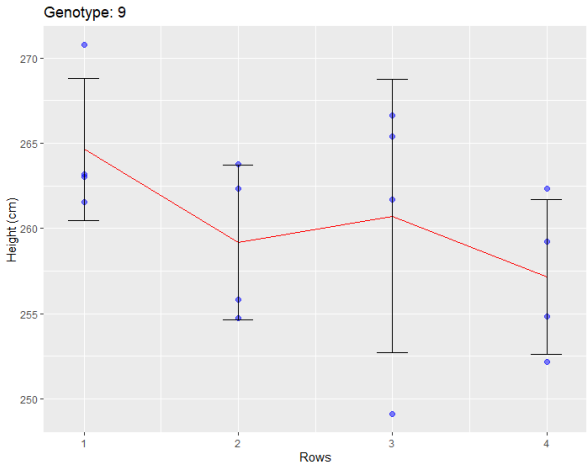
Genotype: 9
Height (cm)
270
265
260
255
250
1
2
3
4
Rows

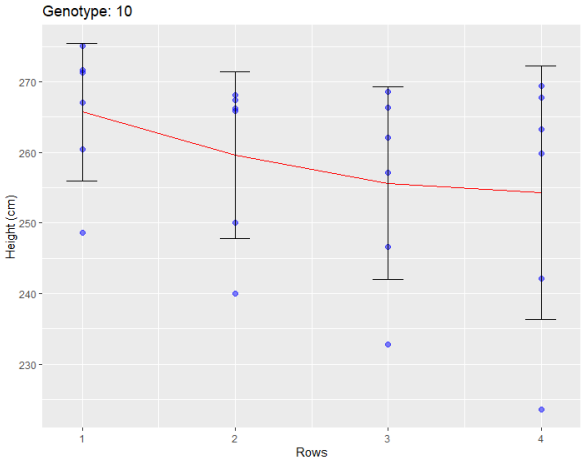
Genotype: 10
Height (cm)
270
260
250
240
230
1
2
3
4
Rows

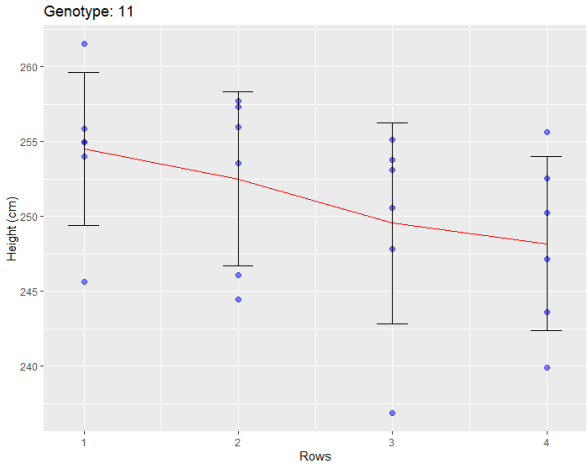
Genotype: 11
Height (cm)
260
255
250
245
240
1
2
3
4
Rows

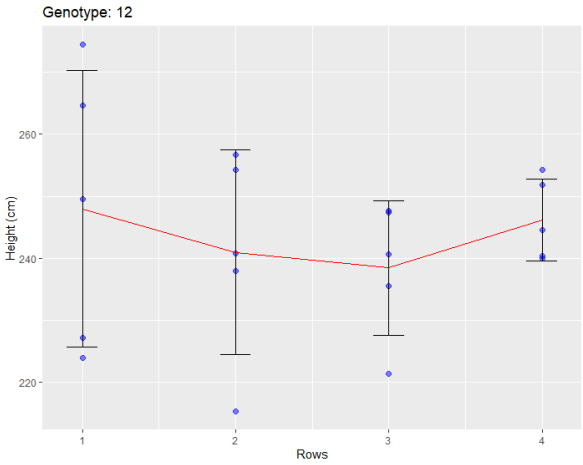
Genotype: 12
Height (cm)
260
240
220
1
2
3
4
Rows

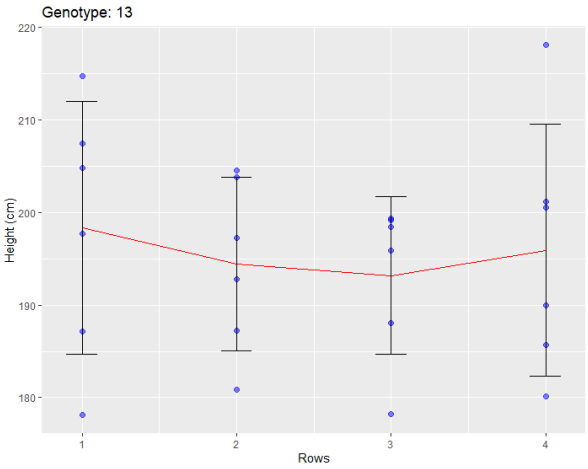
Genotype: 13
Height (cm)
220
210
200
190
180
1
2
3
4
Rows

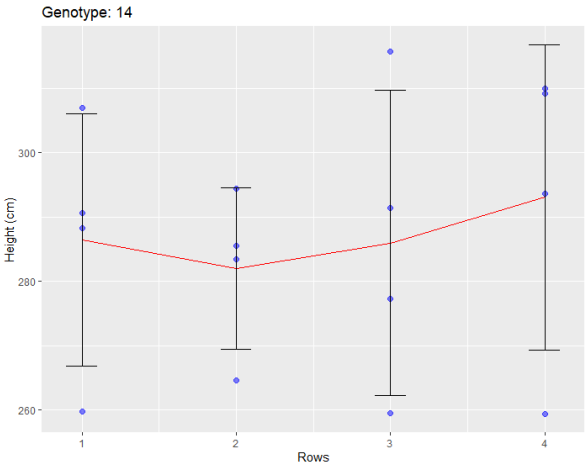
Genotype: 14
Height (cm)
300
280
260
1
2
3
4
Rows

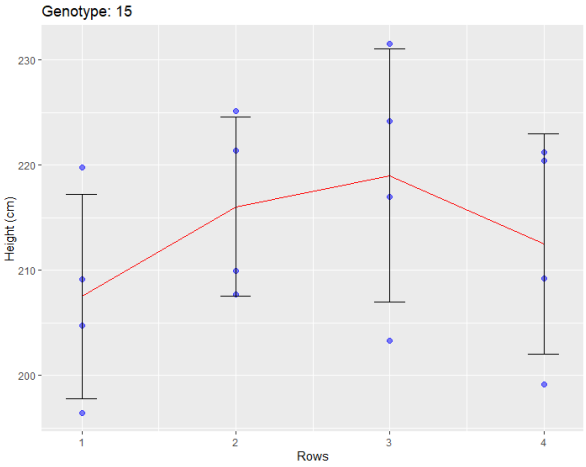
Genotype: 15
Height (cm)
230
220
210
200
1
2
3
4
Rows

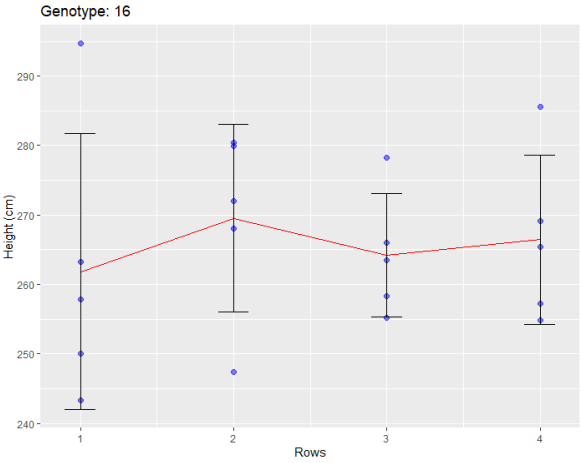
Genotype: 16
Height (cm)
290
280
270
260
250
240
1
2
3
4
Rows

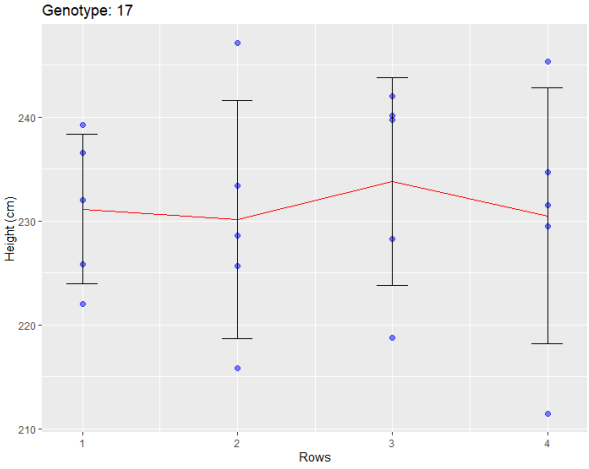
Genotype: 17
Height (cm)
240
230
220
210
1
2
3
4
Rows

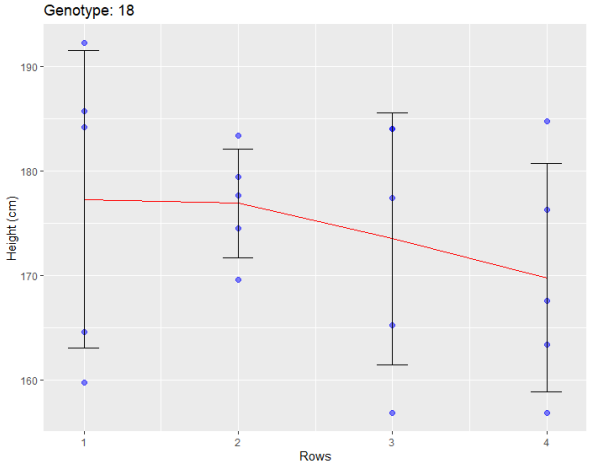
Genotype: 18
Height (cm)
190
180
170
160
1
2
3
4
Rows

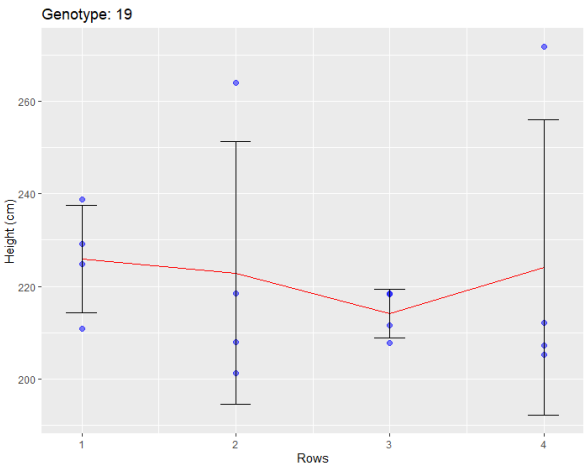
Genotype: 19
Height (cm)
260
240
220
200
1
2
3
4
Rows

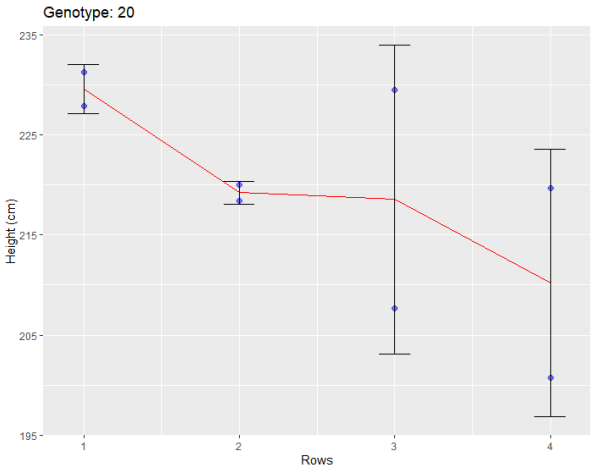
Genotype: 20
Height (cm)
235
225
215
205
195
1
2
3
4
Rows

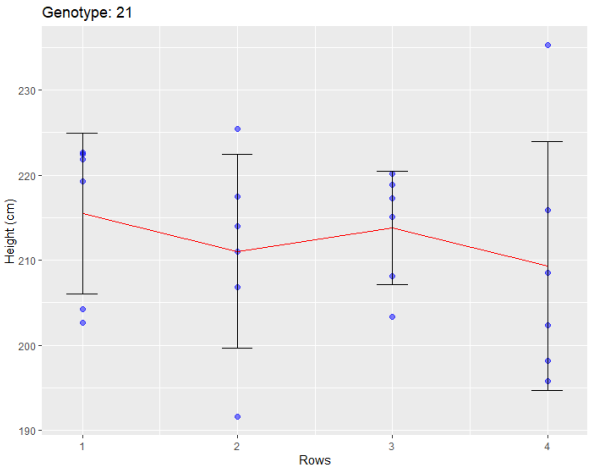
Genotype: 21
Height (cm)
230
220
210
200
190
1
2
3
4
Rows

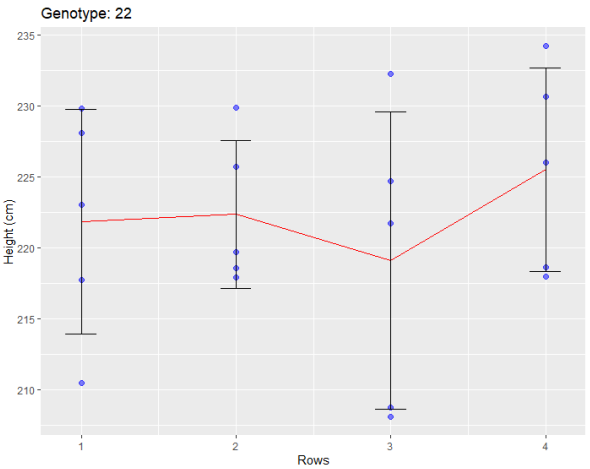
Genotype: 22
Height (cm)
235
230
225
220
215
210
1
2
3
4
Rows

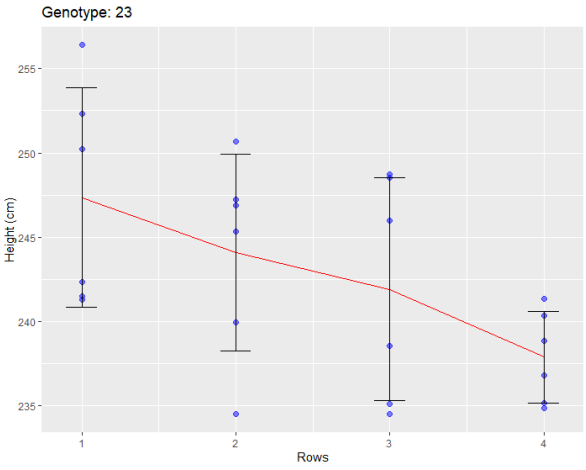
Genotype: 23
Height (cm)
255
250
245
240
235
1
2
3
4
Rows

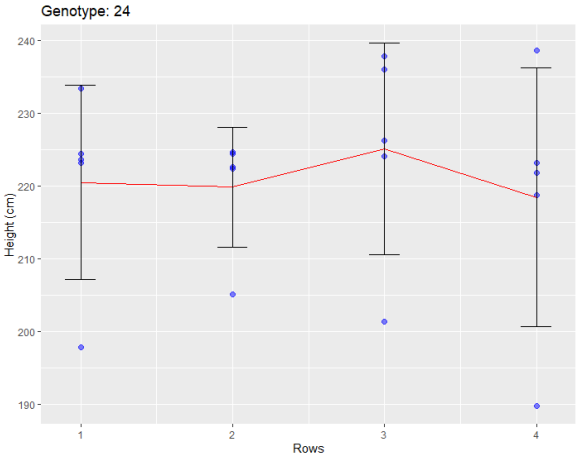
Genotype: 24
Height (cm)
240
230
220
210
200
190
1
2
3
4
Rows

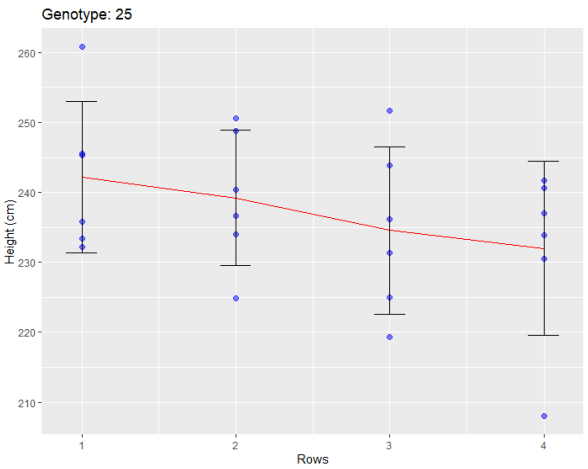
Genotype: 25
Height (cm)
260
250
240
230
220
210
1
2
3
4
Rows

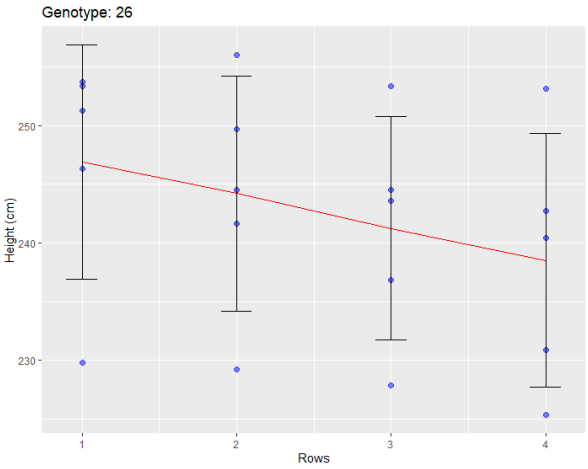
Genotype: 26
Height (cm)
250
240
230
1
2
3
4
Rows

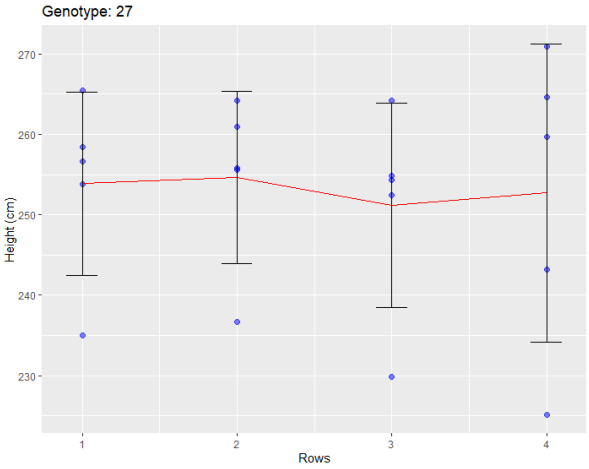
Genotype: 27
Height (cm)
270
260
250
240
230
1
2
3
4
Rows

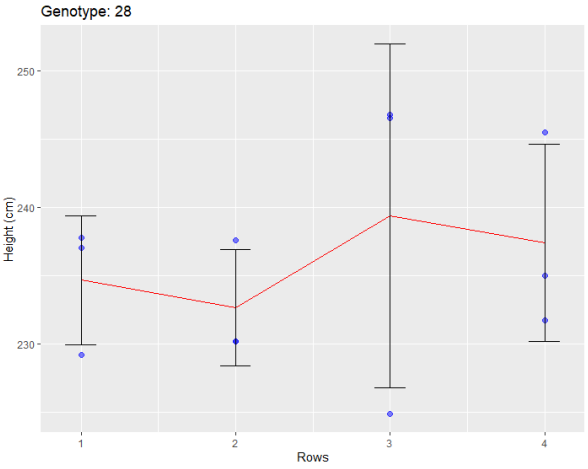
Genotype: 28
Height (cm)
250
240
230
1
2
3
4
Rows

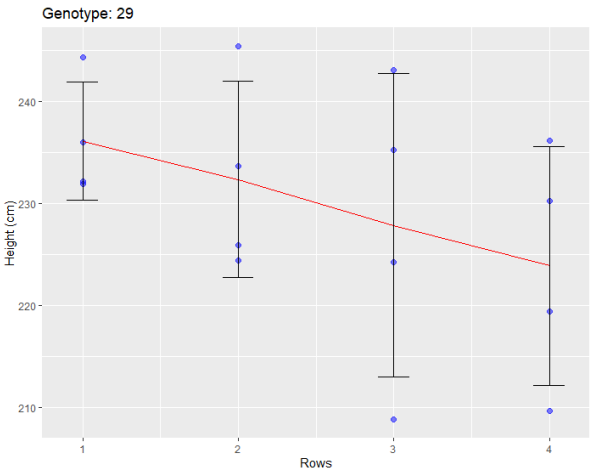
Genotype: 29
Height (cm)
240
230
220
210
1
2
3
4
Rows

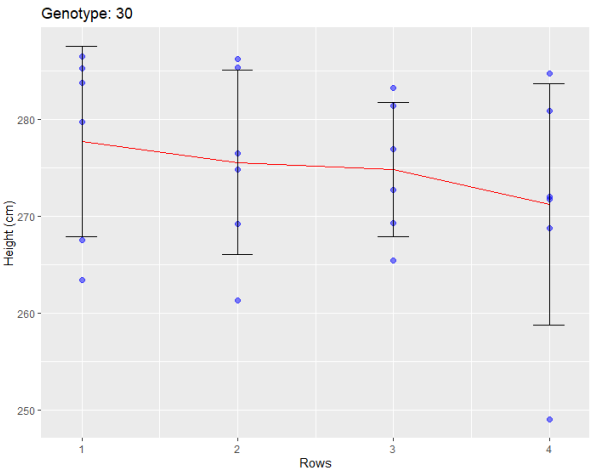
Genotype: 30
Height (cm)
280
270
260
250
1
2
3
4
Rows

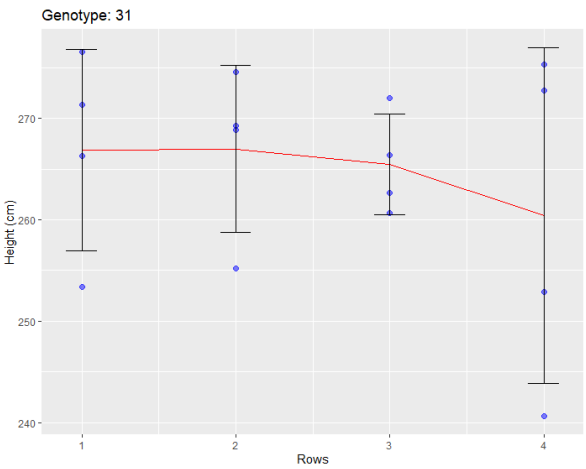
Genotype: 31
Height (cm)
270
260
250
240
1
2
3
4
Rows

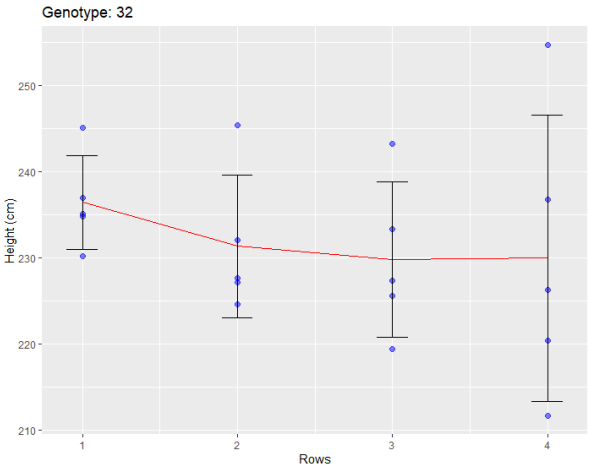
Genotype: 32
Height (cm)
250
240
230
220
210
1
2
3
4
Rows

Appendix B: Height maps for June 7th and July 18th using LiDAR data.

B.1. Average tassel height value for each row on the 7th June. Using the 99.9th percentile value of the LiDAR Imagery.

B.2. Average tassel height value for each row on the 18th July. Using the 99.9th percentile value of the LiDAR Imagery.

Appendix C: Temporal height variations of maize genotypes in an intercropping system.

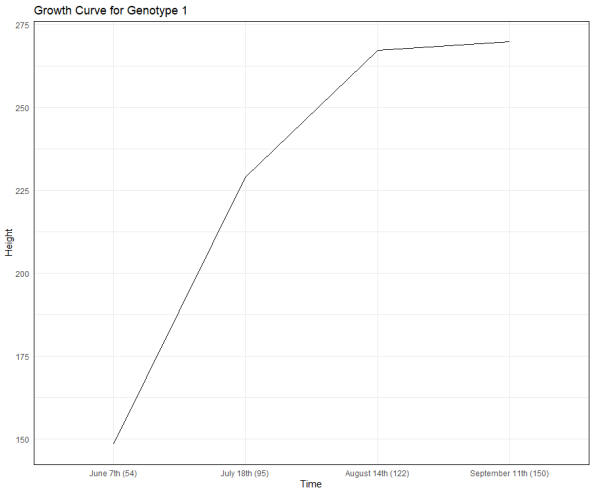

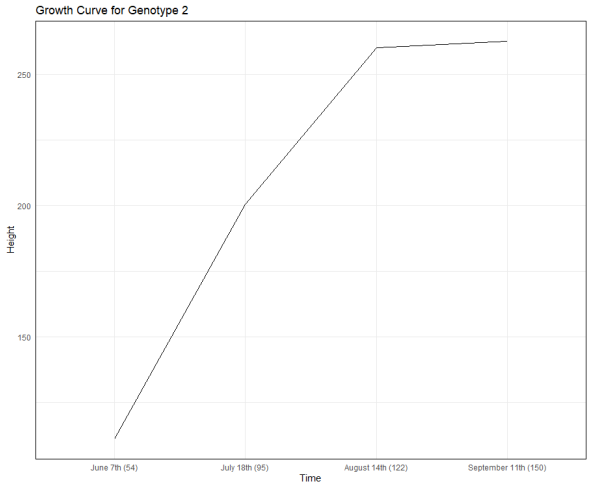

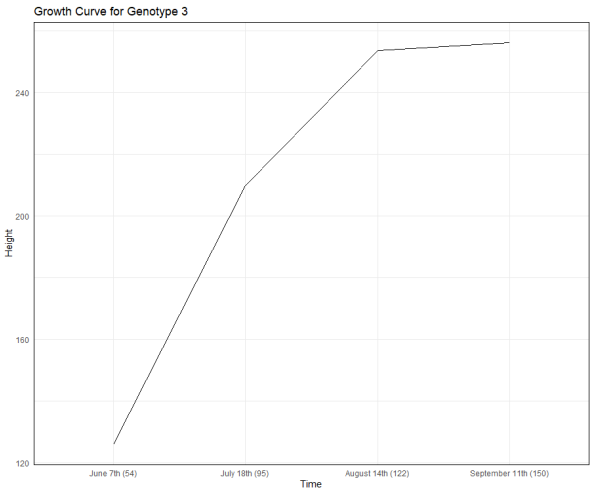

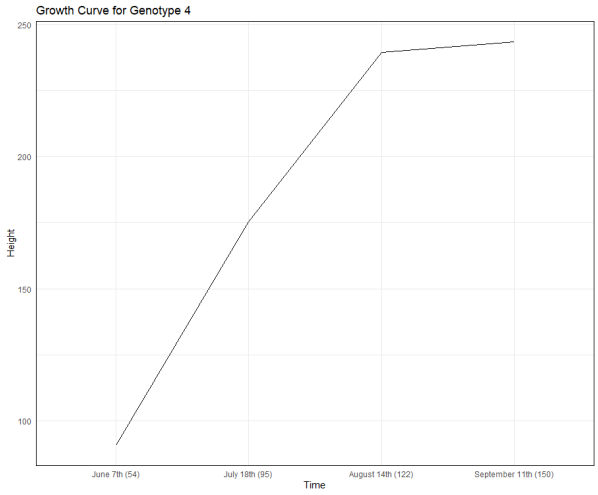

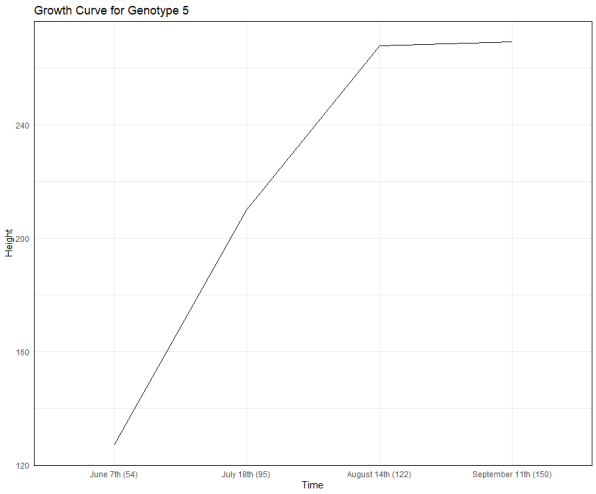

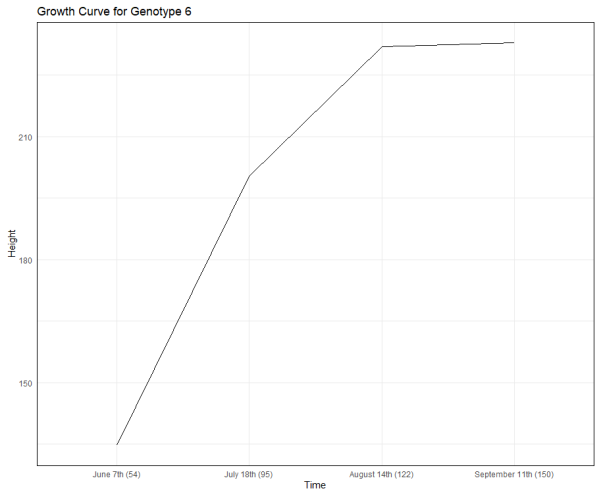

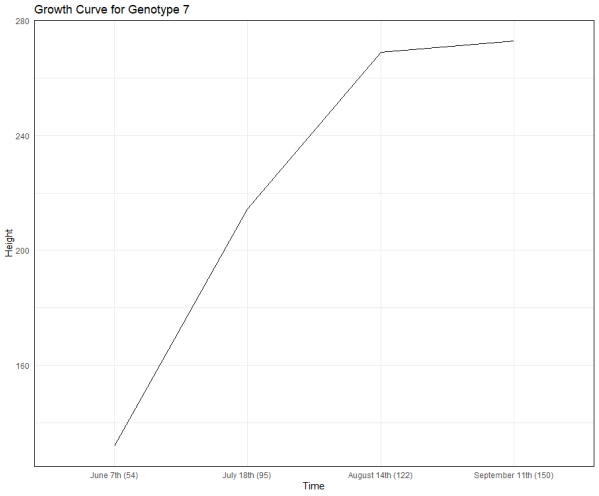
Growth Curve for Genotype 7
Height
280
240
200
160
June 7th (54)
July 18th (95)
August 14th (122)
September 11th (150)
Time

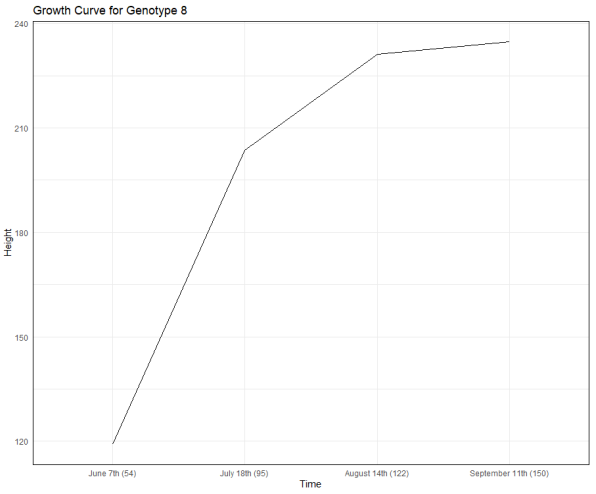
Growth Curve for Genotype 8
Height
240
210
180
150
120
June 7th (54)
July 18th (95)
August 14th (122)
September 11th (150)
Time

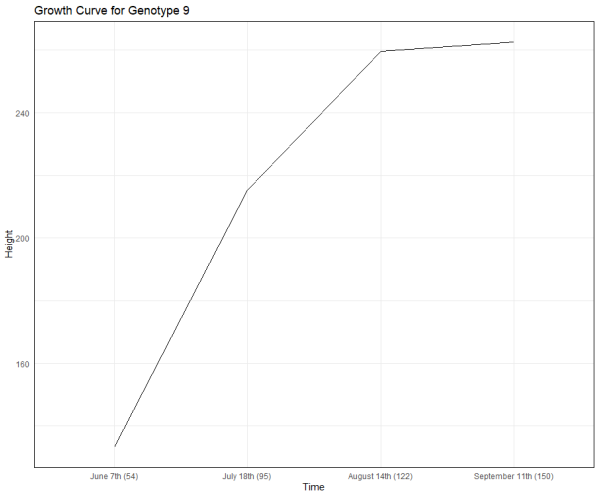
Growth Curve for Genotype 9
Height
240
200
160
June 7th (54)
July 18th (95)
August 14th (122)
September 11th (150)
Time

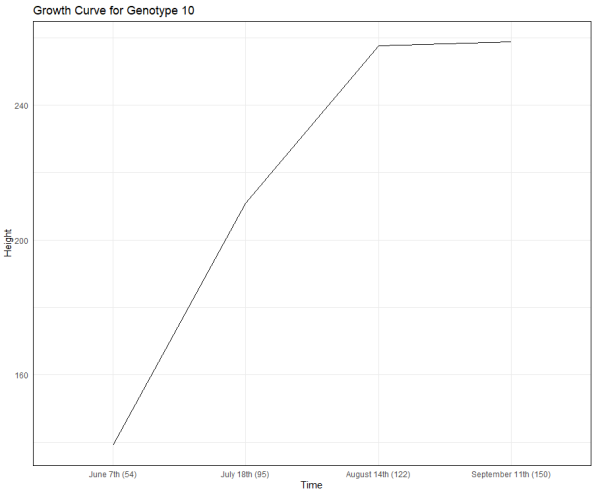
Growth Curve for Genotype 10
Height
240
200
160
June 7th (54)
July 18th (95)
August 14th (122)
September 11th (150)
Time

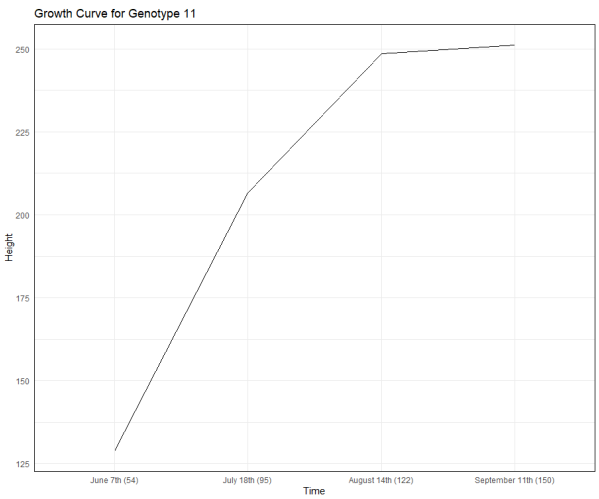
Growth Curve for Genotype 11
Height
250
225
200
175
150
125
June 7th (54)
July 18th (95)
August 14th (122)
September 11th (150)
Time

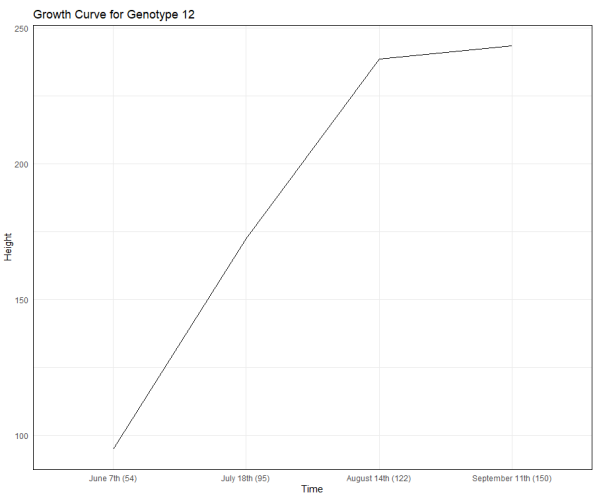
Growth Curve for Genotype 12
Height
250
200
150
100
June 7th (54)
July 18th (95)
August 14th (122)
September 11th (150)
Time

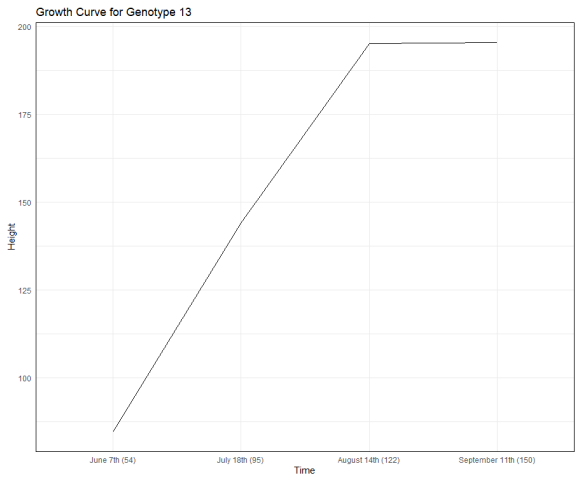
Growth Curve for Genotype 13
Height
200
175
150
125
100
June 7th (54)
July 18th (95)
August 14th (122)
September 11th (150)
Time

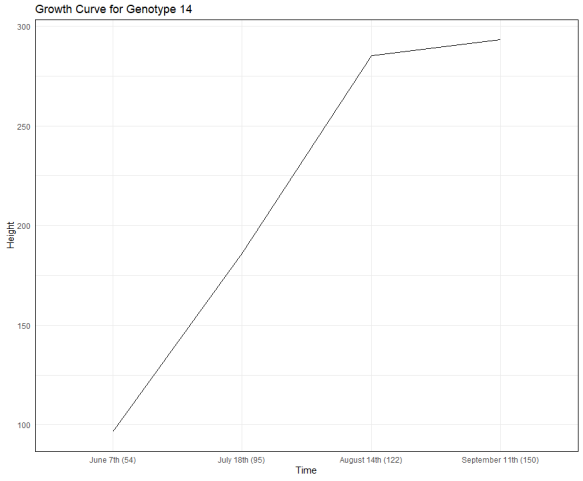
Growth Curve for Genotype 14
Height
300
250
200
150
100
June 7th (54)
July 18th (95)
August 14th (122)
September 11th (150)
Time

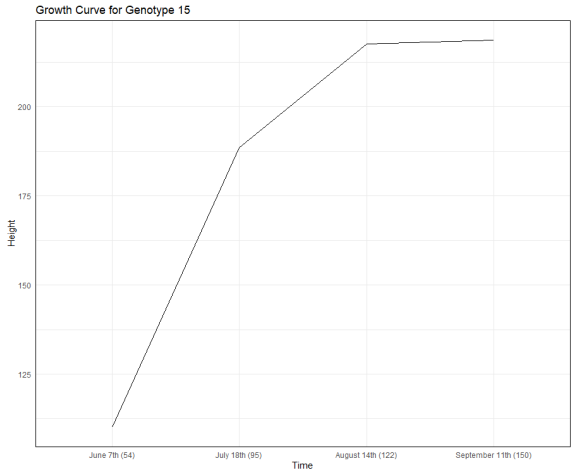
Growth Curve for Genotype 15
Height
200
175
150
125
June 7th (54)
July 18th (95)
August 14th (122)
September 11th (150)
Time

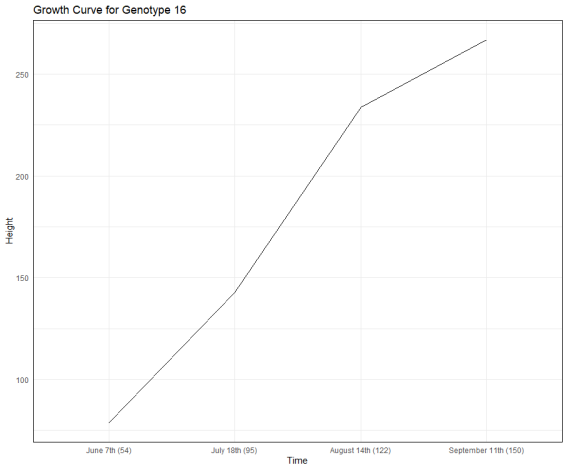
Growth Curve for Genotype 16
Height
250
200
150
100
June 7th (54)
July 18th (95)
August 14th (122)
September 11th (150)
Time

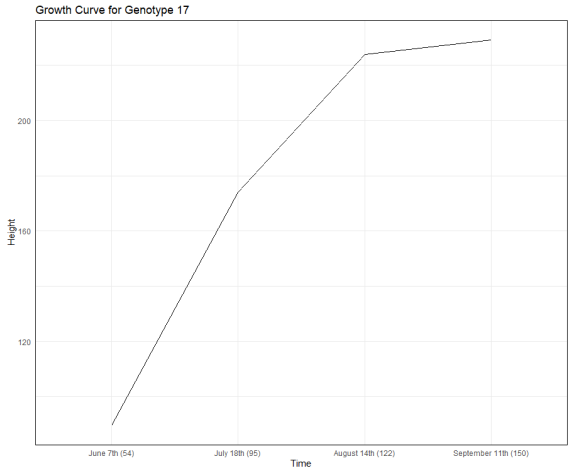
Growth Curve for Genotype 17
Height
200
160
120
June 7th (54)
July 18th (95)
August 14th (122)
September 11th (150)
Time

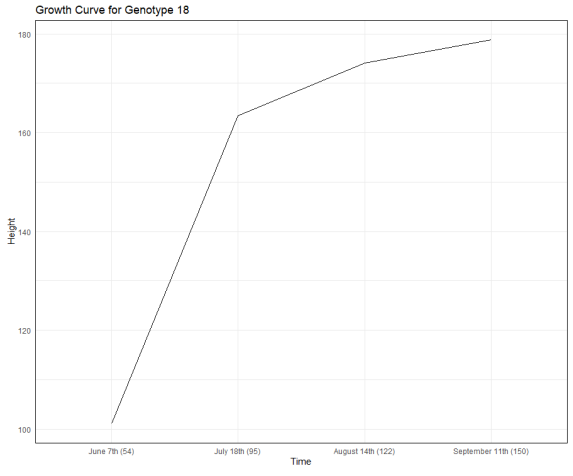
Growth Curve for Genotype 18
Height
180
160
140
120
100
June 7th (54)
July 18th (95)
August 14th (122)
September 11th (150)
Time

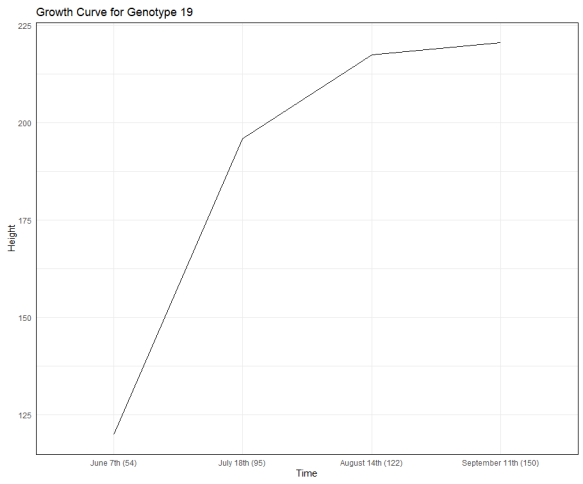
Growth Curve for Genotype 19
Height
225
200
175
150
125
June 7th (54)
July 18th (95)
August 14th (122)
September 11th (150)
Time

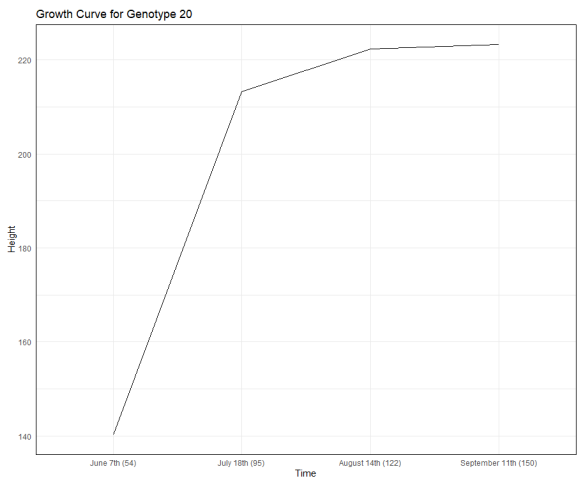
Growth Curve for Genotype 20
Height
220
200
180
160
140
June 7th (54)
July 18th (95)
August 14th (122)
September 11th (150)
Time

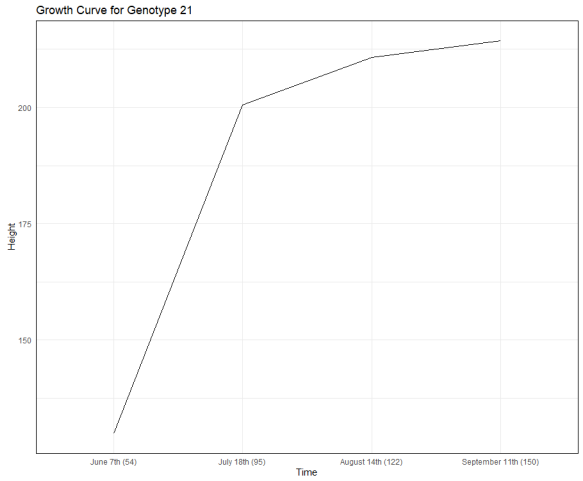
Growth Curve for Genotype 21
Height
200
175
150
June 7th (54)
July 18th (95)
August 14th (122)
September 11th (150)
Time

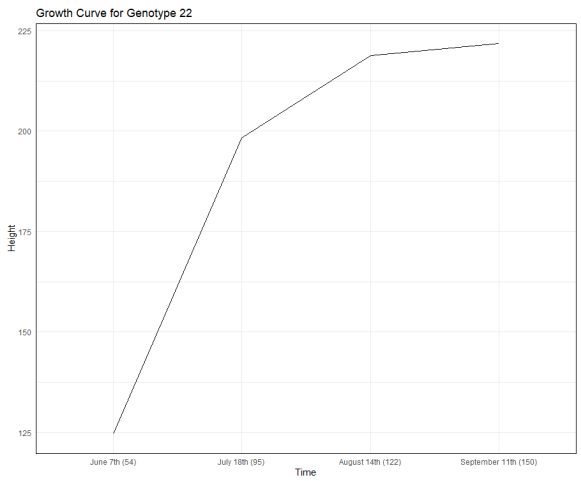
Growth Curve for Genotype 22
Height
225
200
175
150
125
June 7th (54)
July 18th (95)
August 14th (122)
September 11th (150)
Time

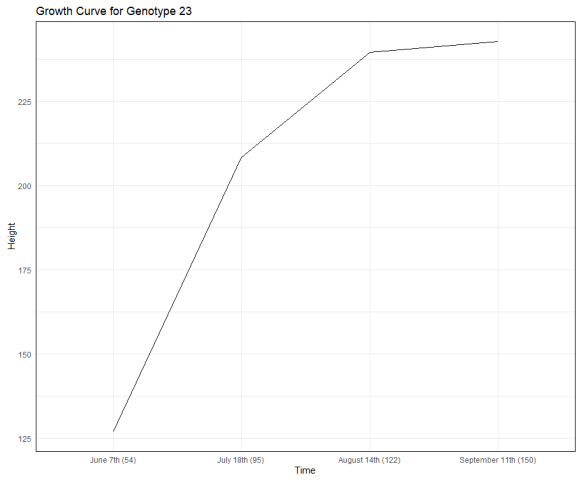
Growth Curve for Genotype 23
Height
225
200
175
150
125
June 7th (54)
July 18th (95)
August 14th (122)
September 11th (150)
Time

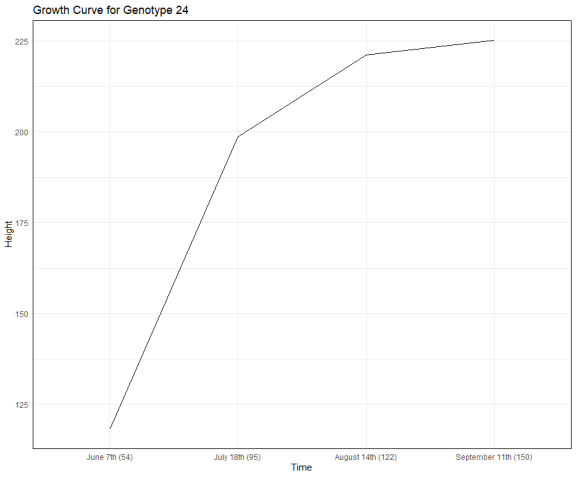
Growth Curve for Genotype 24
Height
225
200
175
150
125
June 7th (54)
July 18th (95)
August 14th (122)
September 11th (150)
Time

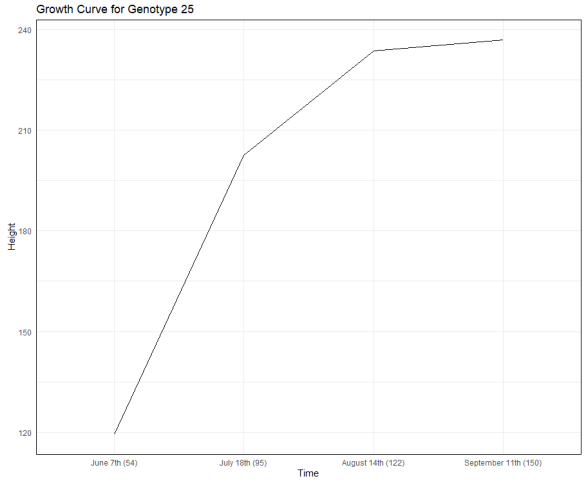
Growth Curve for Genotype 25
Height
240
210
180
150
120
June 7th (54)
July 18th (95)
August 14th (122)
September 11th (150)
Time

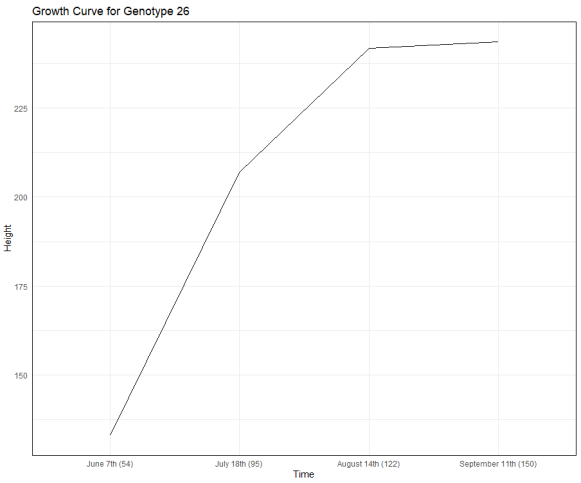
Growth Curve for Genotype 26
Height
225
200
175
150
June 7th (54)
July 18th (95)
August 14th (122)
September 11th (150)
Time

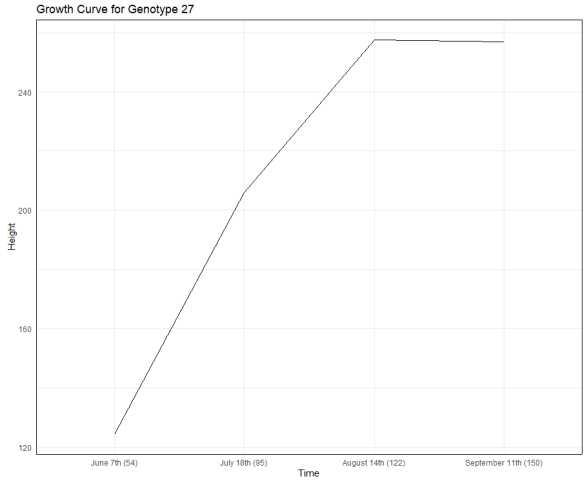
Growth Curve for Genotype 27
Height
240
200
160
120
June 7th (54)
July 18th (95)
August 14th (122)
September 11th (150)
Time

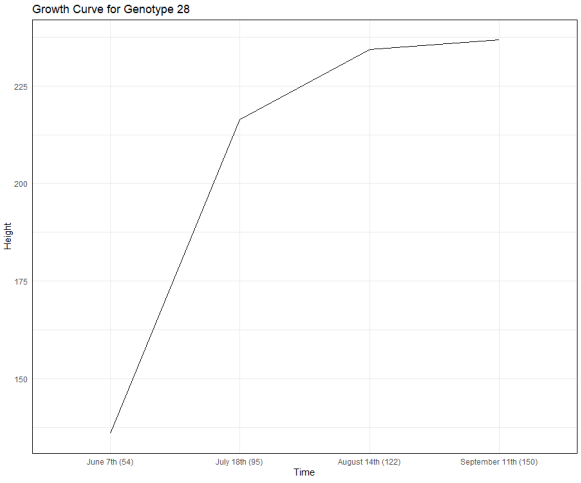
Growth Curve for Genotype 28
Height
225
200
175
150
June 7th (54)
July 18th (95)
August 14th (122)
September 11th (150)
Time

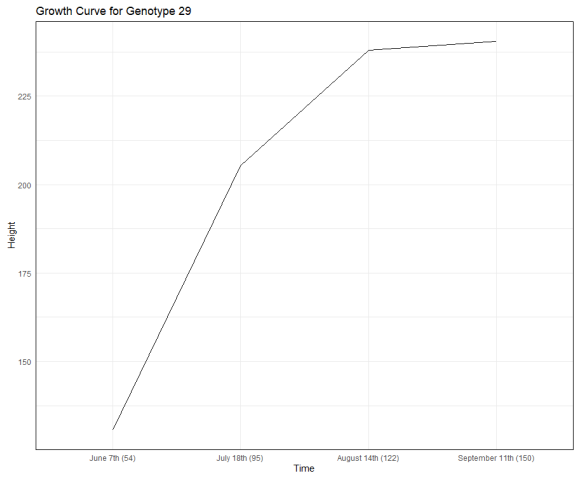
Growth Curve for Genotype 29
Height
225
200
175
150
June 7th (54)
July 18th (95)
August 14th (122)
September 11th (150)
Time

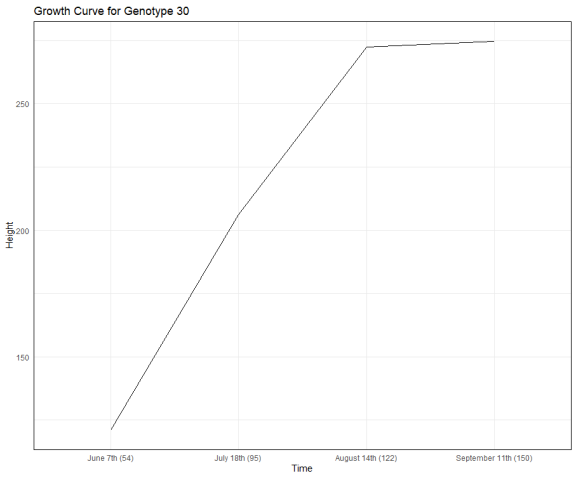
Growth Curve for Genotype 30
Height
250
200
150
June 7th (54)
July 18th (95)
August 14th (122)
September 11th (150)
Time

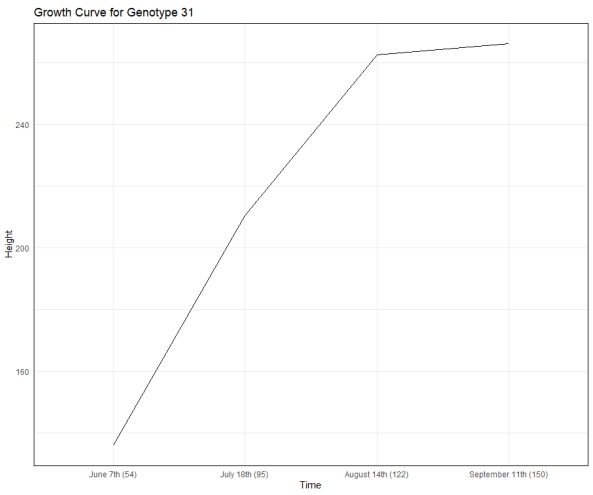
Growth Curve for Genotype 31
Height
240
200
160
June 7th (54)
July 18th (95)
August 14th (122)
September 11th (150)
Time

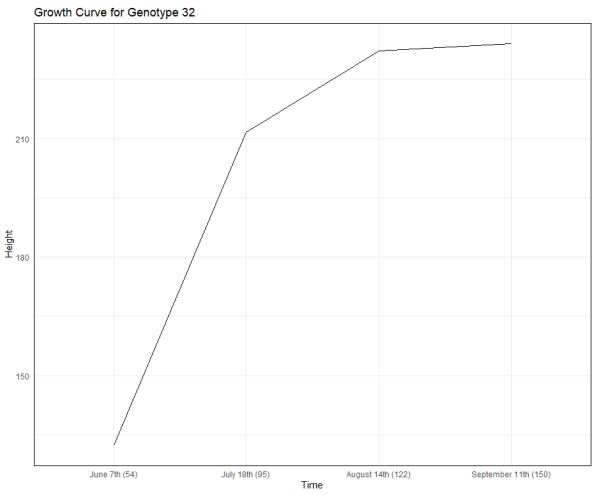
Growth Curve for Genotype 32
Height
210
180
150
June 7th (54)
July 18th (95)
August 14th (122)
September 11th (150)
Time

Appendix D: Average maize height (cm) by genotypes throughout the growing season 2023 (June to September)

Cultivars	June 7th (54 DAP)	July 18th (95 DAP)	August 14th (122 DAP)	Septemebr 11th (150 DAP)
1	148	229	267	270
2	111	200	260	263
3	126	210	254	256
4	91	175	240	244
5	127	210	268	269
6	135	200	232	233
7	132	214	269	273
8	119	204	231	235
9	133	215	260	263
10	139	211	258	259
11	129	207	248	251
12	95	172	239	243
13	84	144	195	195
14	96	186	285	293
15	110	189	218	219
16	79	143	234	267
17	90	174	224	229
18	101	163	174	179
19	120	196	217	221
20	140	213	222	223
21	130	201	211	214
22	125	198	219	222
23	127	208	240	243
24	118	199	221	225
25	119	203	234	237
26	133	207	242	244
27	124	206	258	257
28	136	216	234	237
29	131	205	238	241
30	121	206	272	275
31	136	210	263	266
32	132	212	232	234